I. STUDY OF MACROMOLECULAR BROWNIAN MOTION BY LASER LIGHT SCATTERING

II. LIGHT SCATTERING INVESTIGATION OF AMORPHOUS POLYMETHYLMETHACRYLATE

Thesis by

Vega Dibag Sankur

In partial fulfillment of the requirements

for the degree of

Doctor of Philosophy

California Institute of Technology

Pasadena, California

1977

(Submitted May 27, 1977)

To Haluk

ACKNOWLEDGMENTS

I am grateful to Professor C. J. Pings for his guidance and support during my studies at Caltech.

I would like to thank Dr. Claude Cohen for his collaboration in the study of solid polymers and also for many helpful discussions, and his very careful reading of this thesis. I would like to thank Hollis Reamer for his help and advice in the experimental work.

During these studies I have received financial support from the National Science Foundation, under grant GK34045X.

Finally, I would like to thank Haluk for his love, encouragement and support through the years I spent at Caltech.

ABSTRACT

Part I

We have studied the light scattered from dilute solutions of three different molecular weight (MW = 2 x 10^6, 4.1 x 10^6, 7.1 x 10^6) polystyrene molecules in three solvents (cyclohexane, diethylmalonate, 1-chloroundecane) at their respective theta temperatures. The autocorrelation functions collected at small x = $k^2R_G^2$ (k is the wave vector, R_G is the radius of gyration) were fitted to a single exponential function decay time which yielded the diffusion coefficients D. For concentrations below 1000 μg/cc, D's were found to be independent of concentration and to be well represented by a Stokes-Einstein relation $D = k_BT/6\pi\eta_s\zeta R_G$ where η_s is the solvent viscosity. We determined ζ to be 0.70 ± .02. At higher x, the autocorrelation functions have contributions from the first mode of internal motion and analysis of data in terms of two exponentials yield the relaxation time of this mode, τ_1. τ_1's were measured for four polystyrene-cyclohexane solutions with varying concentrations for both the four and seven million molecular weight samples. The relaxation times were found to be independent of concentration. The same experiment was repeated for both molecular weight samples for one solution each in diethylmalonate and in 1-chloroundecane. The relaxation times obtained agreed well with the theoretical predictions based on Rouse-Zimm model. The results of this research program confirm the accuracy of laser light scattering technique to measure diffusion coefficients of macromolecules. They also establish laser light scattering as a new technique for quanti-

tative determination of terminal relaxation time of linear flexible polymers. The accuracy of these measurements are comparable to those obtained by viscoelastic methods.

Part II

We have studied the light scattered from amorphous polymethylmethacrylate (PMMA) using the correlation technique for a range of temperatures from 6°C to 165°C encompassing the glass transition temperature ($T_g \sim 120°C$). The data were analyzed in terms of two exponential decays and the angular dependence of each of the corresponding relaxation frequencies was examined. The results for the high frequency relaxation mode are angular independent and fall reasonably well on two straight lines of different activation energy ($\sim$ 8 Kcal/mole at high temperatures and $\sim$1 Kcal/mole at low temperatures), indicating the presence of two coupled relaxation mechanisms. The low frequency relaxation results are quite sensitive to the inhomogeneities of unannealed samples and have in this case irregular angular dependences. The angular dependence disappears for samples close to T_g and for annealed samples. Below T_g this relaxation process has a fairly constant frequency of about 3 Hz independent of temperature. Above T_g its frequency increases very rapidly with temperature to reach 130 Hz at 165°C and follows the backbone main-chain relaxation frequency measured by other techniques. The results of this research program show that laser light scattering is a valuable tool to study the various relaxation mechanisms occuring in solids and supercooled liquids.

TABLE OF CONTENTS

Part I: STUDY OF MACROMOLECULAR BROWNIAN MOTION BY LIGHT SCATTERING

Chapter I Introduction 1

II Theory 5

III Experimental 31

IV Results and Discussion 40

Diffusion Measurements 40

Relaxation Times 45

Summary of Results and Conclusion 52

Part II: LIGHT SCATTERING INVESTIGATION OF AMORPHOUS POLYMETHYMETHACRYLATE

Chapter V Introduction 54

VI Background on Glasses 60

VII Experimental 65

VIII Results and Discussion 68

The High Frequency Relaxation Mode 68

The Low Frequency Relaxation Mode 71

Conclusion 74

Literature Cited 75

Tables 79

Figures 88

LIST OF TABLES

I. The eigenvalues λ_k' (from Zimm et al., 1956) 23

II. Eigenvalues λ_k and diagonal elements V_k for N = 100 (from Perico et al., 1975a) 24

III. Solvent Characterization Data 37

IVa. Diffusion coefficients for four million molecular weight polystyrene 41

IVb. Diffusion coefficients for seven million molecular weight polystyrene 42

V. The relaxation times and relative intensities for polystyrene (MW = 4.1×10^6) in cyclohexane. Concentration = 570 μg/cc 46

VI. The relaxation times for polystyrene with MW = 4.1×10^6 46

VII. Relaxation times and relative intensities for polystyrene (MW = 7.1×10^6) in cyclohexane. Concentration = 322 μg/cc 47

VIII. The relaxation times determined for polystyrene with MW = 7.1×10^6 48

IX. Comparison of relaxation times observed with predictions of Rouse-Zimm theory. 51

X. Diffusion coefficients vs concentration for 2×10^6 molecular weight polystyrene 79

XI. Diffusion coefficients vs concentration for 4.1×10^6 molecular weight polystyrene 80

XII. Diffusion coefficients vs concentration for 7.1×10^6 molecular weight polystyrene 81

XIII. Relaxation times and relative intensities for polystyrene (MW = 4.1×10^6) in cyclohexane. Concentration = 431 μg/cc $D = 0.685 \times 10^{-7} cm^2/sec$ 82

XIV. Relaxation times and relative intensities for polystyrene (MW = 4.1 x 10^6) in cyclohexane. Concentration = 307 μg/cc D = 0.661 x 10^{-7} cm^2/sec 82

XV. Relaxation times and relative intensities for polystyrene (MW = 4.1 x 10^6) in cyclohexane. Concentration = 198 μg/cc D = 0.668 x 10^{-7} cm^2/sec 82

XVI. Relaxation times and relative intensities for polystyrene (MW = 4.1 x 10^6) in diethylmalonate. Concentration = 559 μg/cc. D = 0.324 x 10^{-7} cm^2/sec 83

XVII. Relaxation times and relative intensities for polystyrene (MW = 4.1 x 10^6) in 1-chloroundecane. Concentration = 533 μg/cc. D = 0.263 x 10^{-7} cm^2/sec 84

XVIII. Relaxation times and relative intensities for polystyrene (MW = 7.1 x 10^6) in cyclohexane. Concentration = 245 μg/cc D = 0.519 x 10^{-7} cm^2/sec 84

XIX. Relaxation times and relative intensities for polystyrene (MW = 7.1 x 10^6) in cyclohexane. Concentration = 176 μg/cc D = 0.527 x 10^{-7} cm^2/sec 85

XX. Relaxation times and relative intensities for polystyrene (MW = 7.1 x 10^6) in cyclohexane. Concentration = 115 μg/cc D = 0.518 x 10^{-7} cm^2/sec 86

XXI. Relaxation times and relative intensities for polystyrene (MW = 7.1 x 10^6) in diethylmalonate. Concentration = 301 μg/cc. D = 0.254 x 10^{-7} cm^2/sec 87

XXII. Relaxation times and relative intensities for polystyrene (MW = 7.1 x 10^6) in 1-chloroundecane. Concentration = 344 μg/cc. D = 0.210 x 10^{-7} cm^2/sec 87

LIST OF FIGURES

1. The scattering geometry of the experimental set-up used in this study 6

2. Bead-Spring Model 14

3. The relative intensities of various terms contributing to the spectrum vs $x^{1/2}$ (from Pecora, 1968) 88

4a. The total and diffusive intensity vs x (from Perico et al., 1975) 88

4b. The intramolecular intensities vs x (from Perico et al., 1975) 89

5. $P_{NM}(x)$ vs $x^{1/2}$ for flexible molecules (from Fujime and Maruyama, 1973) 90

6. A schematic drawing of the light scattering spectrometer used in this study 91

7. A typical current autocorrelation function with 400 points 92

8. The inverse decay time vs k^2 for the two million molecular weight polystyrene in cyclohexane (C = 735 μg/cc) 93

9. The inverse decay time vs k^2 for the two million molecular weight polystyrene in diethylmalonate (C = 718 μg/cc) 94

10. The inverse decay time vs k^2 for the two million molecular weight polystyrene in 1-chloroundecane (C = 796 μg/cc) 95

11. The inverse decay time vs k^2 for the four million molecular weight polystyrene in cyclohexane (C = 570 μg/cc) 96

12. The inverse decay time vs k^2 for the four million molecular weight polystyrene in cyclohexane (C = 431 μg/cc) 97

13. The inverse decay time vs k^2 for the four million molecular weight polystyrene in cyclohexane (C = 307 μg/cc) 98

14. The inverse decay time vs k^2 for the four million molecular weight polystyrene in cyclohexane (C = 198 μg/cc) 99

15. The inverse decay time vs k^2 for the four million molecular weight polystyrene in diethylmalonate (C = 559 μg/cc) 100

16. The inverse decay time vs k^2 for the four million molecular weight polystyrene in 1-chloroundecane (C = 533 μg/cc) 101

17. The linear part of the inverse decay time vs k^2 plot for the four million molecular weight polystyrene in cyclohexane (C = 570 μg/cc) 102

18. The inverse decay time vs k^2 for the seven million molecular weight polystyrene in cyclohexane (C = 322 μg/cc) 103

19. The inverse decay time vs k^2 for the seven million molecular weight polystyrene in cyclohexane (C = 245 μg/cc) 104

20. The inverse decay time vs k^2 for the seven million molecular weight polystyrene in cyclohexane (C = 176 μg/cc) 105

21. The inverse decay time vs k^2 for the seven million molecular weight polystyrene in cyclohexane (C = 115 μg/cc) 106

22. The inverse decay time vs k^2 for the seven million molecular weight polystyrene in diethylmalonate (C = 301 μg/cc) 107

23. The inverse decay time vs k^2 for the seven million molecular weight polystyrene in 1-chloroundecane (C = 344 μg/cc) 108

24. The linear part of the inverse decay time vs k^2 plot for the seven million molecular weight polystyrene in cyclohexane (C = 322 μg/cc) 109

25. τ_I^{-1} vs k^2 for the four million molecular weight polystyrene in cyclohexane (C = 570 μg/cc). 110

26. The diffusion coefficients vs molecular weight M_w 111

27. The diffusion coefficients vs the solvent viscosity η_s 112

28. The ratio A/(A+B) vs x 113

29. Thermodynamic properties of glucose around glass transition temperature (from Kauzmann, 1948) 114

30. Excess heat content and entropy (from Kauzmann, 1948) 115

31a. Correlation function at 20°C, θ = 130° with the correlator increment time t = 1 msec 116

31b. Correlation function of Fig. 31a repeated with the correlator increment time t = 200 μsec 117

32a. Angular dependence of the high frequency relaxation performed on the same position of a sample at 20°C 118

32b. Angular dependence of the high frequency relaxation performed on various positions of a sample at 20°c 119

33. Angular dependence of the high frequency relaxation performed on various positions of a sample at 40°C 120

34. Angular dependence of the high frequency relaxation performed on various positions of a sample at 55°C 121

35. Angular dependence of the high frequency relaxation performed on various positions of a sample at 81°C 122

36. Angular dependence of the high frequency relaxation performed on various positions of a sample at 100°C 123

37. Temperature dependence of the high frequency relaxation 124

38a. Angular dependence of the low frequency relaxation performed on the same position of an unannealed sample: i) at 20°C; ii) at 40°C 125

38b. Angular dependence of the low frequency relaxation performed on the same position of an unannealed sample: i) at 81°C; ii) at 100°C 126

38c. Angular dependence of the low frequency relaxation performed on one position of an annealed sample: i) at 6°C; ii) at 20°C 127

39. Temperature dependence of the low frequency relaxation 128

PART I

STUDY OF MACROMOLECULAR BROWNIAN MOTION BY LASER LIGHT SCATTERING

CHAPTER I

INTRODUCTION

With the advent of lasers and optical mixing techniques that can resolve very narrow spectra, laser light scattering has become a powerful tool to study dynamics of macromolecules in solution. A series of theoretical papers by Pecora (1964, 1965, 1968, 1968a) have shown that the spectrum of light can be related to the translational diffusion and the internal motion of the molecule. Under the condition that $\ell k \leq 1$ (where ℓ is the characteristic dimension of the molecule and k is the magnitude of the scattering vector) the main contribution to the spectrum comes from the center of mass motion. Thus the resolution of the spectrum in this region yields the diffusion coefficient D of the molecule. Numerous experimental studies conducted earlier (Cummins et al, 1964; Dubin et al, 1967) have established light scattering as a reliable tool to determine D. For $\ell k > 1$, the contribution from the internal motion of the molecule becomes appreciable. Thus analysis of spectrum in this region should yield additional information about the internal modes of motion.

The internal motion of the macromolecules largely contributes to the viscoelastic behavior of the polymer solutions, thus affecting all properties of engineering interest such as viscosity under various flow conditions, stress coefficients, etc. It has been a major problem in rheology to describe the dynamic behavior of macromolecules and to relate flow properties to the known molecular parameters using these models.

The case of random coil molecules has been extensively studied

due to the fact that most synthetic and biological polymers fall into this category. Rouse (1953) was the first to calculate the viscosity of a solution of coiling molecules using a bead-spring representation. A transformation to normal coordinates showed that the internal motion of the molecules can be separated into a series of modes, each with a relaxation time τ_1, τ_2, etc. The flow properties of the solution can then be calculated in terms of these relaxation times. The largest contribution to the viscoelastic parameters arises from the lowest order mode characterized by the first or the so-called terminal relaxation time τ_1. This basic model was later improved by addition of hydrodynamic interaction (Zimm, 1956), solvent molecule interaction (Tschoegl, 1964), etc.

Pecora (1965, 1968) pointed out the possibility of measuring the first relaxation time by light scattering. He calculated the contribution of the various internal modes to the spectrum of light using the Rouse model. He found that for a range of ℓk values ($1 < \ell k < 5$) the spectrum consists of the translational diffusion and the lowest order internal mode contributions. Thus an analysis of the spectrum in this region should yield τ_1. Later the spectrum was calculated by Fujime and Maruyama (1973) using a wormlike molecule model introduced by Harris and Hearst (1966), and by Perico et al (1975) using the Zimm model with varying degrees of hydrodynamic interaction taken into account. Their results agree with Pecora's with only slight numerical differences in the intensities of terms contributing to the spectrum.

The experimental work in this area is limited. Huang and

Frederick (1974) studied the spectrum of light scattered by polystyrene (molecular weight 27.3 million) in cyclohexane and 2-butanone. They determined D and τ_1. Their values for τ_1 agree roughly with theoretical predictions. But the uncertainty in their diffusion coefficient due to the fact that their ℓk values are too high even at small angles, and the large scatter in their data make the results inconclusive. McAdam and King (1974) also studied light scattered from polystyrene solutions. They analyzed the spectrum in terms of an oversimplified function. This fact and their polystyrene samples being highly polydisperse (M_w/M_n = 1.7) introduces ambiguities in their interpretation of the results. This technique was also applied to biological macromolecules (Fujime, 1970 ; Fujime and Ishiwata, 1971; Fujime et al, 1972; Schmidt, 1973; Jolly and Eisenberg, 1976).

The present study was undertaken to evaluate light scattering as a technique to determine the terminal relaxation time of flexible molecules. Polystyrene molecules were chosen due to their availability in fairly monodisperse form. The molecular weights used in this study made it possible to take extensive data at $\ell k \leq 1$ to obtain the diffusion coefficient accurately. The range $1 < \ell k < 5$ was also readily attainable to determine the relaxation time. The solvents were chosen to form ideal solutions with polystyrene where the molecule interactions balance the solvent molecule interactions as evidenced by the disappearance of the second virial coefficient. Diffusion coefficients for three different molecular weight polystyrenes (M_w = 2×10^6, 4.1×10^6, 7.1×10^6), in each of three solvents (cyclohexane,

diethylmalonate and 1-chloroundecone) were determined. The relaxation times were measured for 4 and 7 million molecular weight samples in each solvent. In all cases angular studies were conducted in order to verify anticipated scattering angle dependence.

CHAPTER II

THEORY

Light is scattered from the optical inhomogeneities of the medium it passes through. In the case of macromolecular solutions, these inhomogeneities are due to the large polarizabilities of solute molecules compared with those of the solvent. Light scattered from such a system carries information about the dynamic behavior of these macromolecules. In this chapter we will derive the spectrum of light scattered from a dilute solution of linear flexible molecules and we will relate it to the diffusion coefficient and internal relaxation times for these molecules.

Spectrum of Light

As light passes through a nonabsorbing, nonconducting medium, it induces an oscillating dipole moment in each molecule. In turn, these dipole moments emit a spherical light wave with the same frequency as that of the incident wave (Born & Wolf, 1970).

The electric field of the incident laser light at $\underline{r}$ is

$$\underline{E}_i(t) = \underline{n}_i E_i \exp(\underline{k}_i \cdot \underline{r} - \omega_i t) \tag{1}$$

where $\underline{n}_i$ is the unit vector in the direction of polarization, E_i is the amplitude and ω_i is the frequency of the incident wave. $\underline{k}_i$ is the propagation vector and its magnitude is given by:

$$k_i = |\underline{k}_i| = \frac{n\omega_i}{c} = \frac{2\pi}{\lambda} = \frac{2\pi n}{\lambda_o} \tag{2}$$

where n is the refractive index of the medium, c is the speed of light and λ_o and λ are the wavelengths of light in vacuo and in the scattering

medium respectively.

The scattering geometry for our experimental set-up is shown in Fig. 1. The incident light is polarized in the vertical direction ($\underline{n}_i \,||\, \underline{z}$). The detector is placed in the xy plane and the scattered light detected has the same polarization as the incident one. $\underline{k}_s$ is the

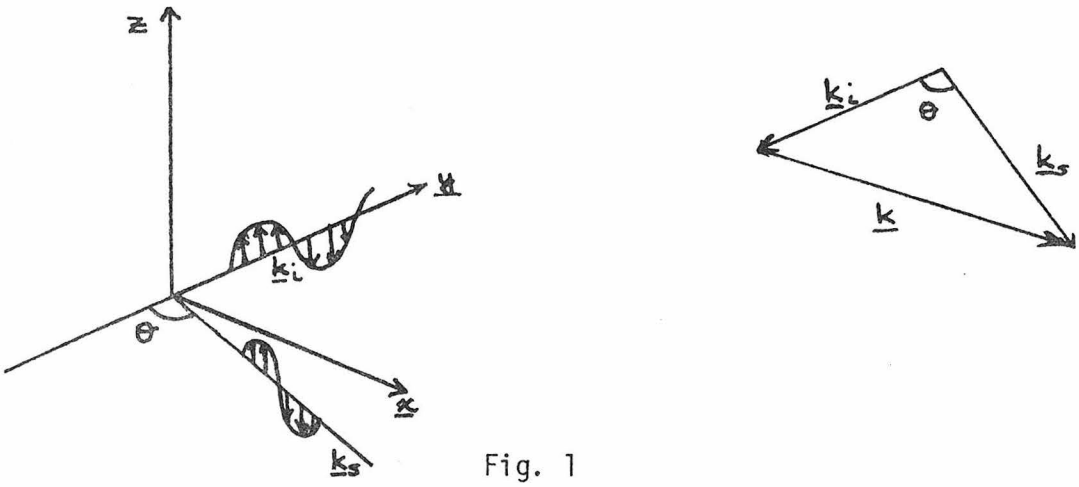

Fig. 1

propagation vector in the scattering direction and its magnitude is approximately equal to k_i due to the fact that the frequency changes in these experiments are very small compared with the incident frequency. θ is the scattering angle.

The electric field of the wave scattered by the j^{th} molecule and detected at $\underline{R}$ is given by (Berne and Pecora, 1976)

$$\underline{E}_{sc_j}(\underline{R},t) = \frac{1}{[|\underline{R} - \underline{r}_j|c]} \exp[i\underline{k}_s \cdot (\underline{R} - \underline{r}_j)] \frac{\partial^2}{\partial t^2} P(\underline{r}_j, t')d^3r \qquad (3)$$

$\underline{P}(\underline{r},t')$ is the polarization induced at $\underline{r}$ at the retarded time t' defined as

$$t' = t - \frac{|\underline{R} - \underline{r}|}{c/n} \tag{4}$$

and takes into account the fact that light scattered from different parts of the medium has to travel different distances to reach the detector. $P(r,t')$ is related to the incident field by the polarizability tensor $\underline{\underline{\alpha}}(r,t')$

$$\underline{P}(\underline{r},t') = \underline{\underline{\alpha}}(\underline{r},t') \cdot \underline{E}_i(\underline{r},t') \tag{5}$$

For isotropic scatterers, the induced polarization is in the same direction as incident wave polarization, and the polarizability $\alpha(r,t')$ reduces to a scalar quantity.

$$\underline{P}(\underline{r},t') = \alpha(\underline{r},t')\, n_i \underline{E}_i \exp i(\underline{k}_i \cdot \underline{r} - \omega_i t') \tag{6}$$

Combining equations 3, 5, and 6, taking the time derivative of $\underline{P}(\underline{r},t)$, and using the far field approximation in the denominator, $\underline{E}_{sc_j}$ can be expressed as follows:

$$\underline{E}_{sc_j}(\underline{R},t) = \frac{\omega_o^2}{c^2 R}[\exp i\underline{k}_s \cdot (\underline{R} - r_j)]\, \alpha(\underline{r}_j,t)[\exp i(\underline{k}_i \cdot \underline{r}_j - \omega_i t)]d^3r \tag{7}$$

The light reaching the detector is a sum of scattered waves from all over the illuminated volume. Thus the scattered field at the detector can be expressed as an integration over the scattering volume,

$$\underline{E}_{sc}(\underline{R},t) \quad \frac{\omega_o^2}{c^2 R}[\exp i(\underline{k}_s \cdot \underline{R} - \omega_i t)] \int_V \alpha(\underline{r},t)[\exp i(\underline{k}_i - \underline{k}_s) \cdot \underline{r}]\, d'\underline{r} \tag{8}$$

The scattering vector $\underline{k}$ is defined as

$$\underline{k} = \underline{k}_s - \underline{k}_i \tag{9}$$

and its magnitude can be obtained using the law of cosines,

$$k = |\underline{k}| = 2k_i \sin \frac{\theta}{2} \tag{10}$$

To simplify the integral in equation 8, the polarizability is expanded in a Fourier series,

$$\alpha(\underline{r},t) = \frac{1}{(2\pi)^{3/2}} \int_{-\infty}^{\infty} \alpha(\underline{q},t) \cdot \exp i\underline{q}\cdot r \, d^3\underline{q} \tag{11}$$

Replacing $\alpha(\underline{r},t)$ in equation 8 by its Fourier expansion and rearranging terms, E_{sc} can be written as

$$E_{sc}(\underline{R},t) = \frac{\omega_i^2}{c^2 R} \frac{1}{(2\pi)^{3/2}} [\exp i(\underline{k}_s\cdot\underline{R} - \omega_i t)]$$

$$\times \left[\int_q \alpha(\underline{q},t) \, d^3\underline{q} \int_r \exp(\underline{q} - \underline{k})\cdot\underline{r} \, d^3\underline{r}\right] \tag{12}$$

The second integral over $\underline{r}$ yields a δ function.

$$\int \exp i(\underline{q} - \underline{k})\cdot\underline{r} \, d^3r = \delta(\underline{q} - \underline{k}) \tag{13}$$

Replacing the integral in equation 12 by the δ function, we find that the electric field is proportional to the $\underline{k}$ Fourier component of the polarizability,

$$\underline{E}(\underline{R},t) = \frac{\omega_i^2}{(2\pi)^{3/2} c^2 R} E_i \, \underline{z} \, [\exp i(\underline{k}_s\cdot\underline{R} - \omega_i t)] \, \alpha(\underline{k},t) \tag{14}$$

The experimentally measured quantities are the spectrum of light or the correlation function of the electric field. According to the Wiener-Khintchine theorem, these are related to each other by a Fourier transformation,

$$C_E(\underline{k},\tau) = \langle E^*(\underline{k},t)\ E(\underline{k},t+\tau)\rangle \tag{15}$$

and

$$I(\underline{k},\omega) = \frac{1}{2\pi}\int_{-\infty}^{\infty} \langle E^*(\underline{k},t)\ E(\underline{k},t+\tau)\rangle \exp\, i\omega\tau\ d\tau \tag{16}$$

Since for a stationary process the correlation function is time invariant independent of the original time t, t in equations 15 and 16 can be replaced by zero and these functions can be written in terms of polarizability as follows:

$$C_E(\underline{k},\tau) \propto \langle \alpha^*(\underline{k},0)\ \alpha(\underline{k},\tau)\rangle \exp(-i\omega_i\tau) \tag{17}$$

and

$$I(\underline{k},\omega) \propto \int_{-\infty}^{\infty} \langle \alpha^*(\underline{k},0)\ \alpha(\underline{k},\tau)\rangle \exp\, i(\omega-\omega_i)\tau\ d\tau \tag{18}$$

The term in the brackets is the correlation function of the $\underline{k}$ component of the polarizability. It will be denoted by $S(\underline{k},\tau)$.

$$S(\underline{k},\tau) \equiv \langle \alpha^*(\underline{k},0)\ \alpha(\underline{k},\tau)\rangle \tag{19}$$

$\alpha(\underline{r},t)$ can be obtained by summing up the individual polarizability α_j of each molecule j in the scattering volume.

$$\alpha(\underline{r},t) = \sum_{j=1}^{N'} \alpha_j\ \delta[\underline{r} - \underline{r}_j(t)] \tag{20}$$

$\alpha(r,t)$ and $\alpha(\underline{k},t')$ are related by equation 11. By taking the inverse Fourier transform of equation 20 one obtains:

$$\alpha(\underline{k},t) = \sum_{j=1}^{N} \alpha_j \exp i\, \underline{k}\cdot\underline{r}_j(t) \tag{21}$$

The polarizabilities of macromolecules are much larger than those of the solvent molecules. For polymer solutions we can therefore neglect the contribution from the solvent and carry out the summation over only the polymer molecules. This approximation is also justified when we consider the time scales involved in these experiments. The macromolecules move much more slowly compared with the small solvent molecules and dominate the slow relaxation part of the spectrum in which we are interested. Therefore,

$$\alpha(\underline{k},t) = \sum_{i=1}^{M} \alpha_i \exp i\, \underline{k}\cdot\underline{r}_i(t) \tag{22}$$

where the summation is carried over the polymer molecules only.

In all the derivations above, the molecules have been treated as point sources: the electric field has been assumed to be uniform throughout the molecule. This is valid only for molecules much smaller than the wavelength of light. For large molecules, the field is not uniform; there is interference between scattering from different parts of the molecule, and equation 21 is not applicable as it stands. This problem can be circumvented by dividing the molecule into segments, the sizes of which are small compared with λ, and carrying out the summation over these segments. The polarizability then, in terms of segmental polarizability, can be written as

$$\alpha(\underline{k},t) = \sum_{\substack{i=1 \\ j=1}}^{N,M} \alpha_{ij}^{s} \exp i\underline{k}\cdot\underline{r}_{ij}(t) \qquad (23)$$

where i,j are summations over segments of a molecule and over different molecules respectively. N is the number of segments. For identical segments and molecules, α_{ij}^{s} are the same and equal to α/N.

The correlation function $S(\underline{k},\tau)$ can now be calculated as

$$S(\underline{k},\tau) = \frac{\alpha^2}{N^2} \sum_{\substack{i=1 \\ j=1}}^{N,M} \sum_{\substack{\ell=1 \\ m=1}}^{N,M} \left\langle \exp[i\underline{k}\cdot\underline{r}_{ij}(0)] \exp[-ik\cdot r_{\ell m}(\tau)] \right\rangle \qquad (24)$$

where i,ℓ are over the segments and j,m are over the molecules.

In sufficiently dilute solutions, the molecules behave independently of each other, so the motion of segments of different molecules are uncorrelated. Thus in equation 23 the terms for which $j \neq m$ vanish and $S(k,\tau)$ is reduced to a correlation over the segments of a single mulecule,

$$S(\underline{k},\tau) = \frac{M\alpha^2}{N^2} \sum_{\substack{i=1 \\ \ell=1}}^{N} \left\langle \exp i\underline{k}\cdot[\underline{r}_{\ell}(\tau) - \underline{r}_{i}(0)] \right\rangle \qquad (25)$$

To calculate $S(\underline{k},\tau)$ an extensive knowledge of the dynamic behavior of a single molecule in solution is required. The spectrum of light has been calculated for a few specific cases such as rigid rods, flexible molecules, etc. using already existing hydrodynamic theories (Pecora 1964, 1965, 1968, 1968a, 1968b; Fujime, 1973; Saito et al. 1967). Before going into these we will show that under certain conditions $S(\underline{k},\tau)$ can be simplified and calculated using the translational diffusion equation. The coordinates of the i^{th} segment, $\underline{r}_i$ can be expressed in terms of center of mass coordinates

$$\underline{r}_i = \underline{R}_{cm} + \underline{r}'_i \tag{26}$$

where $\underline{r}'_i$ is the location of the segment with respect to the center of mass. The correlation function takes the form

$$S(\underline{k},\tau) \propto \left\langle \sum_{i,j}^{n} \exp i\underline{k} \cdot [\underline{R}_{cm}(\tau) + \underline{r}_j(\tau) - \underline{R}_{cm}(0) - r'_i(0)] \right\rangle \tag{27}$$

and assuming that the segmental motion of the molecule is independent of its center of mass motion, it can be factored into two correlation functions,

$$S(\underline{k},\tau) \propto \langle \exp i\underline{k}\cdot[\underline{R}_{cm}(\tau) - \underline{R}_{cm}(0)]\rangle \left\langle \sum_{i,j}^{n} \exp i\underline{k}\cdot[\underline{r}_j(\tau) - \underline{r}_i(0)] \right\rangle \tag{28}$$

For small molecules or small angles where the inequality below holds,

$$\langle \underline{k} \cdot [r'_j(\tau) - \underline{r}'_i(0)]\rangle << 1 \tag{29}$$

the second term in equation 27 can be approximated by one. Thus, $S(\underline{k},\tau)$ is reduced to a correlation over only the center of mass motion of the molecule,

$$S(\underline{k},t) \propto \langle \exp i\underline{k} \cdot [\underline{R}(t) - \underline{R}(0)]\rangle \tag{30}$$

It is recognized that the term in brackets is the space Fourier transform of the van Hove self-spacetime correlation function $G_s(\underline{R},t)$ which is the probability of finding a particle in the neighborhood of point R at time t, given that the particle was at origin at time zero (van Hove, 1954)

$$G_s(\underline{R},t) = \langle \delta(\underline{R} - [\underline{R}_{cm}(t) - \underline{R}_{cm}(0)] \rangle \tag{31}$$

For time scales characteristic of these experiments, $G_s(R,t)$ can be calculated using diffusion equation,

$$\frac{\partial}{\partial t} G_s(\underline{R},t) = -D\nabla^2 G_s(\underline{R},t) \tag{32}$$

$$G_s(\underline{R},0) = \delta(\underline{R}) \tag{33}$$

Taking the Fourier transforms of the above equations, we obtain a first order differential equation for $S(\underline{k},t)$

$$\frac{\partial}{\partial t} S(\underline{k},t) = -Dk^2 S(\underline{k},t) \tag{34}$$

with the initial condition

$$S(\underline{k},0) = S(\underline{k}) \tag{35}$$

which when solved together give $S(\underline{k},t)$ as an exponentially decaying function,

$$S(\underline{k},t) = S(\underline{k}) \exp -k^2Dt \tag{36}$$

The field correlation function and the spectrum of light scattered from small molecules (and/or small angles) can now be calculated

$$C_E(\underline{k},t) \propto (\exp - k^2Dt)(\exp - i\omega_i t) \tag{37}$$

$$I(\underline{k},\omega) \propto \frac{Dk^2}{(\omega-\omega_i)^2 + (Dk^2)^2} \tag{38}$$

$C_E(\underline{k},\tau)$ is an exponentially decaying function with relaxation time equal to $(Dk^2)^{-1}$, and the spectrum is a single Lorentzian function centered around the incident frequency with a half-width at half-height (HWHH) equal to Dk^2. Thus the self-diffusion coefficient D for macromolecules can be obtained from either of these functions using the appropriate equation.

For large molecules or large angles the approximation in equation 29 is no longer valid and $S(\underline{k},t)$ has the contribution from correlation of segmental motions in addition to the center of mass motion. Pecora (1965,1968) evaluated these contributions for the case of flexible linear molecules using the free-draining solution of Rouse-Zimm (bead-spring) model. Recently, Perico and coworkers (1975) derived the spectrum for the same system using the Rouse-Zimm model with varying degrees of hydrodynamic interaction taken into account.

Rouse-Zimm Theory

In this model the molecule is represented by N identical segments interconnected by N+1 identical beads which are also the light scattering centers.

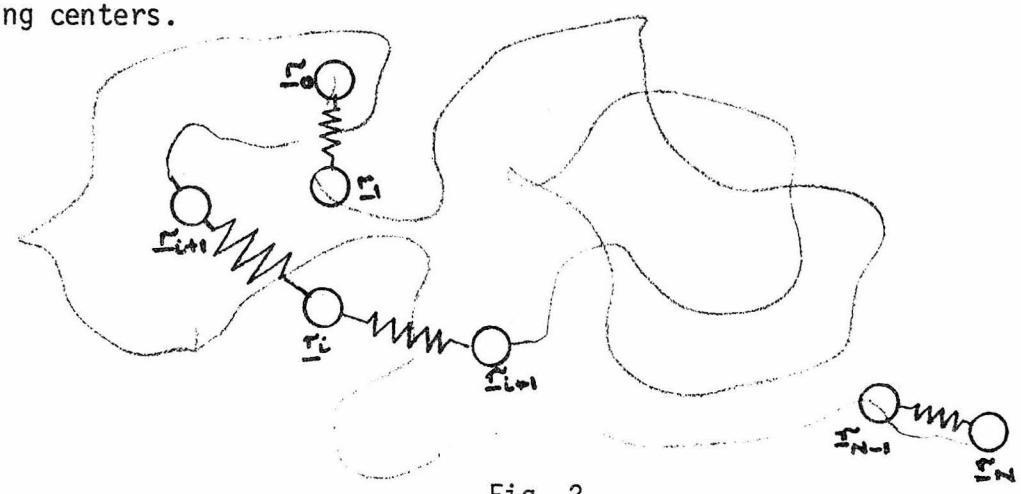

Fig. 2

The segments are long enough so that their end-to-end distance ℓ_s can be represented by a Gaussian probability function,

$$p(\ell_s) = a \exp - \frac{3\ell_s^2}{2b^2} \tag{39}$$

where b^2 is the mean of ℓ_s^2.

The molecule interacts with the viscous medium only through the beads with a friction factor ρ . The viscous force exerted on the J^{th} bead can be written as

$$\underline{F}_j^{visc} = \rho(\dot{\underline{r}}_j - \underline{v}_j') \tag{40}$$

where $\underline{r}_j$'s are the coordinates of the J^{th} bead, the dot denotes the time derivative, and $\underline{v}_j'$ is the velocity the fluid would have at r_j if the J^{th} bead were absent. This velocity can be related to the solvent velocity by Kirkwood-Riseman (1948) approximation of the Oseen interaction formula,

$$\underline{v}_j' = \underline{v}_j + \sum_{J' \neq k} T_{jk}\underline{F}_k \tag{41}$$

where $\underline{v}_j$ is the undisturbed velocity of the solvent. The interaction coefficients T_{jk} in equation (41) are given as

$$T_{jk} = \frac{1}{\eta_s b(6\pi^3)^{1/2}|j-k|^{1/2}} \tag{42}$$

where η_s is the viscosity of the solvent.

The segments exert Hookean restoring forces on the beads that can be written in terms of $\underline{r}_j$ as below:

$$\underline{F}_o^{sp} = -\frac{3kT}{b^2}(\underline{r}_o - \underline{r}_1)$$

$$\underline{F}_j^{sp} = -\frac{3kT}{b^2}(-\underline{r}_{j-1} + 2\underline{r}_j - \underline{r}_{j+1}) \qquad 1 \leq j \leq N-1 \tag{43}$$

$$\underline{F}_N^{sp} = -\frac{3kT}{b^2}(\underline{r}_N - \underline{r}_{N-1})$$

The third force acting on the beams is the effective force resulting from the Brownian motion, and it can be related to the distribution function for the bead positions by

$$\underline{F}^{Br} = -kT\nabla(\ell n\ \psi) \tag{44}$$

where $\psi(\underline{r}_o \cdots \underline{r}_N)$ is the probability of finding each J^{th} bead with coordinates between $\underline{r}_j$ and $\underline{r}_j + d\underline{r}_j$.

The equation of motion for bead j can be obtained combining equations 40, 41 and 44 and satisfying the condition that the sum of forces on each bead is zero:

$$F_j^{Br} + F_j^{sp} + F_j^{visc} = 0 \qquad 0 < j < N \tag{45}$$

$$\dot{\underline{r}}_j = \underline{v}_j - D\,\underline{\nabla}_j\,\ell n\ \psi - \sigma(-\underline{r}_{j-1} + 2\underline{r}_j - \underline{r}_{j+1}) - \sum_{k \neq j} \rho T_{jk}[D\,\underline{\nabla}_k\,\ell n\ \psi + \sigma(-\underline{r}_{j-1} + 2\underline{r}_j - \underline{r}_{j+1}) \tag{46}$$

where $D = \frac{kT}{\rho}$ and $\sigma = \frac{3kT}{b^2\rho}$. For quiescent solutions on which our experiments were performed, the solvent has no net velocity, and $\underline{v}_j$ is set equal to zero. It is more convenient to express equation 46 in vector and matrix notation. Following Zimm's example, the x,y coordinates and

partial derivatives are defined as (N+1)-dimensional column vectors,

$$\underline{x} = \begin{bmatrix} x_o \\ \vdots \\ x_j \\ \vdots \\ x_N \end{bmatrix} \qquad \underline{y} = \begin{bmatrix} y_o \\ \vdots \\ \vdots \\ \vdots \\ y_N \end{bmatrix} \qquad \partial/\partial\underline{x} = \begin{bmatrix} \partial/\partial x_o \\ \vdots \\ \partial/\partial x_j \\ \vdots \\ \partial/\partial x_N \end{bmatrix} \qquad \text{etc} \tag{47}$$

The (N+1) x (N+1) square matrices $\underline{\underline{A}}$ and $\underline{\underline{H}}$ are defined as below:

$$A = \begin{bmatrix} 1 & -1 & 0 & 0 & & & \\ -1 & 2 & -1 & & & & \\ 0 & -1 & 2 & -1 & & & \\ & & & -1 & 2 & -1 & \\ & & & & -1 & 1 & \end{bmatrix} \qquad H = \begin{bmatrix} 1 & \rho T_{01} & \rho T_{02} & \cdots \\ \rho T_{10} & 1 & & \\ \vdots & & & \\ \rho T_{1N} & & & 1 \end{bmatrix} \tag{48}$$

The equation of motion can now be rewritten in this notation

$$\frac{\partial x}{\partial t} = -\frac{kT}{\rho}\,\underline{\underline{H}} \cdot (\partial/\partial\underline{x})\, \ell n\, \psi - \frac{3kT}{b^2\rho} \cdot \underline{\underline{H}} \cdot \underline{\underline{A}} \cdot \underline{x} \tag{49}$$

The distribution function ψ obeys the equation of continuity,

$$\frac{\partial \psi}{\partial t} = -\text{div}\ \psi\ [(\partial\underline{x}/\partial t) + (\partial\underline{y}/\partial t) + (\partial\underline{z}/\partial t) \tag{50}$$

Combining equations 49 and 50, a linear second-order differential equation is obtained for ψ :

$$\frac{\partial \psi}{\partial t} = \sum_{u=x,y,z} \{D(\partial/\partial\underline{u})^T \cdot \underline{\underline{H}} \cdot (\partial\psi/\partial\underline{u}) + \sigma(\partial\psi/\partial\underline{u})^T \cdot \underline{\underline{H}} \cdot \underline{\underline{A}} \cdot \underline{u} + \sigma\psi(\partial/\partial\underline{u})^T \cdot \underline{\underline{H}} \cdot \underline{\underline{A}} \cdot \underline{u}\} \tag{51}$$

where the superscript T denotes the transpose of the vector. Equation (50) has a steady state solution ψ_o that is given by

$$\psi_o = \exp - \frac{3}{2b^2} \{ \sum_{J=0}^{N-1} [(x_j - x_{j+1})^2 + (y_j - y_{j+1})^2 + (z_j - z_{j+1})^2] \} \qquad (52)$$

This result could also be obtained from equation (39) by multiplying the Gaussian probability functions for the individual segments.

Equation 51 can be simplified by changing the coordinates to a set of normal coordinates that diagonalizes the quadratic terms appearing in the equation. This transformation is accomplished using the characteristic vectors $\underline{\alpha}_k$ of the matrix $\underline{\underline{H}} \cdot \underline{\underline{A}}$,

$$\underline{\underline{H}} \cdot \underline{\underline{A}} \cdot \underline{\alpha}_k = \lambda_k \underline{\alpha}_k \qquad (53)$$

The square matrix Q whose N+1 columns are the eigenvectors $\underline{\alpha}_k$ has the property

$$\underline{\underline{Q}}^{-1} \cdot \underline{\underline{H}} \cdot \underline{\underline{A}} \cdot \underline{\underline{Q}} = \underline{\underline{\Lambda}} \qquad (54)$$

where $\underline{\underline{\Lambda}}$ is the diagonal matrix of the λ_k's. It also diagonalizes both $\underline{\underline{A}}$ and $\underline{\underline{H}}$ separately by congruent transformations:

$$\underline{\underline{Q}}^{T} \cdot \underline{\underline{A}} \cdot \underline{\underline{Q}} = \underline{\underline{M}}$$

and (55)

$$\underline{\underline{Q}}^{-1} \cdot \underline{\underline{H}} \cdot \underline{\underline{Q}}^{-1T} = \underline{\underline{N}}$$

$\underline{\underline{M}}$ and $\underline{\underline{N}}$ are diagonal matrices with elements γ_k and ν_k respectively. It can also be shown that $\lambda_k = \sigma_k \nu_k$.

The new set of coordinates $\underline{\mu}(\underline{\xi},\underline{\eta}$ and $\underline{\zeta})$ are related to $\underline{x},\underline{y},\underline{z}$ through the matrix $\underline{\underline{Q}}$,

$$\underline{x} = \underline{\underline{Q}} \cdot \underline{\xi}$$

$$\underline{\xi} = \underline{\underline{Q}}^{-1} \cdot \underline{x} \qquad \text{etc.} \tag{56}$$

The partial derivatives are transformed as follows:

$$(\partial/\partial\underline{x}) = \underline{\underline{Q}}^{-1T}(\partial/\partial\underline{\xi})$$

$$(\partial/\partial\underline{\xi}) = \underline{\underline{Q}}^{T}(\partial/\partial\underline{x}) \tag{57}$$

Under the coordinate transformation the differential equation for the distribution function ψ takes the form

$$\frac{\partial\psi}{\partial t} = \sum_{k=0}^{N} \tau_k^{-1} \left[\frac{1}{3} \langle\mu_k^2\rangle_e \underline{\nabla}_k^2\psi + \underline{\nabla}_k \cdot (\underline{\mu}_k\psi)\right] \tag{58}$$

where τ_k is the relaxation time for the k^{th} mode given by $\tau_k = b^2\rho/3kT\lambda_k$ The mean squared equilibrium length of the k^{th} mode $\langle\mu_k^2\rangle_e$ is related to molecular dimensions by $\langle\mu_k^2\rangle_e = \langle\ell^2\rangle/N\gamma_k$ where $\langle\ell^2\rangle$ is the mean squared end-to-end distance of the molecule. The simple solution ψ_o in normal coordinates is again a product of Gaussian probability functions,

$$\psi_o = \exp(-\frac{3}{2b^2})\left[\sum_{k=1}^{N} \gamma_k(\xi_k^2 + \eta_k^2 + \xi_k^2)\right] \tag{59}$$

The Solution of the Eigenvalue Equation

To determine the elements of the matrix $\underline{\underline{Q}}$ we have to solve the eigenvalue equation

$$\underline{\underline{H}} \cdot \underline{\underline{A}} \cdot \underline{\alpha}_k = \lambda_k \underline{\alpha}_k \tag{60}$$

where $\underline{\underline{H}}$ and $\underline{\underline{A}}$ are $(N+1) \times (N+1)$ square matrices as defined in equation 48.

This equation has been solved employing integrodifferential equations by various authors (Zimm, 1956; Fixmann, 1965; Tschoegl, 1963). In this approach a continuous function is substituted in place of the discrete components of the eigenvector. Let h_o and h_{ij} be defined as below

$$h_o = \frac{\rho}{(n_s b)(6\pi^3)^{1/2}}$$

$$h_{ij} = \begin{cases} 1 & i = j \\ |i-j|^{-1/2} & i \neq j \end{cases} \qquad (61)$$

The eigenvalue equation for the i component of α^k can be written in a more explicit form using the fact that components of matrix $\underline{\underline{A}}$ are zero except for i=j and i=j±1

$$(\alpha^k_{i+1} - 2^k\alpha_i + \alpha^k_{i-1}) + h_o \sum_j h_{ij}(\alpha^k_{j+1} - 2\alpha^k_j + \alpha^k_{j-1})$$

$$+ h_o h_{io}(\alpha^k_1 - \alpha^k_o) + h_o h_{in}(\alpha^k_N - \alpha^k_{N-1}) = -\lambda_k \alpha^k_i \ , \quad 1 \leq i \leq j-1 \qquad (62)$$

α_o and α_N obey this equation in a slightly modified from. Superscript k will be dropped from now on. The sum-difference equation above can be converted into an integrodifferential equation by using a continuous function $\alpha(s)$ related to the components of the eigenvector $\underline{\alpha}$ as below

$$\alpha_j = \left(\frac{2}{N}\right)^{1/2} \alpha(s)$$

and (63)

$$s = \frac{j}{N} - 1 \qquad r = \frac{i}{N} - 1$$

With the boundary condition $\alpha'(\pm 1) = 0$, the eigenvalue equation for $\alpha(r)$ is

$$\alpha''(r) + h \int_{-1}^{1} \frac{\alpha''(s)}{|r-s|^{1/2}}\, ds - h \int_{r-\frac{1}{N}}^{r+\frac{1}{N}} \frac{\alpha''(s)}{|r-s|^{1/2}}\, dx = \frac{N^2}{4} \lambda\, \alpha(r) \tag{64}$$

where h is the measure of the strength of the hydrodynamic interaction between the beads defined as $h = (N/2)^{1/2} h_o$.

In the earlier solutions to this problem the integrodifferential equation was derived without the third term. Consequently h could assume any value between zero and infinity, whereas alternative solutions for the discrete case pointed out some limitations as to the value h can have. Recently Osaki (1972) pointed out that this discrepancy is due to nonexclusion of the i=j term in the integrodifferential equation. He corrected for this fact by including in the equation the third term, which he expanded in a Taylor series around r=s,

$$-h \int_{r-\frac{1}{N}}^{r+\frac{1}{N}} \frac{\alpha''(s)}{|r-s|^{1/2}}\, ds = -\frac{4h}{\sqrt{N}}\, \alpha''(r) \tag{65}$$

The integrodifferential equation in its revised form is

$$\beta\, \alpha''(r) + h \int_{-1}^{1} \frac{\alpha''(s)}{|r-s|^{1/2}}\, ds = -\frac{N^2}{4} \lambda\, \alpha(r) \tag{66}$$

where $\beta = 1 - \frac{4h}{\sqrt{N}}$.

The behavior of the system is determined by the interaction parameter h as can be seen in equation 66. At the one extreme h is zero, and there is no interaction between the beads. For this so-called free-draining case the eigenvalue equation simplifies to:

$$\alpha''(r) = -\frac{N^2}{4}\lambda\,\alpha(r) \tag{67}$$

and with the boundary condition $\alpha'(\pm 1) = 0$, it can easily be solved to yield the eigenvalues λ_k and eigenvectors α_k (Rouse, 1953; Zimm, 1956)

$$\lambda_k = \frac{\pi^2 k^2}{N^2}$$

$$\alpha_k = \begin{cases} a_k \cos\frac{\pi k r}{2} & k = \text{even} \\ b_k \sin\frac{\pi k r}{2} & k = \text{odd} \end{cases} \tag{68}$$

At the other extreme, for the case of complete hydrodynamic interaction, β vanishes and h assumes its maximum value, that is, $\sqrt{N}/4$. The eigenvalue equation can be written as follows:

$$\int_{-1}^{1} \frac{\alpha''(s)}{|r-s|^{1/2}}\,ds = -N^{3/2}\lambda\,\alpha(r) = \lambda'\,\alpha(r) \tag{69}$$

To solve equation 69, the eigenfunction $\alpha(r)$ is expanded in terms of eigenfunctions of the free-draining case:

$$\alpha(r) = \begin{cases} a_o + \sum a_m \cos\frac{\pi m r}{2} & \text{even} \\ \sum a_m \sin\frac{\pi m r}{2} & \text{odd} \end{cases} \tag{70}$$

Substituting these series in equation 69, multiplying by $\cos\frac{\pi \ell r}{2}$ or $\sin\frac{\pi \ell r}{2}$ and integrating over dr, a set of linear equations are obtained for the coefficients a_m

$$\underline{\underline{G}} \cdot \underline{a} = \lambda' \underline{a}$$

where the elements of G can be calculated using Fresnel integrals. The

nondiagonal terms of the matrix $\underline{G}$ are found to be close to zero, allowing the eigenvalues λ_k to be calculated using perturbation techniques. In Table I, the first few eigenvalues are tabulated as reported by Zimm, et al. (1956):

Table I: The Eigenvalues λ_k'

k	λ_k'
1	4.04
2	12.79
3	24.2

The coefficients a_m of the Fourier series (eq. 70) were obtained by using the first order approximation

$$ {}^{k}a_m = \frac{G_{mk}\ {}^{k}a_k}{G_{mm} - \lambda_k'} $$

where ${}^{k}a_k$ is unity within a few percent. Furthermore, the elements γ_k of the matrix M were found to be well represented by the formula $\gamma_k = k^2\pi^2/N^2$. The case of partial hydrodynamic interaction for which the value of n is between 0 and $\sqrt{N}/4$ was solved using the same technique (Tschoegl, 1963).

With the advent of fast computers, solution of the eigenvalue equation for the discrete case became an alternative approach to the problem. Recently Perico and coworkers (1975a) were able to calculate the eigenvalues and eigenvectors for varying degrees of hydrodynamic interaction for the case N = 100. Their results are listed in Table II:

Table II: Eigenvalues λ_k and Diagonal Elements γ_k for N = 100

	λ_k			γ_k	
	h = 0	h = 1	h = 2	h = 1	h = 2
1	0.000967	0.00216	0.00334	0.000968	0.000969
2	0.003868	0.00731	0.01072	0.00382	0.003776
3	0.008701	0.01465	0.02054	0.00865	0.008597

Calculation of Spectrum for a Linear Molecule Using Rouse-Zimm Theory

We have seen that in normal coordinates the distribution function ψ obeys the differential equation

$$\frac{\partial \psi}{\partial t} = \sum_{k=0}^{N} \tau_k^{-1} \left[\frac{1}{3} \langle \mu_k^2 \rangle_e \nabla_k^2 \psi + \nabla_k \cdot (\underline{\mu}_k \psi)\right] \tag{71}$$

The zeroth order mode is the diffusion of the molecule as a whole. This mode will be omitted in the following derivations, since the spectrum arising from it has already been calculated. Equation 71 with the initial condition that $\underline{\mu}_k$ has the value $\underline{\mu}_k^0$ at time zero

$$\psi(\underline{\mu}_k; \underline{\mu}_k^0/0) = \prod_{k=1}^{N} \delta(\underline{\mu}_k - \underline{\mu}_k^0) \tag{72}$$

has the solution (Wang & Uhlenbeck, 1945)

$$\psi(\mu_k; \mu_k^0/t) = \prod_{k=1}^{N} \left[\frac{3}{2\pi \langle \mu_k^2 \rangle_e \left[1 - \exp(-2t/\tau_k)\right.}\right]^{3/2}$$

$$\times \exp\left\{- \frac{3}{2\langle \mu_k^2 \rangle_e} \cdot \frac{\left[\underline{\mu}_k - \underline{\mu}_k^0 \exp(-t/\tau_k)\right]^2}{\left[1 - \exp(-2t/\tau_k)\right]}\right\} \tag{73}$$

Now the correlation between segments $S_s(k,t)$ can be calculated using the distribution function ψ averaged over the initial conditions, i.e., ψ_o

$$S_s(k,t) = \langle \exp i\underline{k} \cdot [\underline{r}_j'(t) - r_i'(0)] \rangle$$

$$= \langle \exp i\underline{k} \cdot [\sum_k Q_{jk}\, \underline{\mu}_k(t) - \sum_k Q_{ik}\, \underline{\mu}_k(0)] \rangle \qquad (74)$$

$$S_s(k,t) = \sum_i^N \sum_j^N \iint \exp \{ i\underline{k} \cdot [\sum_k (Q_{jk}\, \underline{\mu}_k - Q_{ik}\, \underline{\mu}_k)] \}$$

$$\times \ \psi(\mu_1 \cdots \mu_N; \mu_1^o \cdots \mu_N^o/t) \qquad (75)$$

$$\times \psi_o(\mu_1^o \cdots \mu_N^o) \prod_{k=1}^N d\mu_k \, d\mu_k^o$$

$S_s(k,t)$ is obtained by combining equations 59, 73 and 75 and performing the double integration

$$S_s(k,t) = N^{-2} \sum_i^N \sum_j^N \exp(-k^2/6) \times \{ \sum_{k=1}^N (\langle \ell^2 \rangle / N\gamma_k)$$

$$\times \ [Q_{jk}^2 + Q_{ik}^2 - 2Q_{ik}Q_{jk}\exp(-t/\tau_k)] \} \qquad (76)$$

Defining the dimensionless parameter $x = k^2\langle \ell^2 \rangle/6$, expanding the exponential term in equation 76, and combining the segmental and the center of mass correlations, the total correlation function $S(k,t)$ can be written as a series of terms:

$$S(k,t) = \exp(-DK^2 t) \sum_{M=0}^{\infty} P_M(x,t) \qquad (77)$$

where $P_M(x,t)$ is given by:

$$P_M(x,t) = N^{-2} \sum_i^N \sum_j^N \exp[-(-x/N) \sum_k \gamma_k^{-1}(Q_{ik}^2 + Q_j^2)]$$

$$\times \ (M!)^{-1}[(2x/N) \sum_k \eta_k^{-1} \, Q_{ik}Q_{jk} \ x \ \exp(-t/T_k)] \qquad (78)$$

S(k,t) can be rewritten by regrouping terms according to the order M:

$$S(k,t) = \exp(-Dk^2t) \ \{P_o(x) + \sum_{r=1}^N P_1(x,r) \exp(-t/\tau_r)$$

$$+ \sum_{r=1}^N \sum_{s=1}^N P_2(x,r,s) \exp -(t/\tau_r + t/\tau_s) + \cdots \qquad (79)$$

$$+ \sum_{r=1} \sum_{s=1} \sum_{t=1} P_3(x,r,s,t) \exp - (t/\tau_r + t/\tau_s + t/\tau_t) + \cdots\}$$

where $P_M(x,r,s,t,\cdots)$ is given by

$$P_o(x) = N^{-2} \sum_{i=0}^N \sum_{j=0}^N \exp[(-x/N) \sum_{k=1}^N \gamma_k^{-1}(Q_{ik}^2 + Q_{jk}^2)]$$

$$P_1(x,r) = N^{-2} \sum_{i=0}^N \sum_{j=0}^N \exp[(-x/N) \sum_{k=1}^N \gamma_k^{-1}(Q_{ik}^2 + Q_{jk}^2)]$$

$$\times \ [(2x/N) \, \gamma_r^{-1} \, Q_{jr}Q_{ir}] \qquad (80)$$

$$P_2(x,r,s) = N^{-2} \sum_{j=0}^N \sum_{i=0}^N \exp[(-x/N) \sum_{k=1}^N \gamma_k^{-1}(Q_{ik}^2 + Q_{jk}^2)]$$

$$\times \ [(2x^2/N^2) \, \gamma_r^{-1} \, \gamma_s^{-1} \, Q_{ir} \, Q_{jr} \, Q_{is} \, Q_{js}]$$

For large molecules, as can be seen in equation 79, S(k,t) is made up of the purely diffusive term with amplitude $P_o(x)$ plus the various order

intramolecular terms with amplitudes $P_1(x)\cdots P_M(x)$. Pecora (1968) evaluated the contribution of these terms using the free draining values for the Q's and γ's,

$$Q_{ik} = \begin{cases} (\frac{2}{N})^{1/2} \sin \pi k(\frac{i}{N} - \frac{1}{2}) & k \text{ odd} \\ (\frac{2}{N})^{1/2} \cos \pi k(\frac{i}{N} - \frac{1}{2}) & \text{even} \end{cases}$$

$$\gamma_k = \frac{\pi^2 k^2}{N^2} \tag{81}$$

The results of Pecora's calculations are plotted in Fig. 3. $P_o(x)$ was calculated combining equations 80 and 81 and replacing the summation by integration and letting N go to infinity. It is given by

$$P_o(x) = (\frac{\pi}{x}) \exp(-\frac{1}{6} x)[\text{erf } \frac{1}{2} (x^{1/2})]^2 \tag{82}$$

where erf(y) is the error function of argument y. For small values of x ($x \leq 1$), $P_o(x)$ follows very closely the total intensity P(x) given as follows:

$$P(x) = \sum_0^M P_N(x) = (\frac{2}{x^2}) [\exp(-x) - (1-x)] \tag{83}$$

In this case, the amplitudes of intramolecular terms are negligible and the correlation function reduces to a single exponential function. This is the same result we have obtained for small molecules and/or small angles (eq. 37).

$$S(k,t) = P_o(x) \exp -Dk^2t \quad , \qquad x \leq 1 \tag{84}$$

The field correlation and the spectrum of light are the same as in

equations 38 and 39. For values of $x > 1$, the intensity of intramolecular terms $P_I(x) = P(x) - P_o(x)$ gets larger. Its contribution ranges from 15% at $x = 3$ to 50% at $x = 7$. For $x > 1$ the correlation function is a sum of exponential functions containing the relaxation times τ_k.

The lowest order intramolecular term $P_1(x)$ can be shown to be negligible for all x values (Pecora, 1968). $P_2(x)$ involves a double summation over r and s. The term $P_2(x, r = s = 1)$ was also calculated by Pecora and found to be the term that contributes the most to the intensity. For values of x, $1 < x < 5$, this term comprises 65-85% of the intramolecular intensity $P_I(x)$. This allows us to express the correlation function as a sum of two exponentials in this range

$$S(k,t) = P_o(x) \exp - Dk^2 t + P_2(x) \exp -(Dk^2 + \frac{2}{\tau_1})t \qquad (85)$$

The field correlation function and the spectrum of light are related to S(k,t) through equations 17 and 18.

$$C_E(k,t) \propto [P_o(x) \exp -Dk^2 t + P_2(x) \exp -(Dk^2 + \frac{2}{\tau_1})t] \exp - i\omega_i t \qquad (86)$$

$$I(k,w) \propto P_o(x) \frac{Dk^2}{(\omega-\omega_o)^2 + (Dk^2)^2} + P_2(x) \frac{Dk^2 + 2/\tau_1}{(\omega-\omega_o)^2 + (Dk^2 + \frac{2}{\tau_1})^2} \qquad (87)$$

For $x > 5$ the higher order terms start contributing to the intensity appreciably and the correlation function becomes a sum of more than two exponentials.

Recently Perico et al (1975a) calculated the contribution of various order terms to the spectrum for varying degrees of hydrodynamic interaction parameter h. Their results are plotted in Fig. 4. The inclusion of h in the calculations does not change the spectrum except for slight numerical differences in the intensity of various terms. A separate attempt to calculate the spectrum of light scattered by large molecules was made by Fujime and Maruyama (1973). They used the wormlike molecule model introduced by Harris and Hearst (1966). Their correlation function is again a sum of exponentials with amplitudes $P_{00}(x)$, $P_{20}(x)$, $P_{40}(x)$ and with decay times $(Dk^2)^{-1}$, $(Dk^2+\frac{2}{\tau_1})^{-1}$, $(Dk^2+\frac{4}{\tau_1})^{-1}$, respectively. These amplitudes vs $x^{1/2}$ are plotted in Fig. 5. A study of this plot shows that their results are basically the same as Pecora's in that for $x < 1$ the correlation function is a single exponential arising from translational diffusion of the molecule whereas for $1 < x < 5$ $C_E(t)$ is a sum of two exponentials with decay times $(Dk^2)^{-1}$ and $(Dk^2+\frac{2}{\tau_1})^{-1}$ respectively.

All the derivations above show that it is possible to measure the terminal relaxation time of a linear flexible molecule by light scattering. An experiment can be devised where the correlation function would be determined for a large range of x values that include both the regions $x < 1$ and $-x > 1$. This can be accomplished by taking data for a large range of scattering angles since x is proportional to $\sin^2\frac{\theta}{2}$. The data taken at small angles can then be fitted to a single exponential function whose decay time gives the diffusion coefficients of the molecule (equation 32). The correlation function collected at large

scattering angles ($x > 1$) can be analyzed in terms of two exponentials (equation 86). The diffusion coefficient determined at small angles is used in fitting the data. The relaxation time τ_1 can be obtained from the decay time of the second exponential which is given as $(Dk^2 + \frac{2}{\tau_1})^{-1}$.

CHAPTER III

APPARATUS AND EXPERIMENTAL METHODS

Apparatus

The light scattering spectrometer consists of the light source, sample container with its temperature controller, light detection system and the signal processing equipment. A schematic diagram of the apparatus is given in Fig. 6.

The light source is a Coherent Radiation 52A argon ion laser operated at the 4880Å line. The incident light is polarized in the vertical direction. For most of the studies, the laser was operated in single mode through the use of an etalon in the laser cavity. The incident intensity was varied between 300-600 mW through adjustment of the laser tube current.

An optical turntable was constructed by mounting an optical rail on a MicroInch microscope base. The arm could rotate between 0-140° and the scattering angles could be read with an accuracy of 0.1°. The scattering cell could be moved in the x,y,z, directions, independently. The system was aligned such that the axis of rotation of the system coincided with the symmetry axis of the cell and also the plane of rotation was perpendicular to the polarization direction.

The sample was contained in a C-105 Brice-Phoenix cylindrical cell with flat entrance and exit windows. The sample volume required was approximately 20 milliliters. For temperature control the cell was inserted in a cylindrical brass block. Water from a constant temperature PM Thompson viscometer bath was circulated through a helical channel

cut into the brass jacket. The temperature of the bath was constant within 0.01°C. The room temperature was independently kept constant within 0.2°C. The fluctuation in the sample temperature was kept below 0.05°C during a run. The sample temperature was independently measured using a platinum resistance thermometer.

The laser light was focused to the center of the sample cell with the aid of a converging lens with a focal length of 10 cm. The scattered light was passed through two 1/32-inch diameter pinholes before falling on the detector. These pinholes defined the scattering angle to better than 0.2°. The detector was an EMI 9789B photomultiplier tube. It has properties of high gain at the power frequency and a fast response time. The voltage to the phototube was supplied by a Fluke 415B high voltage power supply. The output of the photomultiplier tube was fed into the correlator after being amplified by a Princeton Applied Research 113 preamplifier.

The light source, sample, and detection optics were placed on a Newport Research Corp. vibration isolation table which filtered frequencies higher than 3 Hz, preventing vibrations from external sources to interfere with the experiment.

The photocurrent was processed on a Saicor 43A 400 channel correlator and signal analyzer. The autocorrelation function was collected until the first few points filled the memory. The longest time required was 10 minutes due to the fact that the signal-to-noise ratio is very favorable for these polymer solutions. A typical autocorrelation function is given in Fig. 7. The correlation function was then transferred in binary code to a paper tape and the subsequent analysis of the data was done on an IBM 370 computer.

Signal Processing

The linewidths obtained in the present experiments are of the order of a Hz to a kHz for which the best resolution available with interferometric filters (10 MHz) is completely inadequate. Hence to resolve the spectrum, a nonlinear detector is needed to shift the central frequency to lower levels where narrower filters are available. One such detector is the photomultiplier tube which produces a current proportional to the intensity, that is, to the square of the electric field of light. Forrester (1961) showed that when the photocathode is illuminated by two light beams with frequencies ω_1 and ω_2, the photocurrent has an AC component with frequency $(\omega_1-\omega_2)$. This is called optical beating. When the light has a continuous spectrum the photocurrent has components that arise from beating of different frequency elements with each other. Cummins and Swinney (1970) discuss optical beating spectroscopy in detail.

The probability that an electron will be emitted from a photocathode illuminated by a light beam with an electric field E(t) is (Mandel and Wolf, 1964)

$$W'(t) = \sigma E^*(t)\, E(t) \tag{88}$$

where $I(t) = E^*(t)\, E(t)$ is the instantaneous intensity and σ is the quantum efficiency. The photocurrent is proportional to the probability function $W^{(1)}(t)$

$$i(t) = eW^{(1)}(t) = \sigma e\, E^*(t)\, E(t) \tag{89}$$

The joint probability that one electron will be emitted at time t and another at time $t+\tau$ is

$$W^{(2)}(t,t+\tau) = \sigma^2 E^*(t)\ E(t)\ E^*(t+\tau)\ E(t+\tau) \tag{90}$$

For stationary fields the averages for the above quantities can easily be calculated to yield:

$$\langle i(t)\rangle = e\langle W^{(1)}(t)\rangle = e\sigma\ \langle E^*(t)\ E(t)\rangle = e\sigma\ \langle I\rangle$$

and (91)

$$\langle W^{(2)}(t,t+\tau)\rangle = \sigma^2\ \langle E^*(t)\ E(t)\ E^*(t+\tau)\ E(t+\tau)\rangle = \sigma^2\langle I\rangle^2 g^{(2)}(\tau)$$

$g^{(2)}(\tau)$ is the second order correlation function defined as

$$g^{(2)}(\tau) = \frac{\langle E^*(t)\ E(t)\ E^*(t+\tau)\ E(t+\tau)\rangle}{\langle E^*E\rangle^2} \tag{92}$$

The power spectrum $P_i(\omega)$ and the autocorrelation function $C_i(\tau)$ of the photocurrent are a Fourier transform pair

$$P_i(\omega) = \frac{1}{2\pi}\int_{-\infty}^{\infty} C_i(\tau)\ d\tau \tag{93}$$

where

$$C_i(\tau) = \langle i(t)\ i(t+\tau)\rangle = e^2\langle W^{(1)}(t)\ W^{(1)}(t+\tau)\rangle \tag{94}$$

The photocurrent i(t) actually consists of a series of infinitely narrow pulses. Therefore $C_i(\tau)$ has two distinct contributions. If the electrons at t and t+τ are distinct we have

$$\langle W^{(1)}(t)\ W^{(1)}(t+\tau)\rangle_{\text{distinct}} = \langle W^{(2)}(t,t+\tau)\rangle = \sigma^2\langle I\rangle^2\ g^{(2)}(\tau) \tag{95}$$

and if the same electron is observed at t and t+τ we get

$$\langle W^{(1)}(t)\ W^{(1)}(t+\tau)\rangle_{\text{same}} = \langle W^{(1)}(t)\rangle\ \delta(\tau) = \sigma\langle I\rangle\ \delta(\tau) \tag{96}$$

Therefore,

$$C_i(\tau) = e^2\sigma\langle I\rangle\ \delta(\tau) + e^2\sigma^2\langle I\rangle^2\ g^{(2)}(\tau)$$
$$C_i(\tau) = e\langle i\rangle\ \delta(\tau) + \langle i\rangle^2\ g^{(2)}(\tau) \qquad (97)$$

For the homodyne or self-beating technique which was used for the present study, only the scattered light falls on the detector. The photocurrent carries beat notes between the different frequency spectral elements of the scattered light, and hence shifts the spectrum to much lower frequencies where very narrow tunable filters are available. For laser light scattered by a dilute solution of scatterers, the field is a narrow band Gaussian random process. If the field is characterized by the autocorrelation function

$$C_E(\tau) = \langle E^*(t)\ E(t+\tau)\rangle = \langle I\rangle\ g^{(1)}(\tau) \qquad (98)$$

then the second order correlation function $g^{(2)}(\tau)$ is related to $g^{(1)}(\tau)$ by [Mandel (1963)]

$$g^{(2)}(\tau) = 1 + |g^{(1)}(\tau)|^2 \qquad (99)$$

The current autocorrelation function and the power spectrum then can be written as

$$C_i(\tau) = e\ \langle i\rangle\ \delta(\tau) + \langle i\rangle^2 + \langle i\rangle^2\ |g^{(1)}(\tau)|^2$$
$$P_i(\omega) = \frac{1}{2\pi}\, e\langle i\rangle + \langle i\rangle^2\ \delta(\omega) + \langle i\rangle^2 \int_{-\infty}^{\infty} \exp i\omega\tau |g^{(1)}(\tau)|^2\ d\tau \qquad (100)$$

The first term is the shot noise, the second is the d.c. component. They can easily be subtracted off leaving the third term which contains information about the spectrum of scattered light.

The correlation function $g^{(1)}(\tau)$ has the form (eq. 37)

$$g^{(1)}(\tau) = (\exp -i\omega_i\tau)(\exp -Dk^2\tau) \tag{101}$$

for x values less than 1. Inserting this in the equation for the autocorrelation function and the power spectrum, we obtain

$$C_i(\tau) = e\langle i\rangle\ \delta(\tau) + \langle i\rangle^2 + \langle i\rangle^2\ (\exp -2Dk^2\tau) \tag{102}$$

and

$$P_i(\omega) = \frac{1}{2\pi} e\ \langle i\rangle + \langle i\rangle^2\ \delta(\omega) + \frac{\langle i\rangle^2}{\pi} \frac{2Dk^2}{\omega^2 + (2Dk^2)^2} \tag{103}$$

Thus the autocorrelation function is an exponentially decaying function with a relaxation time equal to $(2Dk^2)^{-1}$ and the power spectrum is a Lorentzian centered at zero frequency with HWHH equal to $2Dk^2$.

For $x > 1$ the autocorrelation function is a sum of two exponential (eq. 86)

$$g^{(1)}(\tau) = \frac{1}{(A+B)}[A \exp Dk^2\tau + B \exp -(Dk^2 + \frac{2}{\tau_1})](\exp -i\omega_i\tau) \tag{104}$$

The autocorrelation function for this case (excluding the shot noise and the d.c. component) is given by

$$C_i(\tau) = \langle i\rangle^2 \frac{1}{(A+B)} [A \exp - Dk^2\tau + B \exp -(Dk^2 + \frac{2}{\tau_1})]^2 \tag{105}$$

Experimental

The polystyrene samples used in this study were prepared by anionic polymerization. Two million molecular weight polystyrene samples were purchased from Pressure Chemical Company, Pennsylvania. The polymer was fairly monodisperse with $M_w/M_n = 1.06$. The four and seven million molecular weight polymers were originally prepared by Dr. Fetter and his research group in the University of Akron, Ohio and characterized by light scattering and intrinsic viscosity measurements (McIntyre et al, 1972).

The solvents used were cyclohexane diethyl malonate and 1-chloro-undecane. They were chosen because they form θ solutions at easily attainable temperatures with polystyrene (Orofino & Mickey, 1963). The solvent refractive indices were determined using a Bausch and Lomb refractometer. Viscosities were measured at the respective θ temperatures using Canon-Fenske size 25 and 50 viscometers. The characterization data for the solvents are given in Table III.

Table III: Solvent Characterization Data

	n_D	ρ gm/cc	t_θ ·c	η cP
cyclohexane	1.418	0.763	34.8	0.76
diethylmalonate	1.410	1.039	35.9	1.6
1-chloro-undecane	1.440	0.867	32.8	1.9

The solutions were prepared by placing a weighed amount of polymer in known weight of solvent. To completely dissolve the polymer, the solutions were kept 3-5 degrees above their respective θ temperatures for two to three days with occasional swirling.

For the two million molecular weight polystyrene, the correlation functions were taken at angles ranging from 35 to 95° in each solvent. The data were analyzed in terms of a single exponential function plus a baseline

$$C_i(t) = A \exp -t/\tau_D + \text{baseline} \qquad (106)$$

where the decay time τ_D corresponds to $(2Dk^2)^{-1}$. Inverse decay times were plotted vs k^2 to obtain the diffusion coefficient.

For the 4 and 7 million molecular weight samples, the correlation function was collected at angles between 32.5° and 120°. Initially, the correlation functions were fitted by a single exponential function as in equation 107. The diffusion coefficients were determined from the linear portion of the inverse decay time vs k^2 plot. Then these diffusion coefficients were used in the analysis of data taken at large angles where the correlation function is the square of the sum of two exponentials (equation 105)

$$C_i(t) = [A \exp -Dk^2t + B \exp -t/\tau_I]^2 + \text{baseline} \qquad (107)$$

The decay time of the second exponential τ_I corresponds to $(Dk^2 + \frac{2}{\tau_1})^{-1}$. A plot of inverse decay time vs k^2 is linear with slope equal to D and intercept equal to $2/\tau_1$. The above experiment was performed for four different concentrations of polymers in cyclohexane for both four and seven million molecular weight polystyrene. The same experiment was repeated for both molecular weight samples for one concentration of polymer in each of the remaining solvents.

A separate study of diffusion coefficient vs concentration was made for all the systems above by taking data at small angles for solutions with different concentrations prepared by repeated dilution of a stock solution.

CHAPTER IV

RESULTS AND DISCUSSION

Diffusion Measurements

Initially all autocorrelation functions were fitted to a single exponential function plus a baseline

$$C_i(t) = A \exp(-t/\tau_D) + B \qquad (108)$$

The inverse decay times obtained from this fit were plotted against the square of the scattering vector k^2 for each solution studied. For the two million molecular weight polystyrene in each of the solvents cyclohexane, diethylmalonate and 1-chloroundecane with respective concentrations 735 μg/cc, 718 μg/cc, 796 μg/cc, the plot of inverse decay times vs k^2 is linear for all scattering angles for which the autocorrelation functions were collected (Figs. 8, 9 and 10). The diffusion coefficients for this polymer determined from the slopes of these lines are $D = (1.004 \pm .015) \times 10^{-7} cm^2/sec$ in cyclohexane, $D = (0.466 \pm .007) \times 10^{-7} cm^2/sec$ in diethylmalonate, and $D = (0.392 \pm .006) \times 10^{-7} cm^2/sec$ in 1-choroundecane.

For the four million molecular weight polystyrene, autocorrelation functions were collected for scattering angles between 35 to 120°. The plots of inverse decay times vs k^2 are linear for small scattering angles corresponding to k^2 values less than $5 \times 10^{10} cm^{-2}$, and they deviate from linearity at higher angles corresponding to larger k^2 values. This experiment was performed for four cyclohexane solutions at the following concentrations: 198 μg/cc, 307 μg/cc, 431 μg/cc, and 570 μg/cc.

Only one concentration in each of the remaining solvents was studied, namely 559 μg/cc in diethylmalonate and 533 μg/cc in 1-chloroundecane. The plots of inverse decay time vs k^2 are given in Figs. 11-16. In each case the diffusion coefficients were determined from the slopes of these curves in the linear region. Figure 17 shows the inverse decay times vs k^2 for the most concentrated cyclohexane solution at low angles. The diffusion coefficients determined for polystyrene (MW = 4.1×10^6) are given in Table IVa.

Table IVa. Diffusion Coefficients for Four Million Molecular Weight Polystyrene

Solvent	Concentration μg/cc	D(c) ($\times 10^7$ cm^2/sec)
cyclohexane	570	0.672 ± .010
	431	0.685 ± .012
	307	0.662 ± .013
	198	0.668 ± .015
diethylmalonate	559	0.324 ± .005
1-chloroundecane	533	0.263 ± .005

For the seven million molecular weight polystyrene, autocorrelation functions were determined at angles ranging from 32.5° to 120°. This experiment was repeated for four cyclohexane solutions with concentrations equal to 322 μg/cc, 245 μg/cc, 176 μg/cc and 115 μg/cc, and one solution in diethylmalonate with concentration 301 μg/cc, and one solution in 1-chloroundecane with concentration 344 μg/cc. The

plots of inverse decay times vs k^2 were linear for scattering angles less than 55° corresponding to k^2 values less than 3×10^{10}. At higher angles they showed deviation from linearity (Figs. 18-23). The diffusion coefficients were again obtained from the low angle part of these plots (Fig. 24). The values are tabulated in Table IVb.

Table IVb. Diffusion Coefficients for Seven Million Molecular Weight Polystyrene

Solvent	Concentration (μg/cc)	D(c) ($\times 10^7$ cm^2/sec)
cyclohexane	322	0.524 ± .008
	245	0.519 ± .010
	176	0.527 ± .012
	115	0.518 ± .013
diethylmalonate	301	0.254 ± .006
1-chloroundecane	344	0.210 .005

The concentration dependence of the diffusion coefficients was also studied in separately performed experiments. For each polymer-solvent system the diffusion coefficients were determined for three different concentration solutions prepared by repeated dilution of a stock solution which had a concentration of less than 1000 μg/cc. Autocorrelation functions were collected at small angles where the data could be fitted to a single exponential function. The diffusion coefficients

were found to be independent of concentration for the concentration ranges studied. The results are shown in Tables X-XII.

The diffusion coefficients determined in this study are accurate within ±1%.for the concentrated solutions and ±2% for the most diluted ones as determined from the least squares fits of the data. Earlier calibration studies done with polystyrene spheres with comparable signal-to-noise ratio and correlation times also confirm the accuracy of our diffusion coefficient values. The effect of polydispersity on D values was estimated according to the calculations of Pecora and Tagami (1969) and found to be negligible for all samples used in this study.

Figures 25 and 26 are the logarithmic plots of the diffusion coefficients vs molecular weight and vs solvent viscosity respectively. The diffusion coefficients are proportional to $M_w^{-1/2}$ and inversely proportional to η_s as can be seen in these figures. This is in agreement with theoretical predictions and earlier experimental work (Yamakawa 1971, Cantow 1962, King et al. 1973). The coiled molecule behaves like a spherical particle and its diffusion coefficient can be expressed in a Stokes-Einstein relation

$$D = \frac{k_B T}{6\pi \eta_s R_E} \tag{109}$$

where R_E is the radius of the equivalent sphere. R_E is related to the radius of gyration R_G of the coil by

$$R_E = \zeta R_G \tag{110}$$

The radius of gyration of a molecule can be measured by various methods, total intensity light scattering being the most extensively used. For coil molecules in theta-solutions the radius of gyration of the macromolecule is related to its molecular weight by

$$R_G^2 = K(MW) \qquad (111)$$

where K is assumed to be a constant. The values of K in the literature, though, show some variations. Berry (1966) reported a value of K equal to 7.6×10^{-18}, whereas Orofino and Mickey (1963) found K equal to 9.6×10^{-18}. Recently Slagowski (1972) reported a value of 8.9×10^{-18}. To calculate the radius of gyration of our molecules we will use $K = 9.0 \times 10^{-18}$, which is the average of the K values in literature that were determined for polystyrene with molecular weights comparable to those used in this study. The R_G's for 2×10^6, 4.1×10^6 and 7.1×10^6 molecular weight polystyrene are 425Å, 608 Å and 801Å, respectively. Using these R_G values in combination with equations 111 and 112 we find that the diffusion coefficients are well represented by

$$D = \frac{k_B T}{6\pi \eta_s \zeta R_G} \qquad (112)$$

where we determine ζ to be $0.70 \pm .02$. This value agrees well with the theoretically predicted value of $\zeta = 0.67$ (Kirkwood & Riseman 1948) or the $\zeta = 0.65 \pm .04$ which was measured in sedimentation experiments (Tanford 1963).

Relaxation Times

We have seen in Figs. 11-16 that the inverse decay times vs k^2 plots for four million molecular weight polystyrene solutions showed deviation from linearity for k^2 values higher than $5 \times 10^{10} cm^{-2}$. In this region the autocorrelation functions were fitted to the function

$$C_i(t) = [A \exp(-Dk^2 t) + B \exp(-t/\tau_I)]^2 + \text{base} \qquad (113)$$

where τ_I represents $(Dk^2 + 2/\tau_1)^{-1}$. A plot of τ_I^{-1} vs k^2 is linear with slope D and intercept $2/\tau_1$. τ_1 for each solution can either be determined from the intercept of this plot or by calculating τ_1 at each scattering angle using

$$\tau_1 = 2(\tau_I^{-1} - Dk^2)^{-1} \qquad (114)$$

and averaging. Figure 27 shows the plot of τ_I^{-1} vs k^2 for polystyrene (4.1×10^6 MW) in cyclohexane with concentration equal to 570 μg/cc. τ_1 determined from the intercept of this plot is 93.5 μsec. Below in Table V the τ_1 calculated at each angle according to equation 115 for the same solution are listed. Also the ratios of B/(A+B) are given. τ_1 obtained by averaging the values in the table is 93.5 μsec. There is complete agreement between the two methods. The τ_1 values reported from now on are calculated by the second method. For other solutions of the four million molecular weight polystyrene, the results are given in Tables XIII-XVII.

Table V. The Relaxation Times and Relative Intensities for Polystyrene (MW = 4.1×10^6) in Cyclohexane. Concentration = 570 μg/cc.

θ	k^2 ($\times 10^{-10}$ cm^{-2})	$x = k^2R_G^2$	τ_1 (μsec)	B/(A+B) %
85	6.08	2.25	91.5	11.2
90	6.66	2.46	94.6	13.8
95	7.24	2.69	91.2	16.9
100	7.82	2.90	99.4	19.2
105	8.39	3.11	91.9	21.6
112	9.16	3.39	93.6	22.3
120	9.99	3.71	93.3	26.1

The x values were calculated using the relation between mean square end to end distance and the radius of gyration given below

$$\langle \ell^2 \rangle = 6\ R_G^2 \quad \text{and} \quad x = k^2R_G^2$$

Table VI. The Relaxation Times for Polystyrene with MW = 4.1×10^6

Solvent	Concentration	τ_1
cyclohexane	570	93.5
	431	98.5
	307	103.5
	198	95.6
diethylmalonate	559	238.1
1-chloroundecane	533	251.7

For the seven million molecular weight polystyrene solutions the plots of inverse decay time vs k^2 start deviating from linearity for k^2 values around 3×10^{10}. The autocorrelation functions taken at higher angles were fitted according to equation 113. The relaxation time τ_1 was obtained at each angle using $\tau_1 = 2(\tau_I^{-1} - Dk^2)^{-1}$. The details for the cyclohexane solution at a concentration of 322 μg/cc are given below

Table VII. Relaxation Times and Relative Intensities for Polystyrene (MW = 7.1×10^6) in Cyclohexane. Concentration = 322 μg/cc

θ (deg)	k^2 1 ($\times 10^{10}$ cm^{-2})	x	τ_1 (μsec)	B/(A+B) %
65	3.85	2.46	200.0	11.8
70	4.38	2.81	207.3	14.5
75	4.93	3.17	200.8	18.9
80	5.51	3.53	191.3	22.4
85	6.08	3.90	205.3	24.9
90	6.66	4.27	185.8	28.2
95	7.24	4.65	188.9	31.8
100	7.82	5.02	194.2	35.4
105	8.39	5.39	193.2	38.5
112	9.16	5.88	182.5	42.7
120	9.99	6.41	169.4	46.0

τ_1 determined for this solution is 196.3 μsec. The last two points are not included in the computation of τ_1. Theoretical calculations indicate (Figs. 3,4 and 5) that for $x > 5$ the autocorrelation function has appreciable contributions from even higher order terms and can no

longer be analyzed in terms of two exponentials. This also explains the downward trend of τ_1's for the scattering angles larger than 112° in Table VII. The detailed results for other solutions are given in Tables XVIII-XXII.

The summary of our results for the seven million molecular weight polystyrene is given below

Table VIII. The Relaxation Times Determined for Polystyrene with MW = 7.1×10^6

Solvent	Concentration (μg/cc)	τ_1 (μsec)
cyclohexane	322	196.3
	245	207.5
	176	218.6
	115	203.8
diethylmalonate	301	472.5
1-chloroundecane	344	572.1

We have based the analysis of our data on the common conclusion of Pecora (1968), Fujime (1973) and Perico (1975) that for a limited range of x values the correlation function of the light is a sum of two exponentials resulting in a current autocorrelation function of the form

$$C_i(t) = [A \exp - Dk^2 t + B \exp(-t/\tau_I)]^2 \qquad (115)$$

where τ_I is $(Dk^2 + \frac{2}{\tau_1})^{-1}$. Due to the fact that there are numerical differences in A and B calculated by different authors, we did not feel

justified in preassigning a value for the relative size of A and B. This parameter was determined by the least squares fit of the data. The ratio B/(A+B) as a function of x is given in Tables V, VII and XIII to XXII for all solutions studied. In Fig. 28 it is plotted vs x for six solutions. (both molecular weight polystyrene in each of the three solvents). The A/(A+B) values as a function of x agree with the theoretical predictions within experimental accuracy. The semi-quantitative nature of the models and the uncertainty in A/(A+B) values does not justify further elaboration.

Before drawing any conclusions it is essential to consider the possible sources of error that can affect the values of the relaxation times measured. One such source of error is the neglect of all intramolecular terms except $P_2(x)$. Depending upon the relaxation times of the terms neglected, τ_1 would change in either direction to become a weighted average of the relaxation times. In the range $1 < x < 5$, the most important terms neglected are with amplitudes $P_1(x)$, $P_3(x)$ and $P_4(x)$ (Fig. 4). The first term has a slower relaxation time (eq. 79) which tends to increase the observed τ_1, whereas the latter terms have faster relaxation times which move τ_1 in the opposite direction. The error caused by neglecting these terms tend to cancel each other; for $x < 3$. At higher x the latter terms become important and may cause the τ_1's observed to be underestimated. We estimate this error to be less than 10% as indicated by the fact that τ_1's are constant within experimental error for the range $1 < x < 5$. The only exception is the case shown in Table VII where the relaxation times show a downward trend with x for $x > 5$. We estimate $x \sim 5$ to be the upper limit for which the correlation function can be analyzed in terms of two exponentials.

The τ_1 values determined were very sensitive to the D value used in the least squares fit of the correlation function. Analysis of several data sets with varying diffusion coefficients showed that 2-4% variation in D causes ∿5-10% variation in τ_1. Due to the accuracy of our diffusion data we estimate the error to be less than 5% for all solutions except the most diluted ones, where the error may be as high as 8%.

The polydispersity of the sample would also affect the τ_1 values. There are no theoretical works in this area, but we estimate the effect would be much more pronounced than for the case of diffusion coefficient due to the fact that the relaxation times have a stronger dependence on molecular weight. We expect the error from this source to be small in our case, since the polystyrene samples used were highly monodisperse ($M_w/M_n < 1.1$). Considering all possible sources of error and the scatter in the data, we estimate the relaxation times measured in this study to be accurate within 15%, except for the most dilute polystyrene solutions where the uncertainty might be closer to 20%.

The experiments done in cyclohexane for both molecular weight polystyrene samples show that the relaxation times do not change with concentration for the low concentrations used in this study. For the cyclohexane solutions the average relaxation times are taken as the infinite dilution values τ_1^o. In all other cases the relaxation times measured at finite concentrations were accepted as τ_1^o.

In Table IX the relaxation times measured in this study are compared with the relaxation times predicted by Rouse-Zimm theory. Recent

experiments (Ferry 1970, Osaki et al. 1972) have shown that the refined versions of this basic model predict the viscoelastic properties of dilute solution well. Before we compare the relaxation times, we would like to point out that the relaxation times measured by light scattering are the relaxation times expressed in equation 58. They are equal to the relaxation times observed in dielectric relaxation experiments, but twice the relaxation times appearing in dynamic viscosity or birefringence expressions.

In the free draining limit (Rouse's case), the first relaxation time is given by (Pecora, 1968)

$$\tau_1^R = \frac{2R_G^2}{\pi^2 D} \tag{116}$$

whereas for the complete hydrodynamic interaction (Zimm) it is given by

$$\tau_1^Z = 0.24 \frac{R_G^2}{D} \tag{117}$$

Table IX. Comparison of Relaxation Times Observed with Predictions of Rouse-Zimm Theory

MW	Solvent	τ_1^o measured	τ_1^R	τ_1^Z
4.1×10^6	cyclohexane	97	113	133
	diethylmalonate	238	235	278
	1-chloroundecane	251	288	341
7.1×10^6	cyclohexane	206	252	298
	diethylmalonate	472	516	612
	1-chloroundecane	572	624	740

As can be seen in Table IX, the τ_1^o values determined in this study agree well with the theoretical predictions of the bead-spring model. For all polymer solutions studied, our τ_1 values are closer to τ_1 predicted by the free draining model. However, the calculated Rouse and Zimm values have uncertainty due to the uncertainty in the radius of gyration values. This fact and the experimental uncertainties would make further comment on the degree of hydrodynamic interaction unjustified.

Summary of Results and Conclusion

We have measured the diffusion coefficients of polystyrene samples with molecular weights 2×10^6, 4.1×10^6, and 7.1×10^6 in each of the solvents cyclohexane, diethylmalonate and 1-chloroundecane at their respective theta temperatures. The diffusion coefficients were found to be independent of concentration and to be well represented by $D = k_D T/6\pi\eta\xi R_G$ where $\xi = 0.70 \pm .02$.

The relaxation time of the first mode of internal motion was measured for the samples with molecular weights 4.1×10^7 and 7.1×10^7 in each of the solvents listed above. The experiments done in cyclohexane for both polystyrene samples showed that τ_1 is independent of concentration. The relaxation times measured are in close agreement with the predictions of bead-spring model, which is known to represent the viscoelastic properties of polymer solutions well.

These experiments have established light scattering as a technique to measure the relaxation time of the coil molecules. The experiments are easy to perform and data accumulation and analysis are fast.

It also has the advantage of being performed on quiescent solutions. This is important for the study of high molecular weight polymers for which the shear degradation represents a major problem for viscoelastic measurements. Most of the biological polymers of interest fall into this category. The major drawback of the technique is that with visible light it is limited to high molecular weight polymers. It can be extended to smaller molecules using shorter wavelength lasers and photomultipliers sensitive in this region.

PART II

LIGHT SCATTERING INVESTIGATION OF AMORPHOUS POLYMETHYLMETHACRYLATE

CHAPTER V

INTRODUCTION

We have demonstrated in Part I of this thesis that light scattering is a valuable tool to study the diffusion and the internal motion of macromolecules. However, the domain of this technique is not limited to polymer solutions. It can be used to probe the dynamics of any medium that is transparent at the incident wavelength. One such area of interest is that of supercooled liquids that undergo a transition at approximately 50°C below their melting points, to become amorphous solid glasses.

As is well known, some materials can be kept in the liquid phase at temperatures well below their freezing points. Materials in this metastable state are called supercooled liquids. When the temperature of the supercooled liquid is sufficiently lowered, the material undergoes a transition in which the specific heat (C_p) and the thermal expansion coefficient (α) undergo an abrupt change (Fig. 29). Materials below this transition temperature (denoted by Tg) are called glasses. The wide chemical diversity of materials that undergo this transition show that this phenomenon does not depend on the chemical properties but it is a general property of the liquid state.

X-ray diffraction studies show that the structure of glass closely resembles that of a liquid (Randall, 1934). Furthermore, the volume and the heat content of the supercooled liquid show no change upon transition to a glass. Thus the glass maintains the structure, volume and energy of the liquid. However, changes in volume and energy

of a glass with temperature and pressure are similar to those of the corresponding crystalline material as indicated by the closeness of their α and C_p values. Thus a glass can be described as a liquid in which certain degrees of freedom are "frozen in" and can no longer contribute to the redistribution of energy and volume (Kauzmann, 1948).

It has been widely believed that this freezing in of degrees of freedom is dynamic in origin. In other words, a relaxation phenomenon that plays an important role in the redistribution of volume and energy becomes so sluggish with the lowering of temperature that it can no longer contribute to α and C_p during the duration of measurements of these quantities. The prolongation of equilibration times allowed in the experiments will then allow this relaxation process to be completed and to contribute to α and C_p. This is confirmed by experiments in which the glass transition temperature is changed by simply changing the duration of the experiment. The implication of this assumption is that if experiments are done infinitely slowly the material will stay in the supercooled state without going through the glass transformation. However, the curves of excess volume and entropy of the supercooled liquid (over that of the crystal) when extrapolated to lower temperatures ($< Tg$) go to zero at finite temperatures (Fig. 30). Since the entropy and the volume of the liquid cannot be lower than those of the crystal (Kauzmann's paradox), this extrapolation to low temperatures is not valid and the ΔS and ΔV curves must level off at some temperature. The glass transition must then be viewed as an

intervention of this freezing in of relaxation processes to prevent this thermodynamic impossibility.

Recent theories of free volume (Turnbull and Cohen, 1961,1970) and excess configurational entropy (Gibbs and DiMarzio, 1958) give better explanations to this apparent paradox by interpreting the glass transition phenomenon as a quasithermodynamic transition. In these models the relaxation time of the process that contributes to glass transition goes to infinity when the excess volume or the excess entropy goes to zero. This, however, never takes place; before it happens, the glass transition phenomenon sets in and freezes in an excess free volume or excess configurational entropy. The glassy state is then a nonequilibrium state at temperatures below Tg, where true equilibrium is not attainable. The glass has a locked-in free volume and configurational entropy which are unaffected by the real temperature and are only a function of the transition temperature, and the specimen sees only a constant "fictive" temperature (Davis, 1953; Saito et al. 1963).

Most of the industrially important polymers--acrylates, styrenes, PVC's, to mention a few--are glasses. Extensive studies done on these high polymer glasses by NMR, dielectric and mechanical relaxation experiments indicate that the backbone main-chain motion (commonly called α relaxation) is responsible for the glass transition. The relaxation time of this motion in the supercooled liquid region between Tg and Tg + 100°C obeys the empirical WLF (Williams, Landel, Ferry) equation. It can also be described by the relaxation time expressions derived from the theories of glass transition mentioned before.

Although the α relaxation is completely suppressed below Tg, there are still short range molecular motions which account for the various viscoelastic and dielectric dispersions in the glassy state. The side chain reorienting itself around the bond linking it to the main chain is the cause of β relaxation in methacrylate polymers (Ferry, 1970). Linear polymers with no side chains also exhibit a β-relaxation phenomenon with characteristic time scale and free energy comparable to that of the side chain mechanism (Saito, 1975). For the linear polymers two mechanisms were suggested a) torsional oscillation of the backbone chain (Saito, 1975), and b) rotational motion of the segments of the main chain via a "crankshaft process" (McCall, 1969). These two mechanisms would couple to the side-chain reorientation process when the latter is present. There is also another relaxation mechanism observed by Johari and Goldstein (1971) and Goldstein (1972) in glasses of small molecules above and below Tg. They suggest that this relaxation arises from molecular motions solely caused by the intermolecular interactions of the glassy phase. They claim that this relaxation would be present and strongly coupled to β relaxation for polymer glasses with side chains.

The spectrum of light scattered from an amorphous small molecule glass has been calculated by Cohen et al. (1976). The configurational rearrangements of molecules were described as the fluctuations of a concentration of unoccupied ("free") volume defined as

$$C = 1 - n/n_o$$

where n is the number density and n_o is a reference density defined as

the number density at infinite pressure. This model leads to a Rayleigh peak that is composed of two modes. The density fluctuation mode relaxes very rapidly and can be detected by interferometric techniques, whereas the configurational rearrangement mode relaxes at much slower rates, making detection by correlation techniques possible.

Only very recently, light scattering was applied to the study of relaxation processes in supercooled liquids and glasses. Jackson et al (1973) studied the correlation function of the light scattered from amorphous PMMA (polymethylmethacrylate) below Tg. They analyzed the signal in terms of two exponential decays. The faster relaxation was assigned to the side chain reorientational motion. The slower relaxation process was temperature insensitive up to Tg and could not be explained. The other work in this area is by Demoulin et al. (1974) where they studied the structural relaxation of supercooled glycerol. At low temperatures the relaxation time for this mechanism increases rapidly permitting the correlation technique to be used. The relaxation times they measured compared well with extrapolated results of the sound absorption measurement done at higher temperatures.

This part of the thesis investigates the relaxation mechanisms in polymer glasses above and below the glass transition temperature using the laser light scattering technique. PMMA was chosen in this study for several reasons: It is widely used and commercially available; it has an easily attainable glass transition temperature (Tg $\sim$ 120°C); and the abundance of data in the literature on this polymer makes the interpretation of our data easier. We have studied the light scattered

from this polymer in the temperature range from 6°C to 165°C. The data were analyzed in terms of two exponential decays. In each case we have studied the angular dependence of these relaxation times in order to elucidate the physical mechanisms behind each one.

CHAPTER VI

BACKGROUND ON GLASSES

In the previous chapter we have described the physical mechanisms underlying the glass transition phenomenon. It has appeared that the glass transition as manifested by the discontinuity in α and C_p was caused by the"freezing in" of the relaxation mechanism that plays the major role in the redistribution of energy and volume. Below Tg, the relaxation time of this mechanism is too long to permit equilibration during the time the measurements are done ("time scale" of minutes to hours). The recent theories of glass transition associate this increase in relaxation times to the small values of "excess configurational entropy" (Gibbs and DiMarzio, 1958) or of the "free volume" (Turnbull and Cohen 1961, 1970) around Tg. In this chapter we will briefly review these models and the relaxation time expressions derived from them.

In the excess configurational entropy model of Gibbs and DiMarzio a polymeric material composed of linear semiflexible chains was treated by the quasilattice model of Flory-Huggins. The configurational entropy of the supercooled liquid calculated using this model was seen to go to zero at a finite temperature T_2 (approximately 100° below the melting temperature T_m). Furthermore, it was shown that the energy and entropy are continuous at this temperature, whereas the temperature (and pressure) derivatives of these quantities are discontinuous. Hence the material is said to undergo a second order phase transition at T_2. The behavior of the material predicted at T_2 by this model

agrees with the experimental observations around Tg. The experimental breaks in the slopes of the thermodynamic quantities and the discontinuities of their derivatives at Tg are well reproduced by these parameters at T_2. However, T_2 always lies below Tg. Thus T_2 can be viewed as the ultimate glass transition temperature which will be reached only at infinitely slow experiments, but must always be present. The predictions of this model thus resolve the Kauzmann's paradox: The material cannot exist as a supercooled liquid below T_2. At this temperature the configurational entropy is zero and stays zero for temperatures below T_2.

The sluggish behavior of the material near T_2 is interpreted as a manifestation of the smallness of the configurational entropy in the region close to T_2. There is only a very small number of states the system can be in, with a large energy barrier separating them. Thus the system responds very slowly to any change in the external forces applied to it in the temperature region immediately above T_2. The relaxation time reaches infinity at T_2.

Adam and Gibbs (1965) derive an expression for the relaxation time using the configurational entropy model. They define the "cooperatively rearranging region" as the smallest region that can undergo a transition to a new configuration independent of its environment. The relaxation time is related to the probability of configuration rearrangements in this region. Adam and Gibbs show that the majority of transitions are undergone in regions whose size is very close to the smallest (critical) size that permits a transition at all. As T_2 is

approached, the critical size tends towards the size of the whole sample. The relaxation time is then expressed

$$\tau(T) = A \exp(B/TS_c) \tag{118}$$

where A and B are weakly dependent on temperature and assumed to be constant. S_c is the configurational entropy as defined in the Gibbs and DiMarzio model. As T_2 is approached S_c goes to zero and the relaxation time becomes infinite.

The free volume model of Turnbull and Cohen (1961,1970) was proposed for small molecule glasses. The atomic motions in the supercooled region are separated into two categories: purely diffusive as in a dilute fluid, or purely oscillatory as in an ideal solid. The diffusivity D is related to Enskog self-diffusivity by

$$D = fD_E \tag{119}$$

where D_E is the actual diffusivity calculated by random walk analysis and f is a correlation factor that changes from 1 for dilute fluids to 0 for solids. Cohen and Turnbull assumed that the particle can move diffusively only when the volume of its cage (formed by its nearest neighbors) exceeds a critical volume v*. They also assume that the total free volume Nv_f, where N is the number of particles, is randomly partitioned among the cages. On the basis of this model the following expression was derived for the self-diffusion coefficient:

$$D = \frac{1}{3} \alpha \langle c \rangle [v^* + (v_f/\gamma)] \exp(-\gamma v^*/v) \tag{120}$$

$\langle c \rangle$ is the average speed of particles, γ is a factor of order 0.5 - 1.0. This expression extrapolates to the correct limiting values as $v_f \to \infty$ and $v_f \to 0$. For the high density region for which $v^* >> v_f$, it reduces to a Doolittle type expression:

$$D = \frac{1}{3} \alpha v^* \langle c \rangle \exp(-\gamma v^*/v_f) \tag{121}$$

Thus the relaxation time for this model is exponentially dependent on the free volume fraction f defined as v_f/v^*. Around Tg, due to the small value of f, the relaxation time increases very rapidly.

Most materials that undergo a glass transition obey the well-known empirical equation of Williams Landel and Ferry (WLF equation)

$$-\log \frac{\tau(T)}{\tau(T_s)} = c_1(T-T_s)/[c_2 + (T-T_s)] \tag{122}$$

where the values $c_1 = 8.86$ and $c_2 = 101.6°C$ are appropriate for a large number of substances provided that T_s is chosen appropriately in each case. Both models of the glass transition discussed above lead, under appropriate assumptions, to a relaxation time of the WLF form. On one hand, S_c of the configurational model can be easily calculated as a function of temperature if c_p is assumed to be a constant for the glass forming liquid, i.e.,

$$S_c(T) = \Delta c_p \, \ell n(T/T_2) \tag{123}$$

Introducing $S_c(T)$ into the relaxation time expression (118) and re-arranging the terms, a WLF type expression is obtained:

$$-\log \frac{\tau(T)}{\tau(T_s)} = a_1(T-T_s)/[a_2+ (T-T_s)] \qquad (124)$$

where a_1 and a_2 are no longer universal and weakly temperature dependent. On the other hand, the relaxation time predicted by the free volume model can also be written in terms of temperature if the free volume is expressed in terms of T. The assumption that the free volume varies linearly with T results in the Vogel or Fulcher equation

$$\tau = A \exp[b/(T-T_0)] \qquad (125)$$

which is known to represent the relaxation time well in the high temperature regime but deviates at low temperatures around Tg.

CHAPTER VII

EXPERIMENTAL

The light scattering spectrometer used in this study was the same as that described in Part I of this thesis. A schematic drawing of the apparatus is given in Fig. 6.

The PMMA (commonly known as lucite or plexiglass) samples were obtained from two sources: a) commercially available 1/4-inch rods from Rohm and Haas Company, and b) 1/4-inch PMMA rods prepared by Polysciences, Inc., Pennsylvania. The commercial PMMA samples were studied in the temperature range 6°C to 142°C. At higher temperatures this sample turned yellow due probably to oxidation of either plasticizers, impurities, or excess initiators. The Polysciences samples were studied in the temperature range 20°C to 165°C. Unlike the commercial samples, only a very slight yellow discoloration occurred even at the highest temperature due to the higher purity of these samples. At low temperatures where the samples were hard solids, they were placed vertically in the center of a Brice Phoenix C-105 quartz cylindrical cell with flat entrance and exit windows. The rest of the cell was filled with glycerine, which has a refractive index of 1.47 at 20°C. The latter matches fairly well to the refractive indices of both quartz, 1.46, and the PMMA, 1.49, and falls in between these two. Thus the stray light due to reflections from various surfaces was minimized. Both the commercial and the Polysciences samples studied by this technique gave similar results. Above 135°C the PMMA was soft and the experiments were performed on samples which were melted in a test tube and kept at $\sim$160°C

for ten days. The temperature control below 80°C was provided by circulating water from a constant temperature Walter Thompson viscosity bath through the brass jacket that surrounded the cell. Above 80°C, a heating tape coupled to a Variac was found to provide adequate temperature control at steady state. The fluctuations in the sample were less than 0.5°C due to the fact that the laboratory temperature is independently controlled within 0.2°C. The samples were allowed to equilibrate for several hours to their new temperature after every temperature change.

The current autocorrelation functions were collected at two different time scales each (Fig. 31a,b) and analyzed in terms of two exponential decays. The period required to accumulate a correlation function varied from 30 minutes to several hours with an average of approximately two hours. The correlation function taken with the longer time increment was fitted to a single exponential plus a baseline after neglecting a proper number of initial points representing the faster decaying exponential. The decay time of this slow relaxation was then used to fit the correlation function taken at smaller time increment, to a sum of two exponentials and thence to obtain the decay time of the faster exponential. Most of the data was analyzed by computer except in a few instances where non-rapid convergence made the graphical evaluation of data preferable.

The autocorrelation functions collected in this work were in the heterodyne mode which differs from the homodyne detection used in the first part of this thesis by the fact that not only scattered light, but

also a large amount of incident laser light falls on the photomultiplier tube. This is due to laser light being scattered unshifted by the large static inhomogeneities that are present in the samples used. In the heterodyne mode the current autocorrelation function (or the power spectrum) is exactly the same as the correlation function of the electric field (or the spectrum of light).

CHAPTER VIII

RESULTS AND DISCUSSION

The following data were taken in collaboration with Dr. Claude Cohen. The relaxation mechanisms were characterized in terms of their relaxation frequency (ω in Hertz) defined as $\omega = (2\pi\tau)^{-1}$ where τ is the relaxation time of the process. The relaxation frequency of the slow mechanism was obtained by analyzing the autocorrelation function taken with longer time increment (Fig. 31a) in terms of a simple exponential plus a baseline. A proper amount of initial points representing the faster decaying exponential was neglected. This number was determined by trial and error, making sure that the faster decaying exponential had reached a negligible value by the end of this interval. The decay time of the faster decaying exponential was obtained by analyzing the smaller time increment correlation function (Fig. 31b) in terms of two exponentials. The value obtained for the slow exponential as explained above was used to represent the decay time of the first exponential.

The High Frequency Relaxation Mode

We have studied this relaxation mode at 8 temperatures from 6°C to 135°C (just above Tg). At higher temperatures the amplitude of scattering from this relaxation mechanism became too small, rendering a quantitative study impossible. We have examined the angular dependence of this relaxation mode up to 100°C. Figure 32a represents the results of the angular dependence all obtained for the same position of the sample. Figure 32b represents the results obtained again at

20°C for various positions of the sample. The results indicate that the relaxation frequency is independent of the scattering angle θ. Furthermore, the relaxation frequency is unaffected by the inhomogeneities of the sample as indicated by the similarity of data taken at various different positions of the sample. Figures 33, 34, 35 and 36 represent the relaxation frequency of this mechanism vs angle, taken at various positions, at 40°C, 57°C, 81°C and 100°C, respectively. The error bars in these figures represent the uncertainty as given by the least squares fit. Figure 37 is the plot of relaxation frequency against $1/T$. The data points on this graph represent the values obtained by averaging over the results at various angles and for various positions.

Figure 35 shows that the data points fall reasonably well on two straight lines of different slope. The high temperature line corresponds to an activation energy of 8 Kcal/mole, whereas the low temperature line corresponds to an activation energy of $\sim$1 Kcal/mole. The time scale of this relaxation is similar to that of the side chain reorientation mechanism (β relaxation) in PMMA as measured by dielectric relaxation or NMR. However, the activation energy we observe for the high temperature region is lower than the one reported for this process. Our lower value may be due to either varying amounts of plasticizers which are known to change the activation energy, or more probably due to a coupling to a low activation energy mechanism. Our results in Fig. 37 also confirm the suggestion that there exists a low activation mechanism coupled to the reorientation of the side chain. At low

temperatures when the side chain reorientation is very slow this mechanism is observed, whereas at higher temperatures when the side chain orientation becomes faster the two mechanisms merge into one, dominated by the reorientation of the side chain. This merging of two mechanisms with different activation energies was observed by dielectric techniques for the α- and β-relaxations in isotactic PMMA (Mikhailov and Borisova, 1961) and is expected to take place between the α- and β-relaxations of conventional PMMA at higher temperatures (Jackson et al., 1973; Goldstein, 1972). We would like to suggest that the low energy mechanism that is dominant at low temperature and is coupled to the side chain reorientation at higher temperatures is due to the torsional oscillations of the chain segments about their equilibrium positions. This is also supported by the recent work of Jones and Wang (1976) on depolarized Rayleigh scattering of polypropylene glycol. The relaxation times measured by these authors for the backbone segmental motion of the molecule show an activation energy of $\sim$4 Kcal/mole, whereas dielectric relaxation experiments report a value of 11.7 Kcal/mole for the same mechanism. They explain this discrepancy as due to torsional oscillations of low activation energy which are detected by light scattering, but could not be observed by dielectric measurement techniques.

The relaxation frequency of this correlation shows no angular dependence as shown in Figs. 32-36. Furthermore, in unannealed samples, the inhomogeneities in the scattering volume do not affect the values observed. In the first part of this thesis we have shown

that the correlation function can be written as

$\left\langle \sum_{i,j} \alpha(r_i,0)\ \alpha_{22}(r_j,t) \exp ik \cdot [\underline{r}_j(t) - \underline{r}_i(0)] \right\rangle$ where the $\alpha\cdot\alpha$ part represents the polarizability contribution, whereas the exponential part is the displacement contribution. In view of the small size of the side chain and the small displacements involved in torsional oscillations, we would expect the exponential term to be one and the correlation function to have only the polarizability contribution which is k, and hence is angular independent.

The Low Frequency Relaxation Mode

We have studied this relaxation mode at temperatures ranging from 6°C to 165°C and examined its angular dependence up to 120°C. The angular dependence of this relaxation shows a marked difference between annealed and unannealed samples. Figure 38a represents the data of an unannealed sample at one position at 20°C and at two positions at 40°C. The angular dependence is irregular and markedly different for different positions of the same sample at the same temperature. Figure 38b is the angular dependence of this relaxation at temperatures close to glass transition temperature (81°C and 100°C) and the relaxation frequency for this case shows no dependence on the scattering angle. Figure 38c is the result for an annealed sample at low temperatures (6°C and 20°C) and again the dependence on scattering angle vanishes. These figures indicate that this relaxation mechanism is strongly affected by the imperfections of the sample. Figure 39 is the variation of this relaxation frequency as a function of 1/T. The data points on this graph are again obtained by averaging

the relaxation frequencies measured at various angles and for various positions. The error bars represent the uncertainty as given by the least squares fit of the data.

To rule out the possibility that this relaxation frequency is caused by experimental deficiency on our part, we have examined all possible sources, and did not find any. In particular, we have studied the light scattered from a solution of polystyrene spheres known to have no low frequency component, and did not observe any. The 4880Å line of the argon laser has been used by others to go to even lower frequencies with no complications (Demoulin et al., 1974). Also, this relaxation below has been previously observed by Jackson, et al. (1973).

As seen in Fig. 38a, this relaxation frequency is very sensitive to the inhomogeneities of the sample. This is also confirmed by the disappearance of angular dependence for annealed samples or for unannealed samples at high temperatures where it is known that these inhomogeneities even out. This shows that this mechanism is largely dependent on the overall structure of the scattering volume and is likely to represent a rearrangement of "free" volume or "configurational entropy". The almost constant value of this relaxation frequency shows that the mechanism has no activation energy, that is, no energy barrier to cross. This is exactly the same assumption Turnbull and Cohen (1961,1970) make about the redistribution of "free" volume in their derivation of the WLF equation, which is known to be obeyed by polymers. Since at Tg an excess "free" volume is frozen

into the solid, it should be able to redistribute itself with no energy and thus be temperature independent. A further argument in favor of such a mechanism is the merging of this temperature independent relaxation frequency with the main chain motion (α-relaxation) which requires a large activation energy above Tg. This behavior is similar to the theoretical behavior (below and above Tg) of the ratio f of the "free" volume to the critical free volume used in the "free" volume theories where the relaxation time τ is related to f by a Doolittle type equation

$$\tau = \tau_0 \exp f^{-1}$$

The behavior of the low frequency relaxation mode can also be interpreted in terms of the configuration entropy model if we accept the "fictive" temperature concept for solids below Tg. Adam and Gibbs (1965) find that the relaxation time obeys an equation of the form

$$\tau^{-1} = A \exp -B/TS_c$$

where A and B are constants, T is the temperature, and S_c is the excess configurational entropy. Above Tg this equation leads to an expression similar to WLF equation; below Tg, S_c remains constant and T is substituted by a fictive temperature due to nonequilibrium state of the amorphous glass. In that case, this equation leads to a constant relaxation frequency below Tg and a WLF type equation above it. As indicated in Fig. 39, the relaxation frequency of this mode increases very rapidly above Tg and follows the behavior of the main chain

relaxation observed by mechanical dielectric and NMR techniques (dotted area of Fig. 39).

The relaxation frequency of this mode is angular independent (Fig. 38b,c) except for some irregularities due to inhomogeneities of the sample used (Fig. 38a). Hydrodynamic model of amorphous solids predicts that the relaxation mode that is due to "free" volume or configurational rearrangement will be diffusive in character and thus be k^2 dependent. However, this model is essentially for glasses made up of small molecules with no internal degrees of freedom. In this case the α-relaxation mode above Tg is molecular diffusion which is k^2 dependent and one expects it would lead to a k^2 dependent "free" volume diffusion below Tg. For polymeric glasses however, the α-relaxation is the internal motion of the chain which was demonstrated to give rise to a k^2 independent correlation function in Part I of this thesis. Thus it may be expected that the "free" volume diffusion which merges into a k^2 independent mode above Tg will itself be k^2 independent.

Conclusion:

This study shows that the light scattered from glasses carry a wealth of information about the relaxation mechanisms, some of which are not observable by other techniques. After this initial study, work may be extended to linear polymers with different side chains to better understand the mechanism(s) that is contributing to the high frequency relaxation mode. Also a study of small molecule glasses would be helpful to resolve the ambiguities concerning the k^2 dependence of the low frequency mode.

LITERATURE CITED

Adam, G. and J. H. Gibbs, J. Chem. Phys. 43, 139 (1965)

Berne, B. J. and R. Pecora, Dynamic Light Scattering with Applications to Chemistry, Biology and Physics (Wiley, 1976).

Berry, G. C., J. Chem. Phys. 44, 4550 (1966).

Born, M. and E. Wolf, Principles of Optics (Pergamon Press, 1970), Ch. II.

Cantow, H. J., Macromol. Chem. 53, 91 (1962).

Cohen, C., P. D. Fleming and J. H. Gibbs, Phys. Rev. B13, 866 (1976).

Cummins, H. Z., N. Knable, and Y. Yeh, Phys. Rev. Lett. 12, 150 (1964).

Cummins, H. Z. and H.L. Swinney, Progr. Opt. 8, 1351 (1970).

Davis, R. O. and G. O. Jones, Proc. Roy. Soc. A217, 26 (1953).

DiMarzio, E. A. and J. H. Gibbs, J. Chem. Phys. 28, 807 (1958).

Demoulin, C., C. J. Montrose and N. Ostrowsky, Phys. Rev. A9, 1740 (1974).

Dubin, S. B., J. H. Lunacek and G. B. Benedek, Proc. Nat. Acad. Sci. U.S. 57, 1164 (1967).

Ferry, J. D., Viscoelastic Properties of Polymers (Wiley, 1970), Ch. 9.

Fixman, M., J. Chem. Phys. 42, 3831 (1965).

Forrester, A. T., J. Opt. Soc. Amer. 51, 253 (1961).

Fujime, S., J. Phys. Soc. Jap. 29, 416 (1970).

Fujime, S., Ibid. 29, 751 (1970a).

Fujime, S. and S. Ishiwata, J. Mol. Biol. 62, 251 (1971).

Fujime, S., M. Maruyama and S. Asakura, J. Mol. Biol. 68, 347 (1972).

Fujime, S. and S. Maruyama, Macromolecules 6, 237 (1973).

Gibbs, J. H. and E.A. DiMarzio, J. Chem. Phys. 28, 373 (1958).

Goldstein, M. A., in Amorphous Materials, ed. by R. W. Douglas and B. Ellis (Wiley-Interscience, 1972).

Harris, R. A. and J. E. Hearst, J. Chem. Phys. 44, 2595 (1966).

Huang, W. N. and J. E. Frederick, Macromolecules 7, 34 (1974).

Jackson, D. A., E. R. Pike, J. G. Prowles and J. M. Vaughn, J. Phys. C6, 155 (1973).

Johari, G. P. and M. Goldstein, J. Chem. Phys. 53, 2372 (1970).

Johari, G. P. and M. Goldstein, Ibid. 55, 4245 (1971)

Jolly, D. and H. Eisenberg, Biopolymers 15, 61 (1976).

Jones, D. R. and J. H. Wang, J. Chem. Phys. 65, 1835 (1976).

Kauzmann, W., Chem. Rev. 43, 219 (1949).

King, T. A., A. Knox, W. I. Lee and J.D.G. McAdam, Polymer 14, 151 (1973)

Kirkwood, J. G. and J. Riseman, J. Chem. Phys. 16, 565 (1948).

Mandel, L., Prog. Opt. 2, 181 (1963).

Mandel, L. and E. Wolf, Rev. Modl Phys. 37, 231 (1964).

McAdam, J.D.G. and T. A. King, Chem. Phys. 6, 109 (1974).

McCall, D. W., in Molecular Dynamics and Structure of Solids, ed. by R. S. Carter and J. S. Rush (NBS Special publication 301, 1969).

McIntyre, D., L. J. Fetters and E. Siagowski, Science 176, 1041 (1972).

Mikhailov, G. P. and T. I. Borisova, Polym. Sci., USSR 2, 387 (1961).

Orofino, T. A. and J. W. Mickey, J. Chem. Phys. 38, 2512 (1963).

Osaki, K., Macromolecules 5, 141 (1972).

Osaki, K., J. L. Schrag and J. D. Ferry, Macromolecules 5, 144 (1972).

Pecora, R., J. Chem. Phys. 40, 1604 (1964).

Pecora, R., J. Chem. Phys. 43, 1562 (1965).

Pecora, R., J. Chem. Phys. 49, 1032 (1968).

Pecora, R., Ibid., 1636 (1968a)

Pecora, R., J. Chem. Phys. 48, 4126 (1968b)

Pecora, R. and Y. Tagami, J. Chem. Phys. 51, 3298 (1969).

Perico, A., P. Piaggio and C. Cuniberti, J. Chem. Phys. 62, 2690 (1975).

Perico, A., P. Piaggio and C. Cuniberti, Ibid., 4911 (1975a).

Randall, J. T., Diffraction of X-rays and Electrons by Amorphous Solids, Liquids and Gases (Wiley, 1934)

Rouse, P. E. Jr., J. Chem. Phys. 21, 1272 (1953).

Saito, N., K. Takahashi and Y. Yunoki, J. Phys. Soc. Japan 22, 219 (1967).

Schmidt, R. L., Biopolymers 12, 1427 (1973).

Slagowski, E., PhD Dissertation, The University of Akron (1972).

Saito, S., in Treatise on Solid State Chemistry, ed. by N. B. Hannay (Plenum Press, 1975), Ch. 11.

Saito, N., K. Okano, S. Iwayanagi and T. Hideshima in Solid State Physics ed. by F. Seitz and D. Turnbull, Vol. 14 (Academic Press, 1963).

Tagami, I., and R. Pecora, J. Chem. Phys. 51, 3293 (1969).

Tanford, ., Physical Chemistry of Macromolecules (Wiley, 1963), Ch. 6.

Tschoegl, N. W., J. Chem. Phys. 39, 149 (1963).

Tschoegl, N. W., J. Chem. Phys. 40, 473 (1964).

Turnbull, D. and M. H. Cohen, J. Chem. Phys. 34, 120 (1961).

Turnbull, D. and M. H. Cohen, J. Chem. Phys. 52, 3038 (1970).

Van Hove, L., Phys. Rev. 95, 249 (1954).

Wang, M. C. and G. E. Uhlenbeck, Rev. Mod. Phys. 17, 323 (1945).

Williams, M. L., R. F. Landel and J. D. Ferry, J. Am. Chem. Soc. 77, 3701 (1955).

Yamakawa, H., Modern Theory of Polymer Solutions (Harper & Rowe, 1971), Ch. 4.

Zimm, B. H., J. Chem. Phys. 24, 269 (1956).

Zimm, B. H., G. M. Roe and L. F. Epstein, J. Chem. Phys. 24, 279 (1956).

Table X: Diffusion Coefficient vs Concentration for 2×10^6 Molecular Weight Polystyrene

Solvent	Concentration (μg/cc)	$D(c) \times 10^7$ cm^2/sec
cyclohexane	923	0.991
	461	1.010
	230	0.997
diethylmalonate	948	0.472
	474	0.467
	237	0.474
1-chloroundecane	896	0.394
	448	0.391
	224	0.395

Table XI: Diffusion Coefficient vs Concentration for 4.1×10^6 Molecular Weight Polystyrene

Solvent	Concentration (μg/cc)	D(c) $\times 10^7$ cm^2/sec
cyclohexane	736	0.671
	368	0.682
	184	0.665
diethylmalonate	783	0.322
	391	0.322
	196	0.327
1-chloroundecane	812	0.265
	406	0.261
	203	0.265

Table XII: Diffusion Coefficient vs Concentration for 7.1×10^6 Molecular Weight Polystyrene

Solvent	Concentration (μg/cc)	D(c) $\times 10^7$ cm^2/sec
cyclohexane	537	0.519
	269	0.528
	135	0.516
diethylmalonate	525	0.256
	262	0.252
	131	0.256
1-chloroundecane	621	0.213
	311	0.209
	155	0.214

Table XIII: Relaxation Times and Relative Intensities for Polystyrene ($MW = 4.1 \times 10^6$) in Cyclohexane. Concentration = 431 μg/cc $D = 0.685 \times 10^{-7} cm^2/sec$

θ (deg)	k^2 ($\times 10^{-10} cm^{-2}$)	x	τ_1 (μsec)	B/(A+B) %
85	6.08	2.25	95.9	10.9
90	6.66	2.46	99.2	14.2
95	7.24	2.69	95.4	17.1
100	7.82	2.90	105.4	19.2
105	8.39	3.11	96.3	21.0
112	9.16	3.39	98.7	23.0
120	9.99	3.71	98.4	26.5

Table XIV: Relaxation Times and Relative Intensities for Polystyrene ($MW = 4.1 \times 10^6$) in Cyclohexane. Concentration = 307 μg/cc $D = 0.661 \times 10^{-7} cm^2/sec$

θ (deg)	k^2 ($\times 10^{-10} cm^{-2}$)	x	τ_1 (μsec)	B/(A+B) %
85	6.08	2.25	100.4	11.0
90	6.66	2.46	104.4	13.9
95	7.24	2.69	102.3	16.9
100	7.82	2.90	112.6	19.3
105	8.39	3.11	101.1	20.9
112	9.16	3.39	101.2	23.4
120	9.99	3.71	101.8	26.0

Table XV: Relaxation Times and Relative Intensities for Polystyrene ($MW = 4.1 \times 10^6$) in Cyclohexane. Concentration = 198 μg/cc $D = 0.668 \times 10^{7} cm^2/sec$

θ (deg)	k^2 ($\times 10^{-10} cm^{-2}$)	x	τ_1 (μsec)	B/(A+B) %
85	6.08	2.25	90.8	10.8
90	6.66	2.46	94.3	14.6
95	7.24	2.69	90.3	17.8
100	7.82	2.90	103.8	17.8
105	8.39	3.11	91.6	21.4
112	9.16	3.39	92.2	24.8
120	9.99	3.71	92.2	27.4

Table XVI: Relaxation Times and Relative Intensities for Polystyrene ($MW = 4.1 \times 10^6$) in Diethylmalonate. Concentration = 559 g/cc. $D = 0.324 \times 10^{-7} cm^2/sec$

θ (deg)	k^2 ($\times 10^{-10} cm^{-2}$)	x	τ_1 (μsec)	B/(A+B) %
90	6.59	2.44	229.6	9.31
95	7.17	26.5	231.4	11.8
100	7.73	2.87	227.8	14.6
105	8.30	3.08	235.4	18.9
112	9.06	3.37	247.3	20.6
120	9.89	3.67	234.2	23.2

Table XVII: Relaxation Times and Relative Intensities for Polystyrene ($MW = 4.1 \times 10^6$) in 1-Chloroundecane. Concentration = 533 g/cc. $D = 0.263 \times 10^{-7} cm^2/sec$

θ (deg)	k^2 ($\times 10^{-10} cm^{-2}$)	x	τ_1 (μsec)	B/(A+B) %
90	6.88	2.55	253.0	10.9
95	7.47	2.77	247.4	14.3
100	8.07	2.99	241.6	17.8
105	8.65	3.21	254.4	21.9
112	9.45	3.51	246.5	22.7
120	10.31	3.82	267.4	25.3

Table XVIII: Relaxation Times and Relative Intensities for Polystyrene ($MW = 7.1 \times 10^6$) in Cyclohexane. Concentration = 245 μg/cc. $D = 0.519 \times 10^{-7} cm^2/sec$

θ (deg)	k^2 ($\times 10^{-10} cm^{-2}$)	x	τ_1 (μsec)	B/(A+B) %
65	3.85	2.46	212.0	12.2
70	4.38	2.81	218.2	14.3
75	4.93	3.16	213.0	19.2
80	5.51	3.53	202.1	22.1
85	6.08	3.90	219.7	24.8
90	6.66	4.27	195.6	27.2
95	7.24	4.65	199.6	31.1
100	7.82	5.02	199.9	34.9

Table XIX: Relaxation Times and Relative Intensities for Polystyrene (MW = 7.1×10^6) in Cyclohexane. Concentration = 176 μg/cc
$D = 0.527 \times 10^{-7} cm^2/sec$

θ (deg)	k^2 ($\times 10^{-10} cm^{-2}$)	x	τ_1 (μsec)	B/(A+B) %
65	3.85	2.46	223.0	11.6
70	4.38	2.81	229.6	14.0
75	4.93	3.16	222.6	20.0
80	5.51	3.53	210.6	22.5
85	6.08	3.90	231.9	23.8
90	6.66	4.27	220.1	29.6
95	7.24	4.65	204.9	31.1
100	7.82	5.02	206.1	34.7

Table XX: Relaxation Times and Relative Intensities for Polystyrene ($MW = 7.1 \times 10^6$) in Cyclohexane. Concentration = 115 μg/cc
$D = 0.518 \times 10^{-7} cm^2/sec$

θ (deg)	k^2 ($\times 10^{-10} cm^{-2}$)	x	τ_1 (μsec)	B/(A+B) %
65	8.85	2.46	206.1	11.8
70	4.38	2.81	212.5	15.0
75	4.93	3.16	207.1	19.8
80	5.51	3.53	195.7	22.8
85	6.08	3.90	219.4	23.0
90	6.66	4.27	201.5	28.7
95	7.24	4.65	192.5	31.4
100	7.82	5.02	195.1	34.8

Table XXI: Relaxation Times and Relative Intensities for Polystyrene (MW = 7.1 x 10^6) in Diethylmalonate. Concentration = 301 μg/cc. D = 0.254 x 10^{-7} $cm^2 sec$

θ (deg)	k^2 (x $10^{-10} cm^{-2}$)	x	τ_1 (μsec)	B/(A+B) %
65	3.81	2.45	462.9	11.0
70	4.34	2.78	471.4	13.9
75	4.89	3.14	492.1	16.3
80	5.45	3.50	489.2	20.4
85	6.02	3.87	451.0	22.1
90	6.59	4.23	468.3	23.5
95	7.17	4.61	472.5	30.2

Table XXII: Relaxation Times and Relative Intensities for Polystyrene (MW = 7.1 x 10^6) in 1-Chloroundecane. Concentration = 344 μg/cc. D = 0.210 x $10^{-7} cm^2/sec$

θ (deg)	k^2 (x $10^{-10} cm^{-2}$)	x	τ_1 (μsec)	B/(A+B)
65	3.97	2.55	547.6	7.51
70	4.52	2.90	565.3	9.8
75	5.10	3.27	590.3	12.2
80	5.68	3.64	579.4	14.7
85	6.28	4.03	559.3	17.8
90	6.88	4.41	565.2	22.7
95	7.47	4.79	597.3	25.4

FIGURES

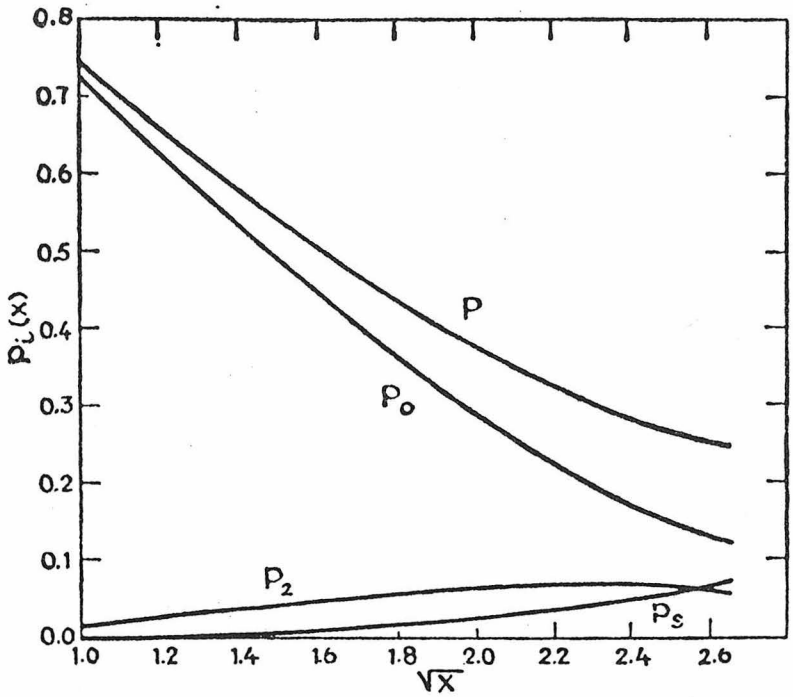

Fig. 3. Relative intensities of various terms contributing to the spectrum vs $x^{1/2}$ (from Pecora 1968).

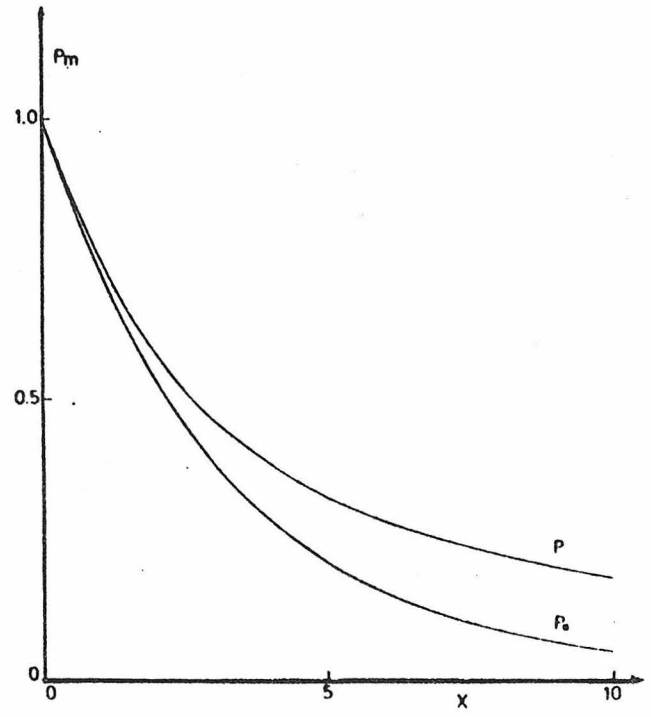

Fig. 4a. The total intensity and the diffusive intensity vs x (from Perico et al 1975).

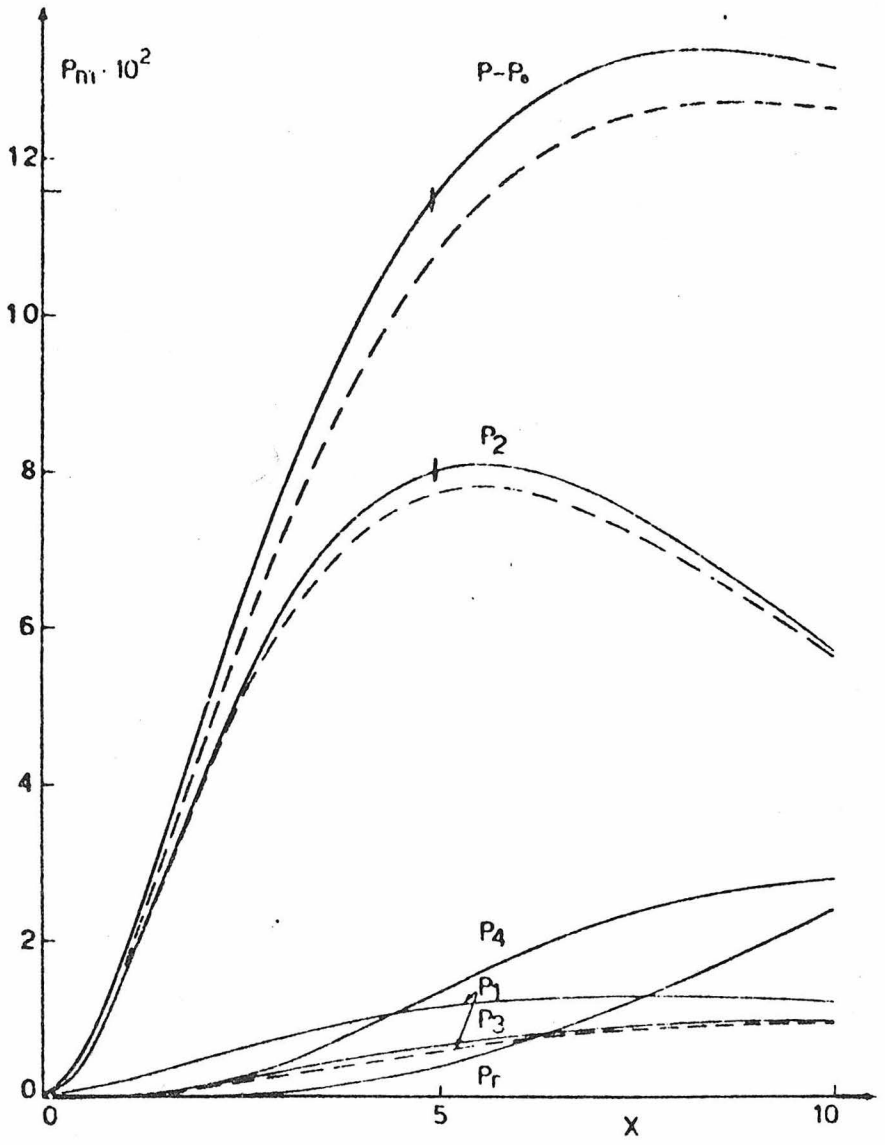

Fig. 4b. The intramolecular intensities vs x (from Perico et al. 1975).

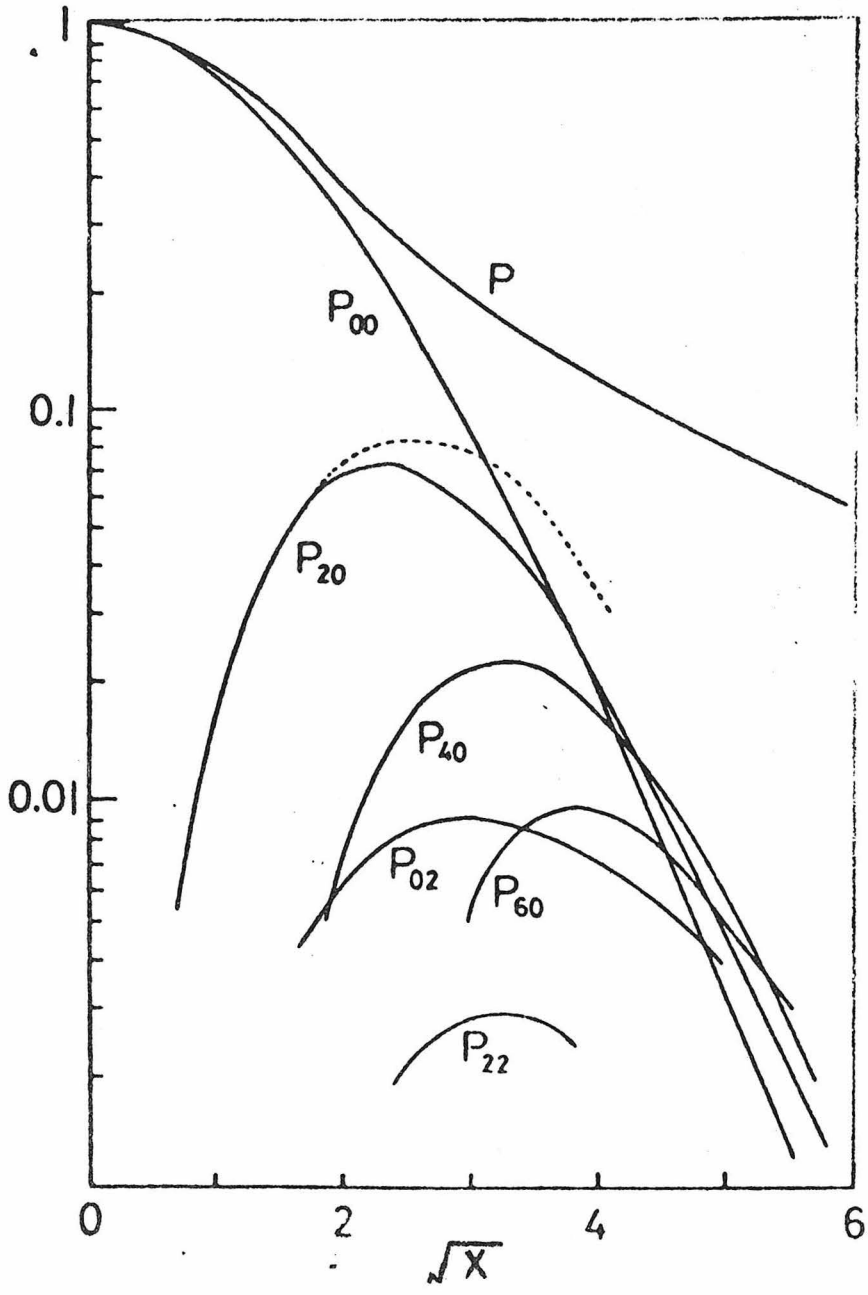

Fig. 5. $P_{NM}(x)$ vs $x^{1/2}$ for flexible molecules. ----- $P_{20}+P_{40}$ (from Fujime and Maruyama 1973)

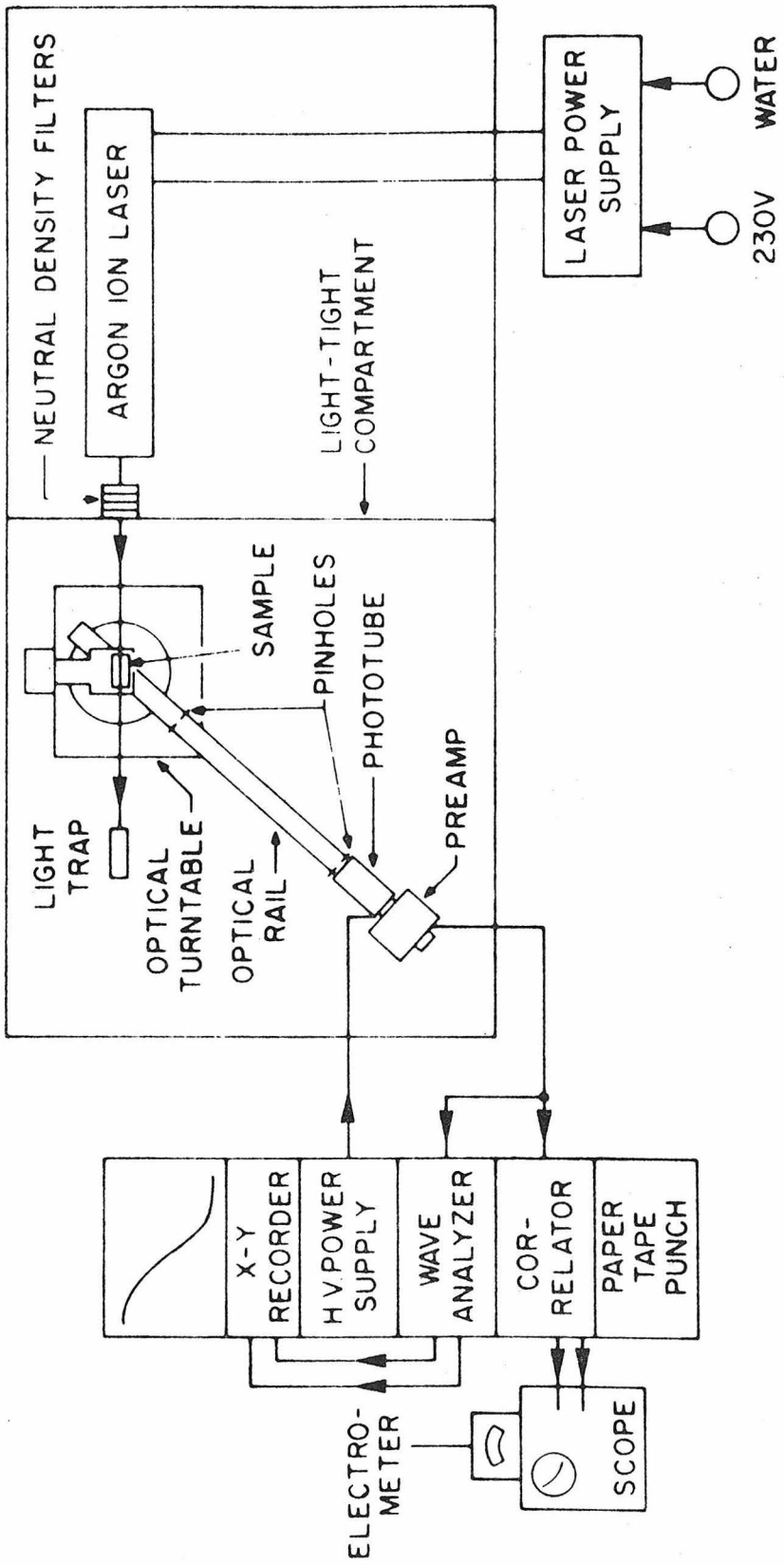

Fig. 6. A schematic drawing of the light scattering spectrometer used in this study.

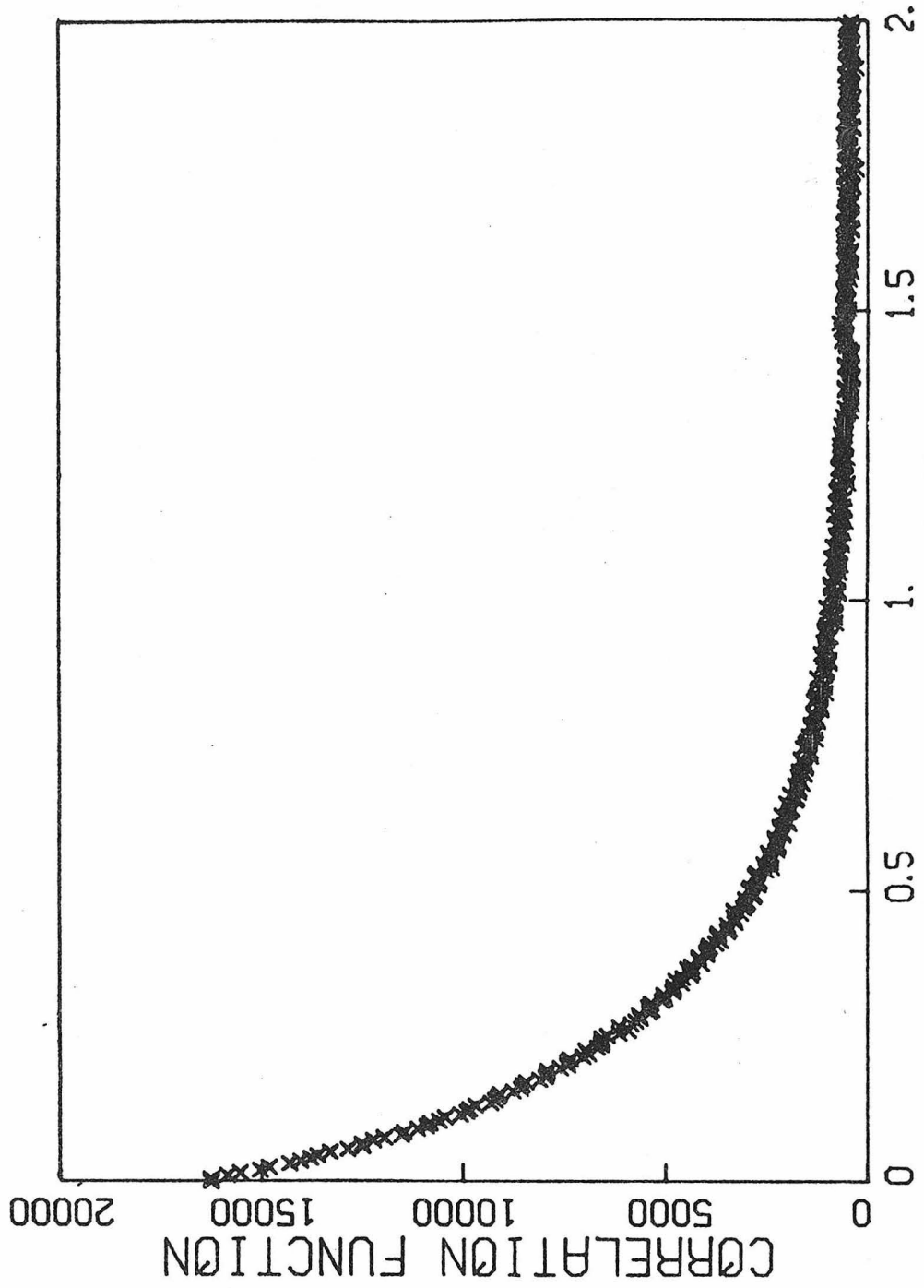

Fig. 7. A typical current autocorrelation function with 400 points

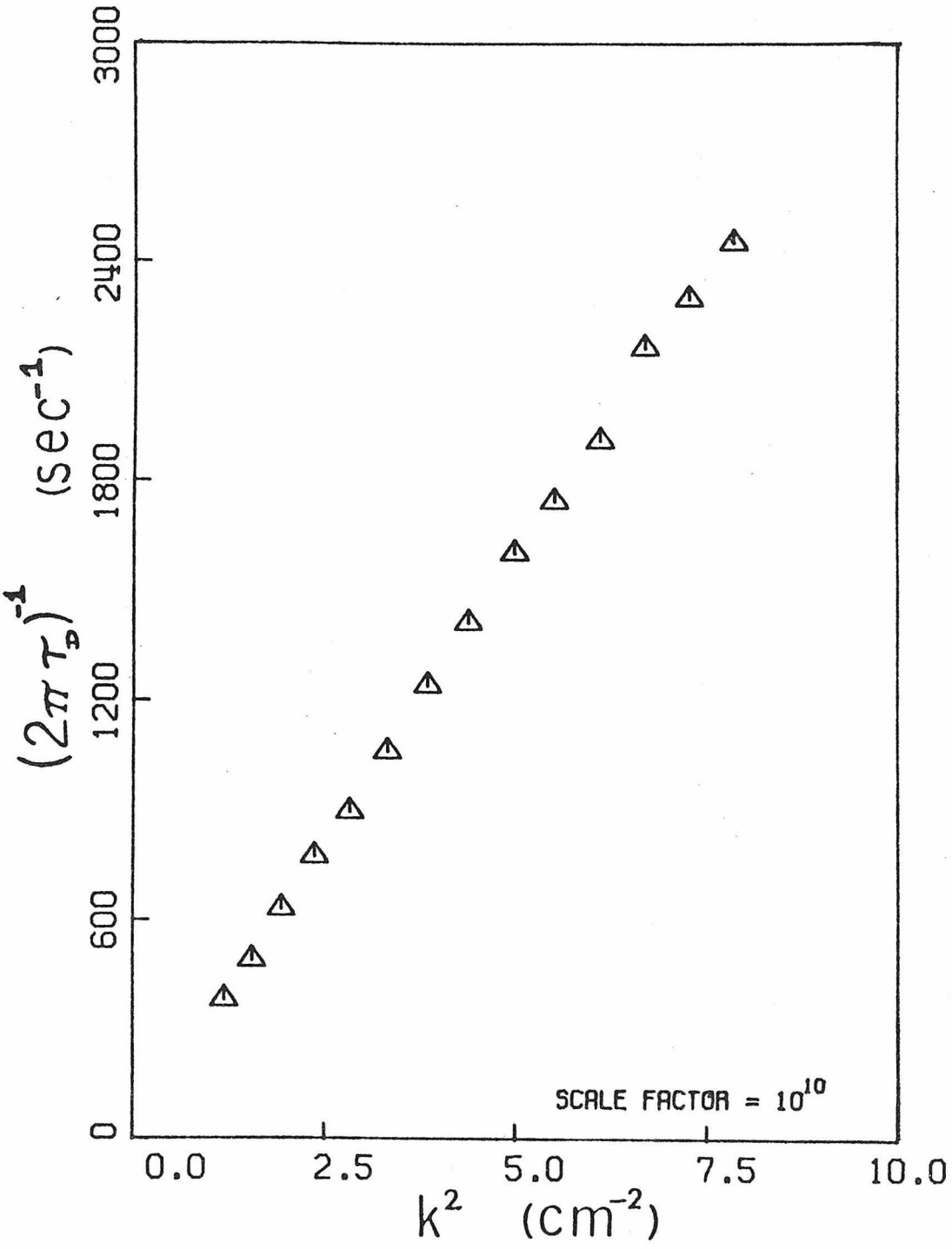

Fig. 8. The inverse decay time vs k^2 for the two million molecular weight polystyrene in cyclohexane (C = 735 µg/cc).

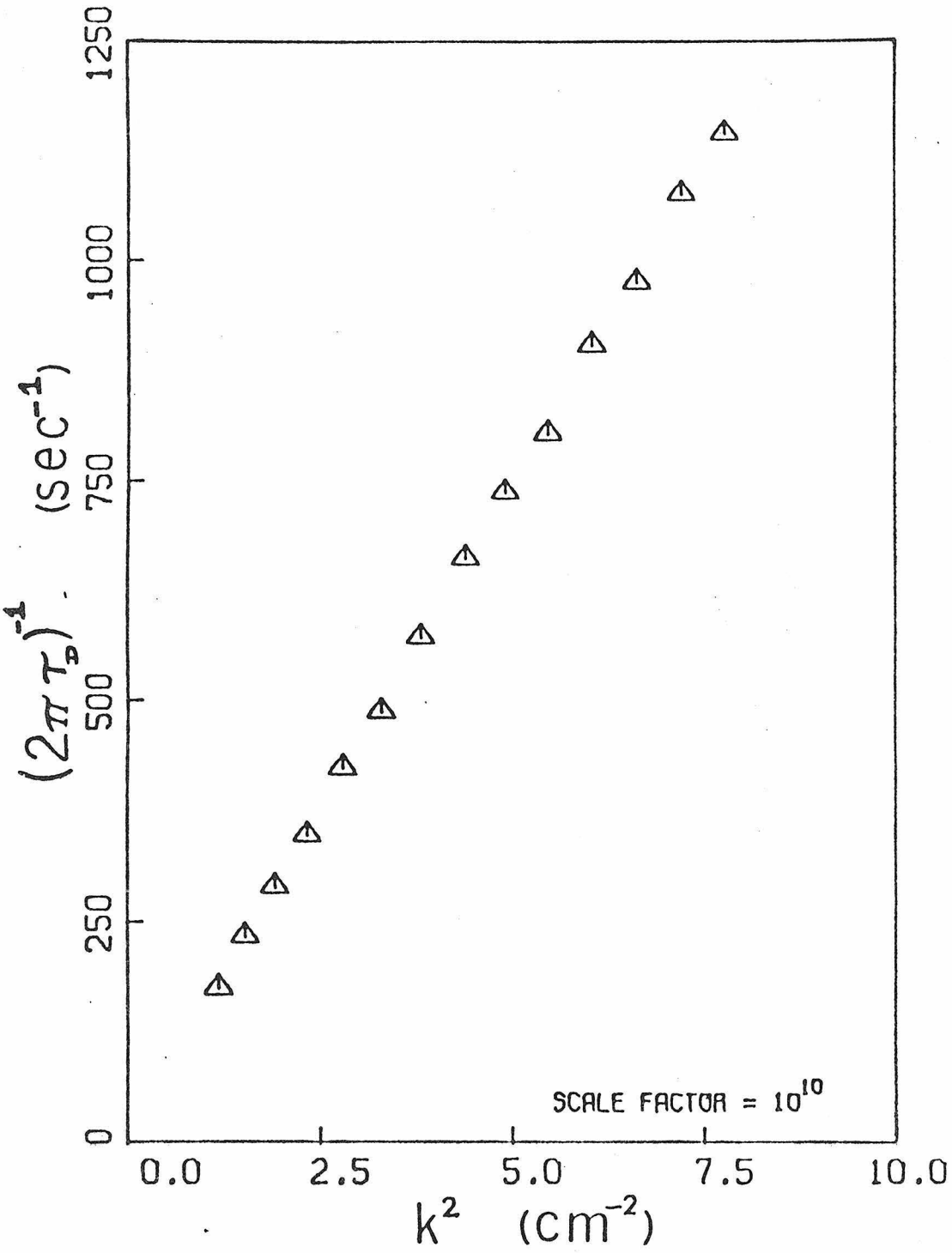

Fig. 9. The inverse decay time vs k^2 for the two million molecular weight polystyrene in diethylmalonate (C = 718 μg/cc).

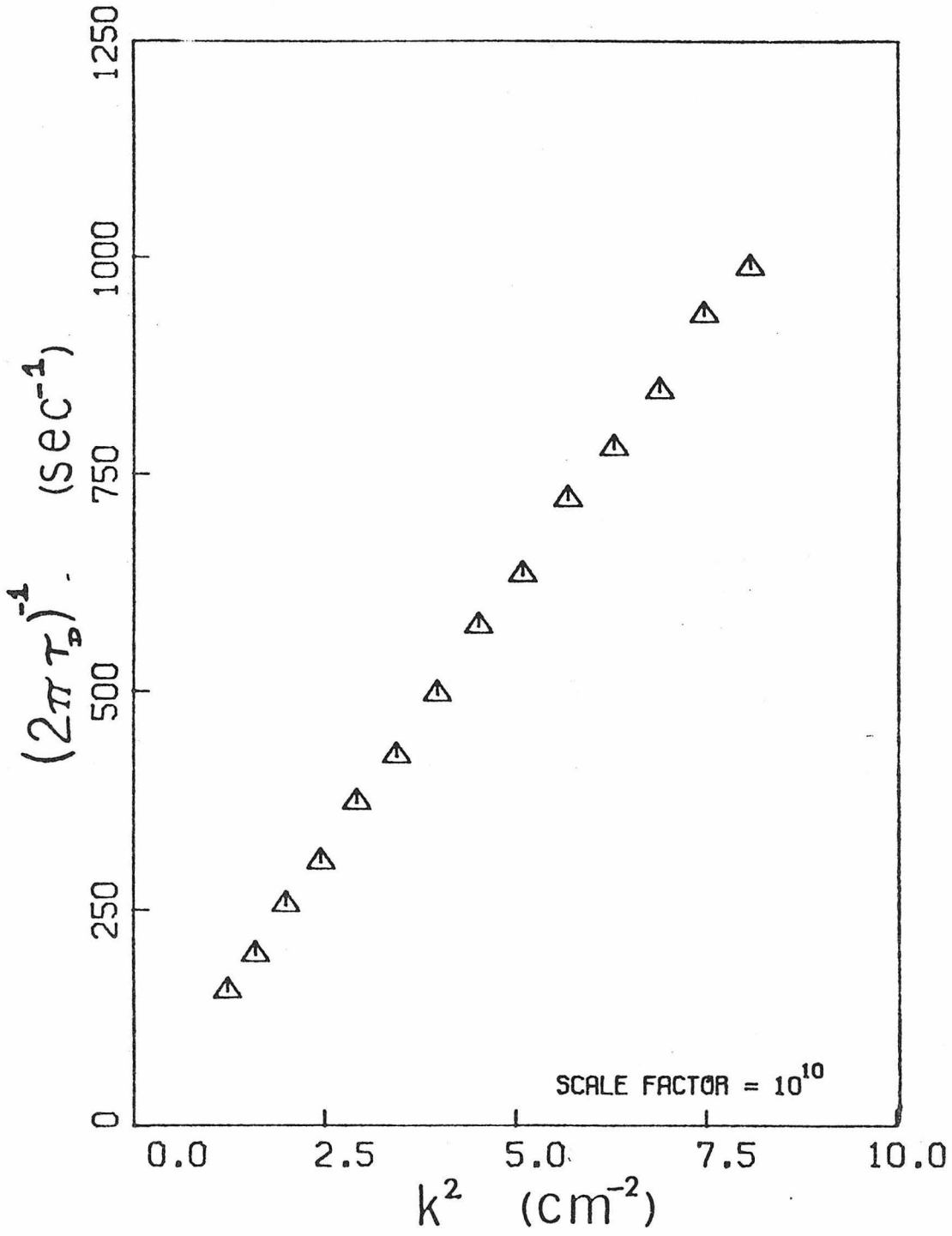

Fig. 10. The inverse decay time vs k^2 for the two million molecular weight polystyrene in 1-chloroundecane (C = 796 μg/cc).

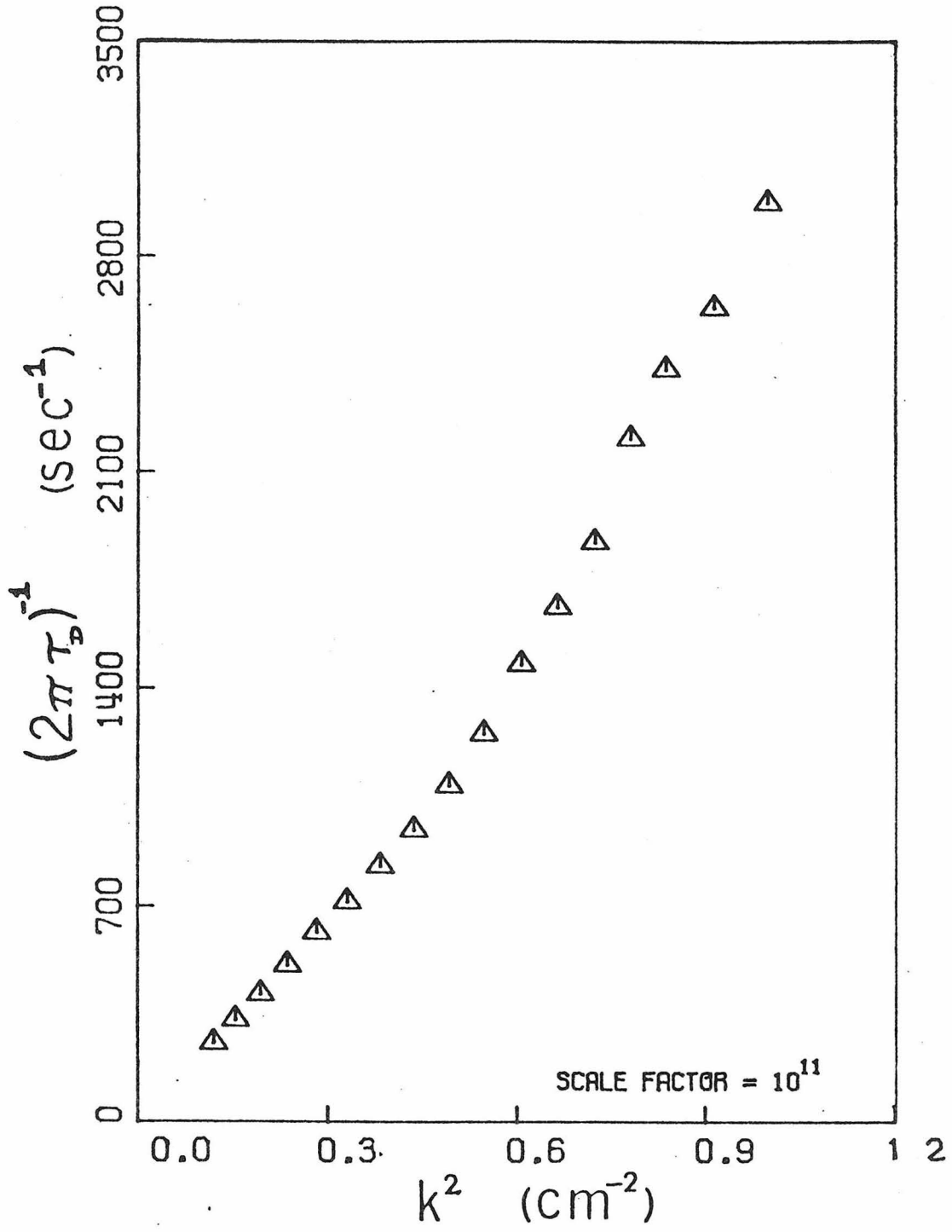

Fig. 11. The inverse decay time vs k^2 for the four million molecular weight polystyrene in cyclohexane (C = 570 μg/cc)

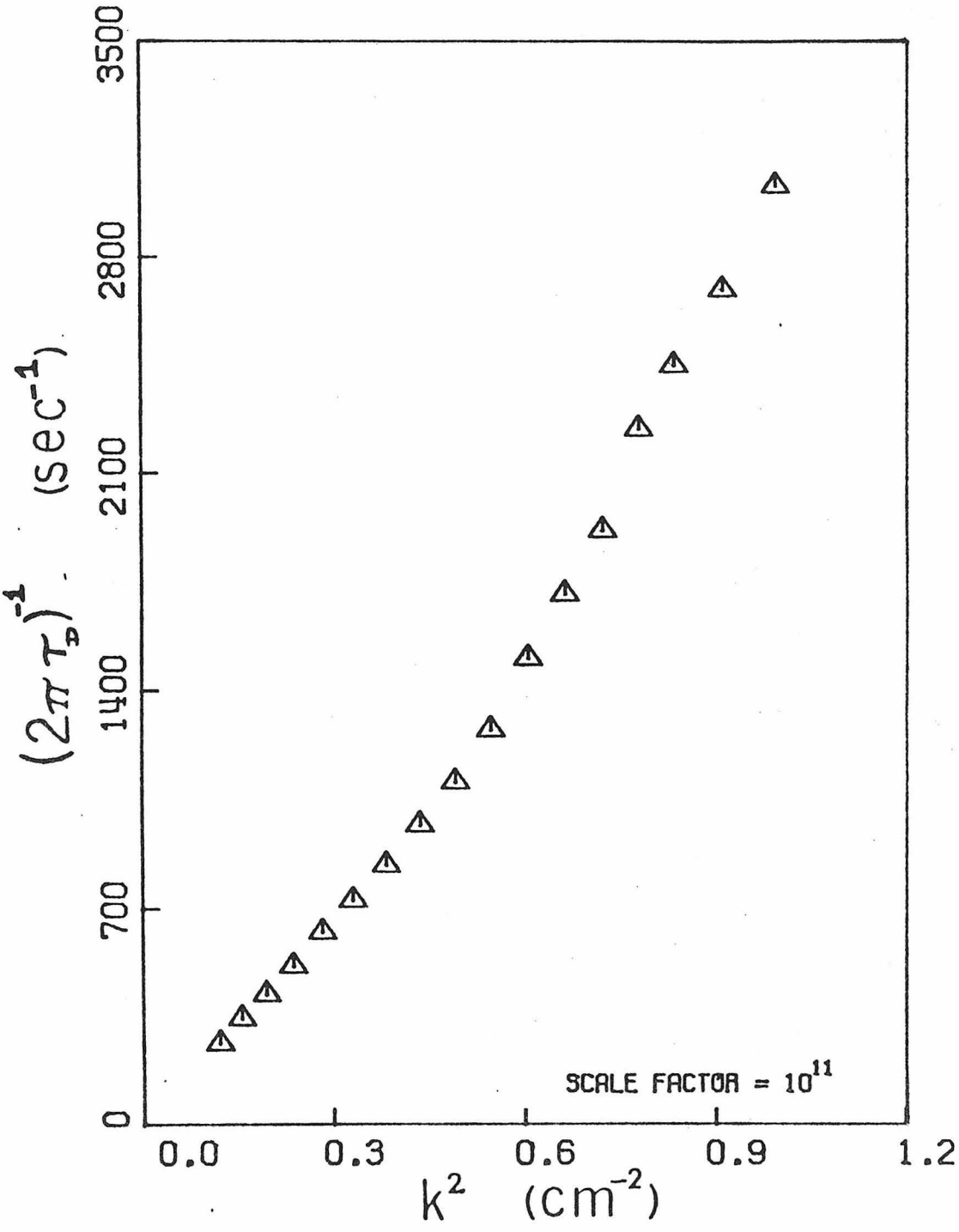

Fig. 12. The inverse decay time vs k^2 for the four million molecular weight polystyrene in cyclohexane (C = 431 μg/cc).

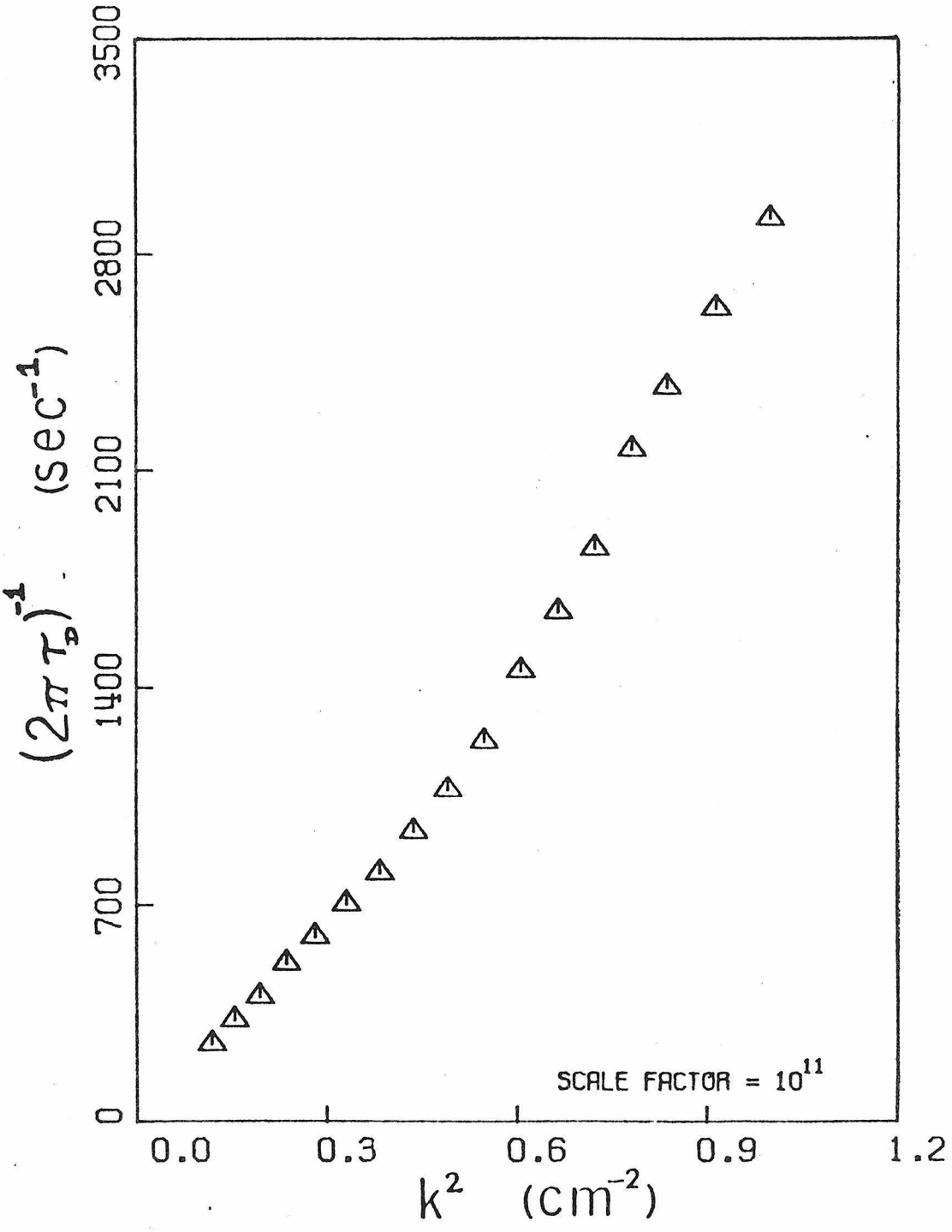

Fig. 13. The inverse decay time vs k^2 for the four million molecular weight polystyrene in cyclohexane (C = 307 μg/cc).

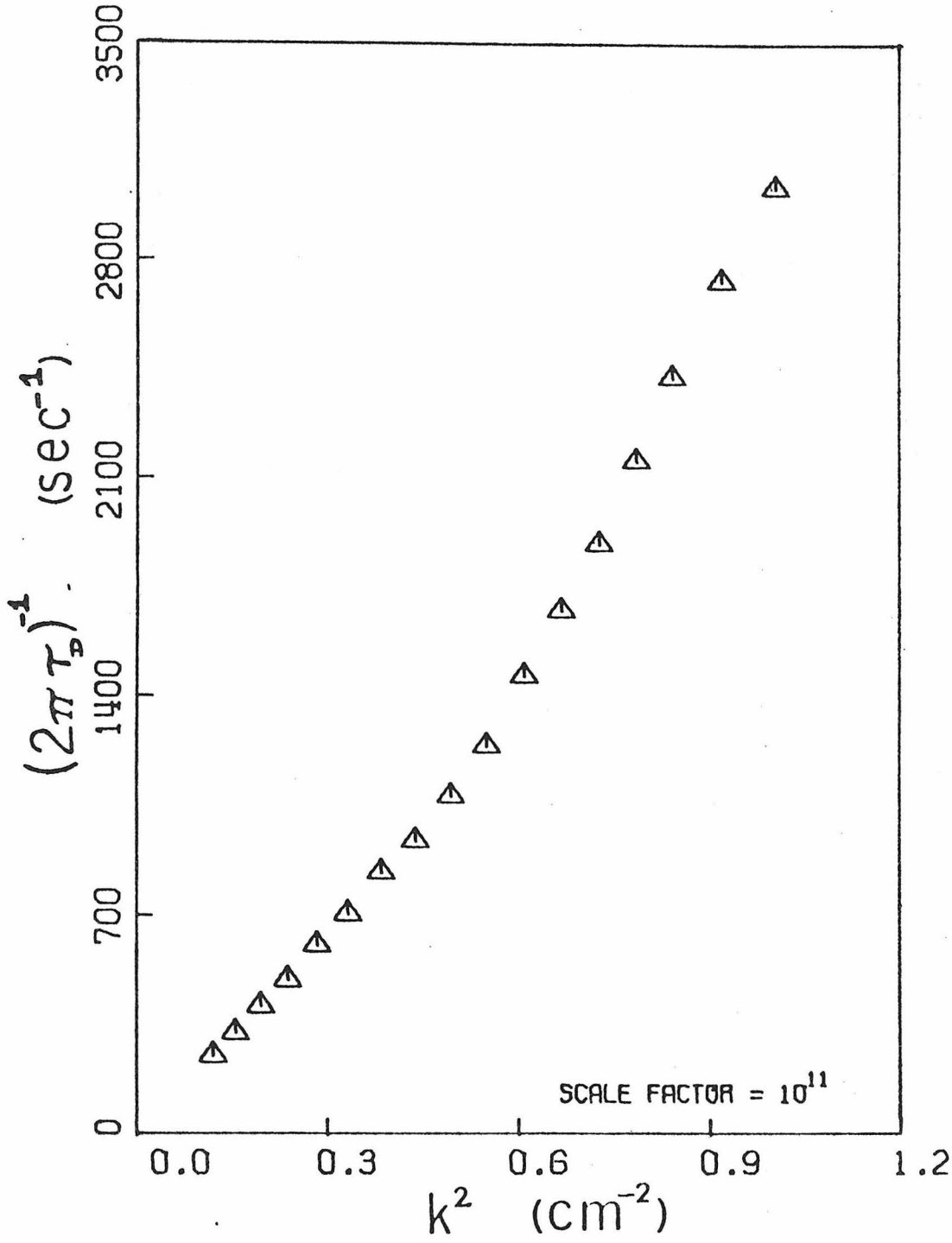

Fig. 14. The inverse decay time vs k^2 for the four million molecular weight polystyrene in cyclohexane (C = 198 μg/cc).

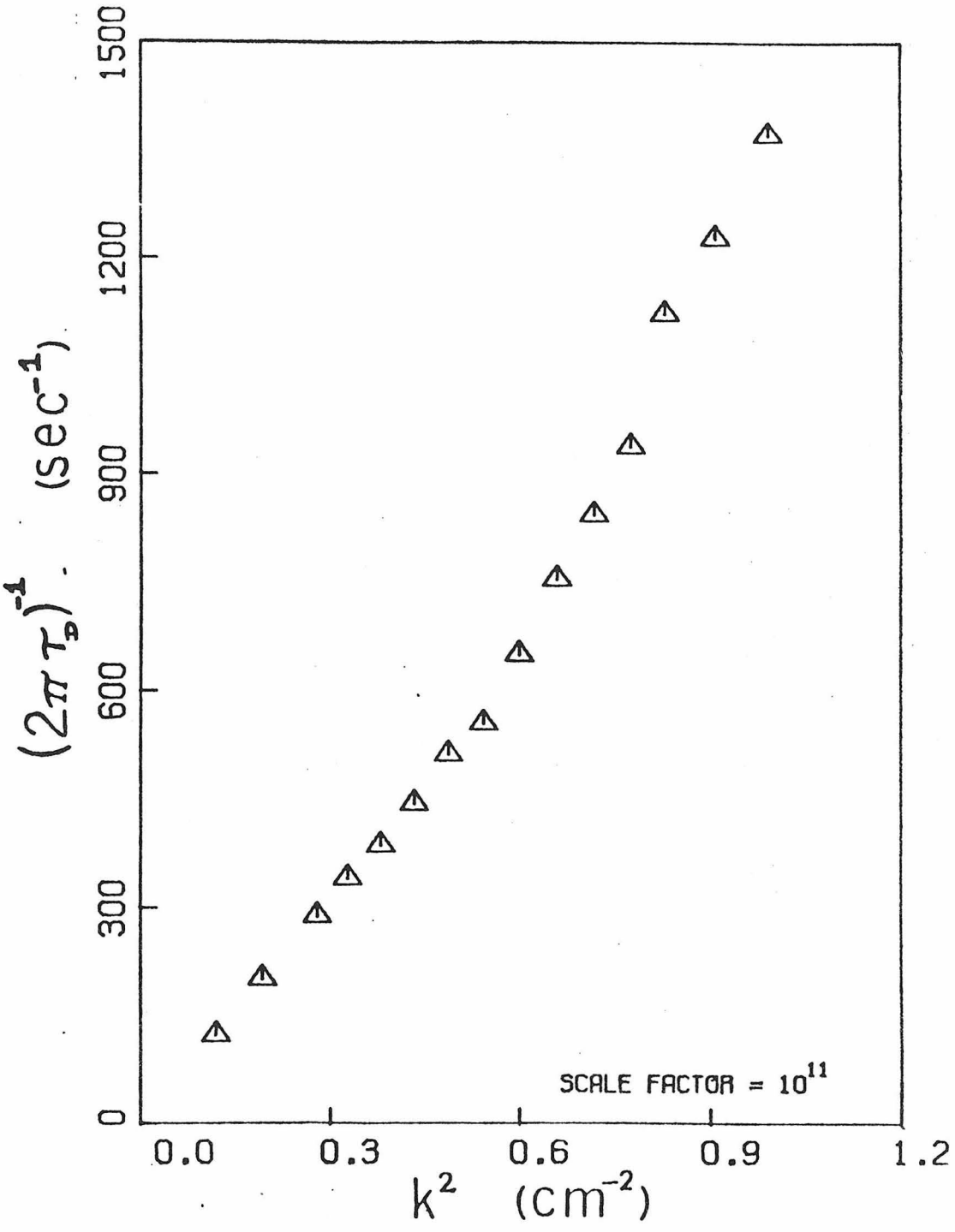

Fig. 15. The inverse decay time vs k^2 for the four million molecular weight polystyrene in diethylmalonate (C = 559 μg/cc).

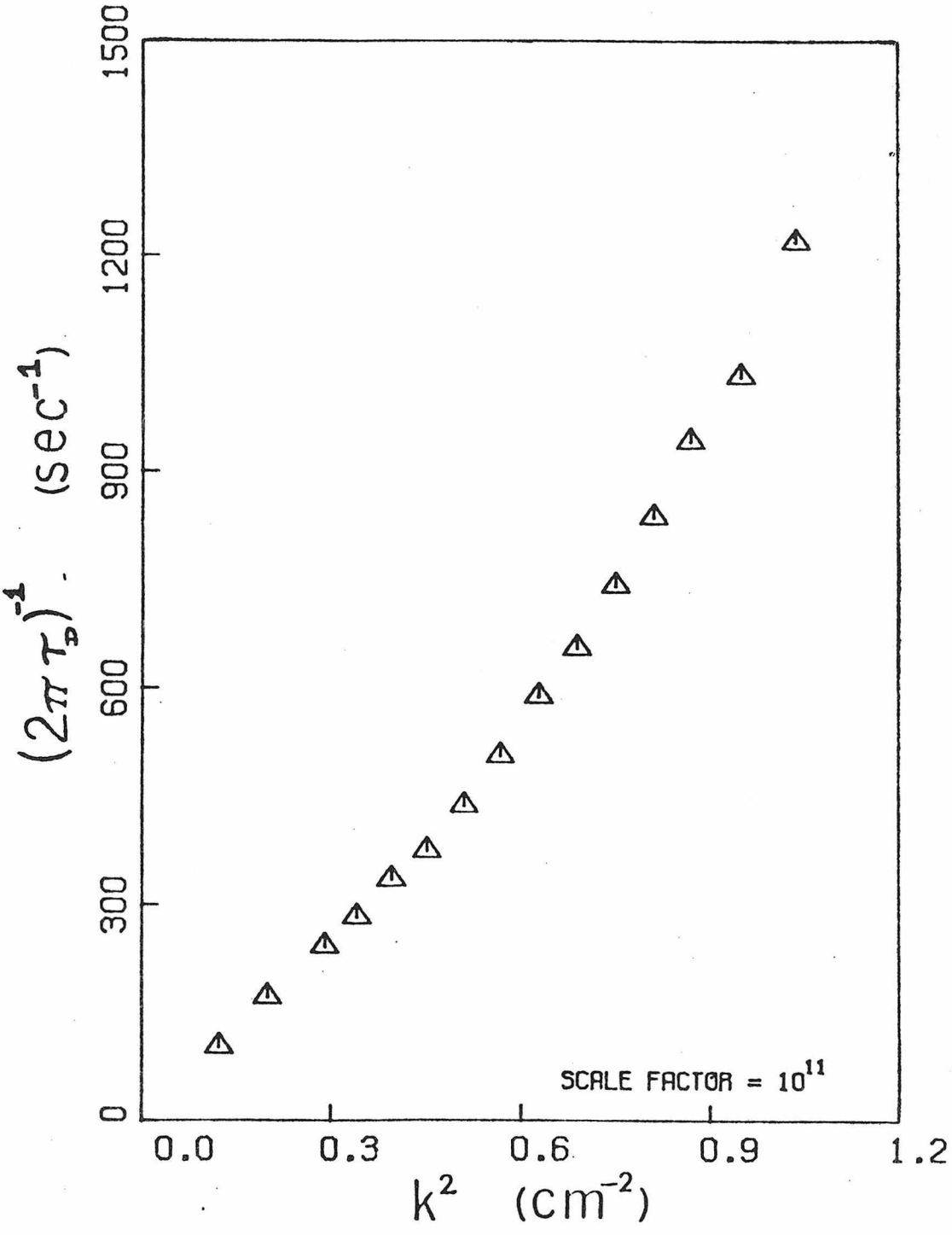

Fig. 16. The inverse decay time vs k^2 for the four million molecular weight polystyrene in 1-chloroundecane (C = 533 μg/cc).

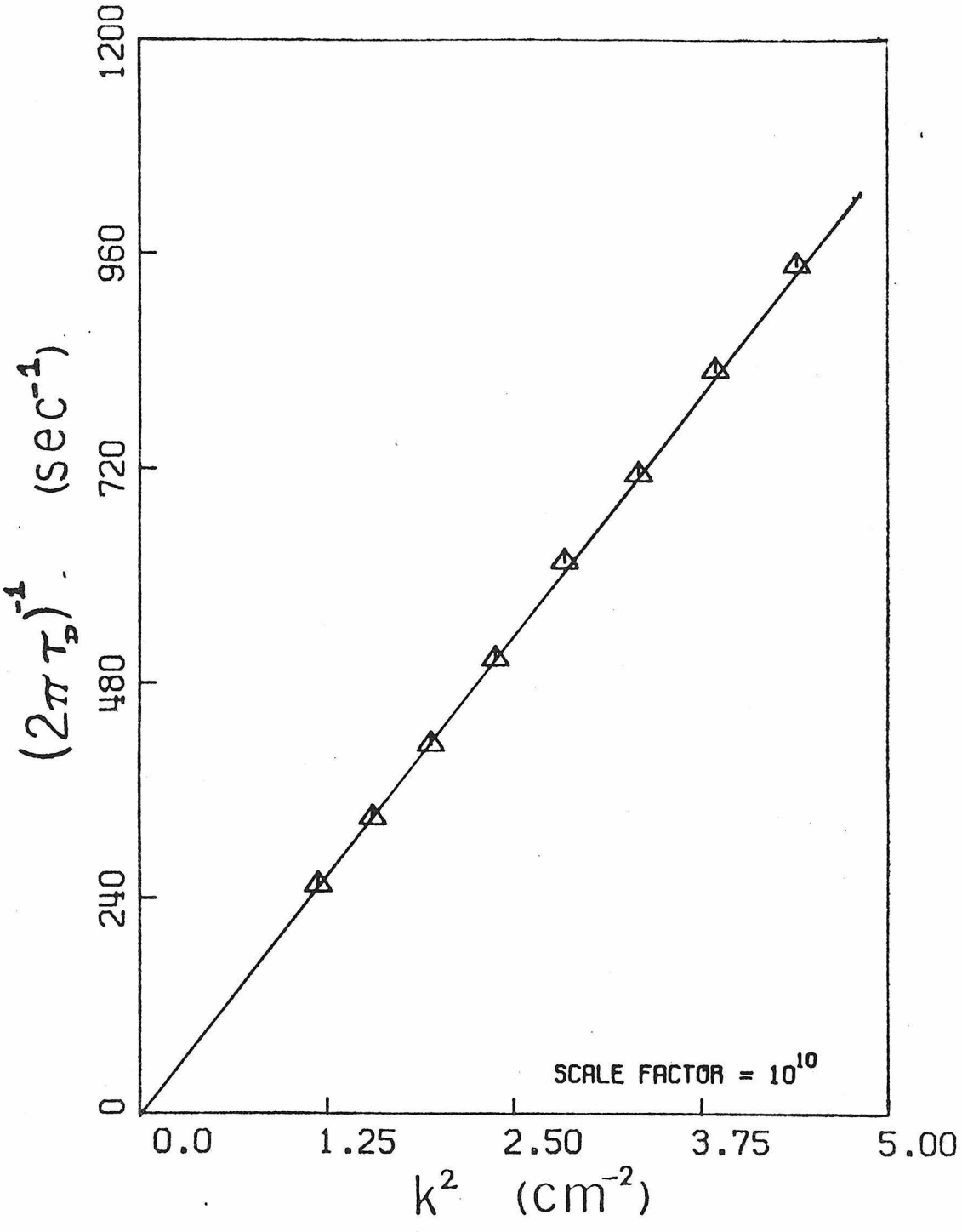

Fig. 17. The linear part of the inverse decay time vs k^2 plot for the four million molecular weight polystyrene in cyclohexane (C = 570 μg/cc).

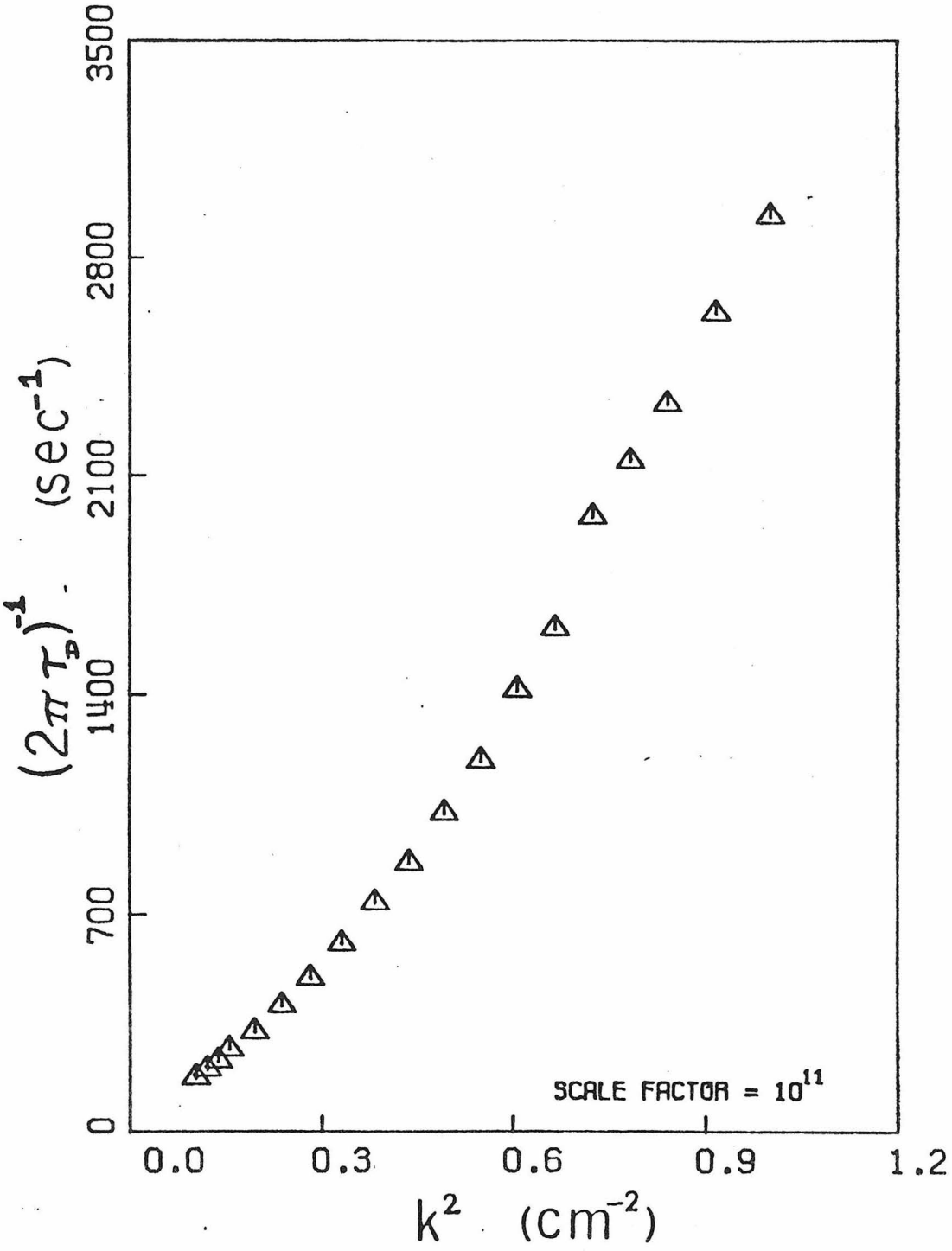

Fig. 18. The inverse decay time vs k^2 for seven million molecular weight polystyrene in cyclohexane (C = 322 μg/cc).

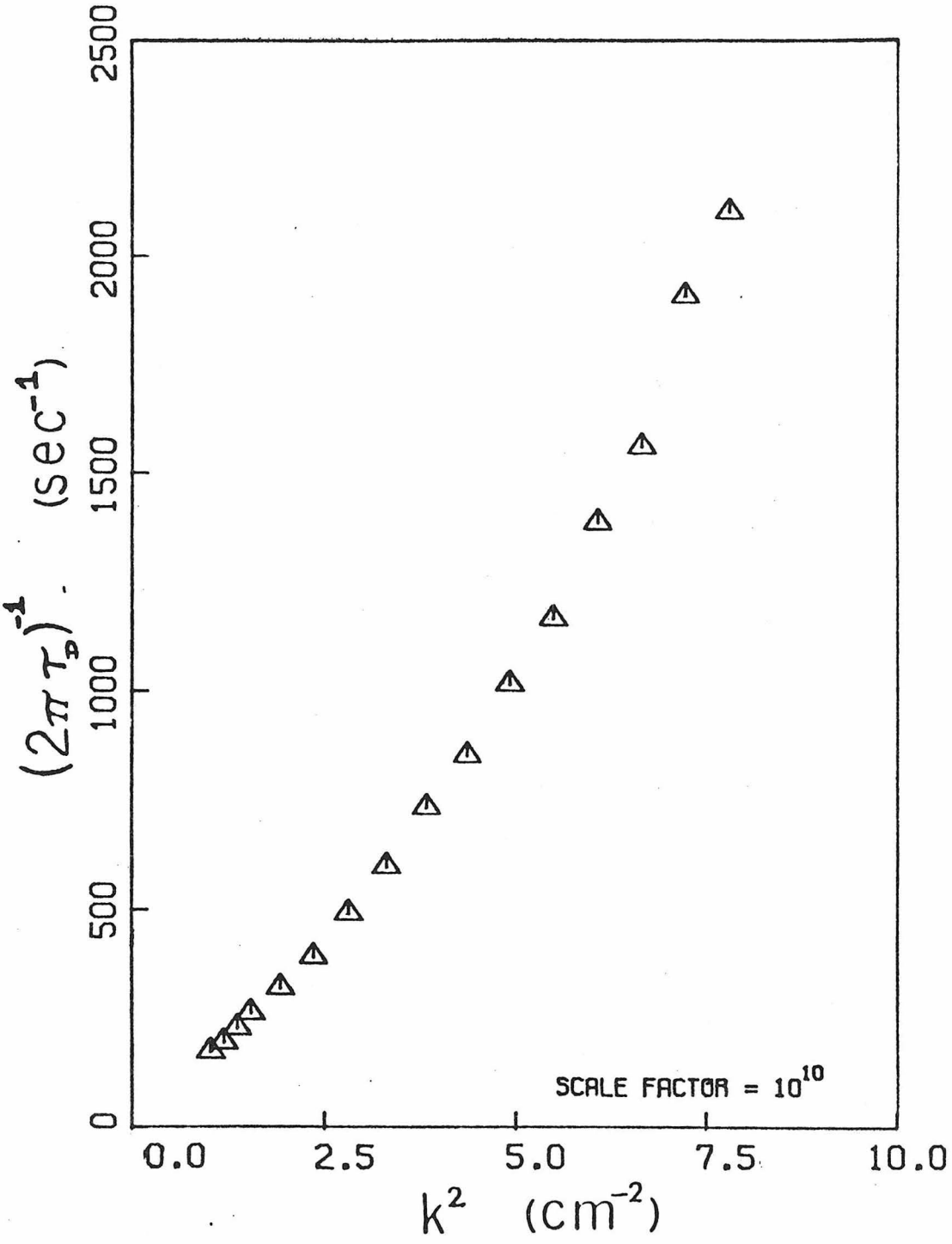

Fig. 19. The inverse decay time vs k^2 for seven million molecular weight polystyrene in cyclohexane (C = 245 μg/cc).

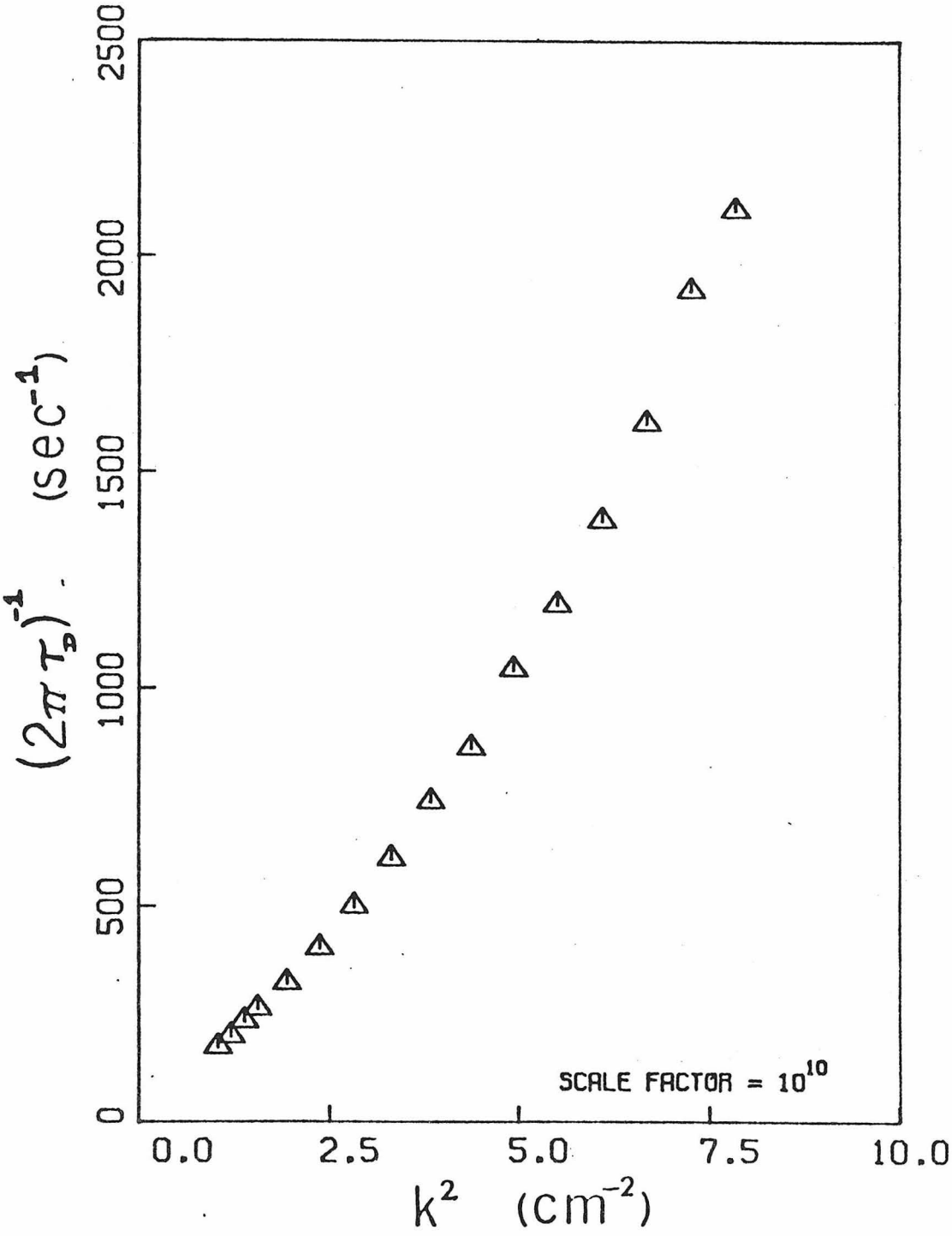

Fig. 20. The inverse decay time vs k^2 for seven million molecular weight polystyrene in cyclohexane (C = 176 μg/cc).

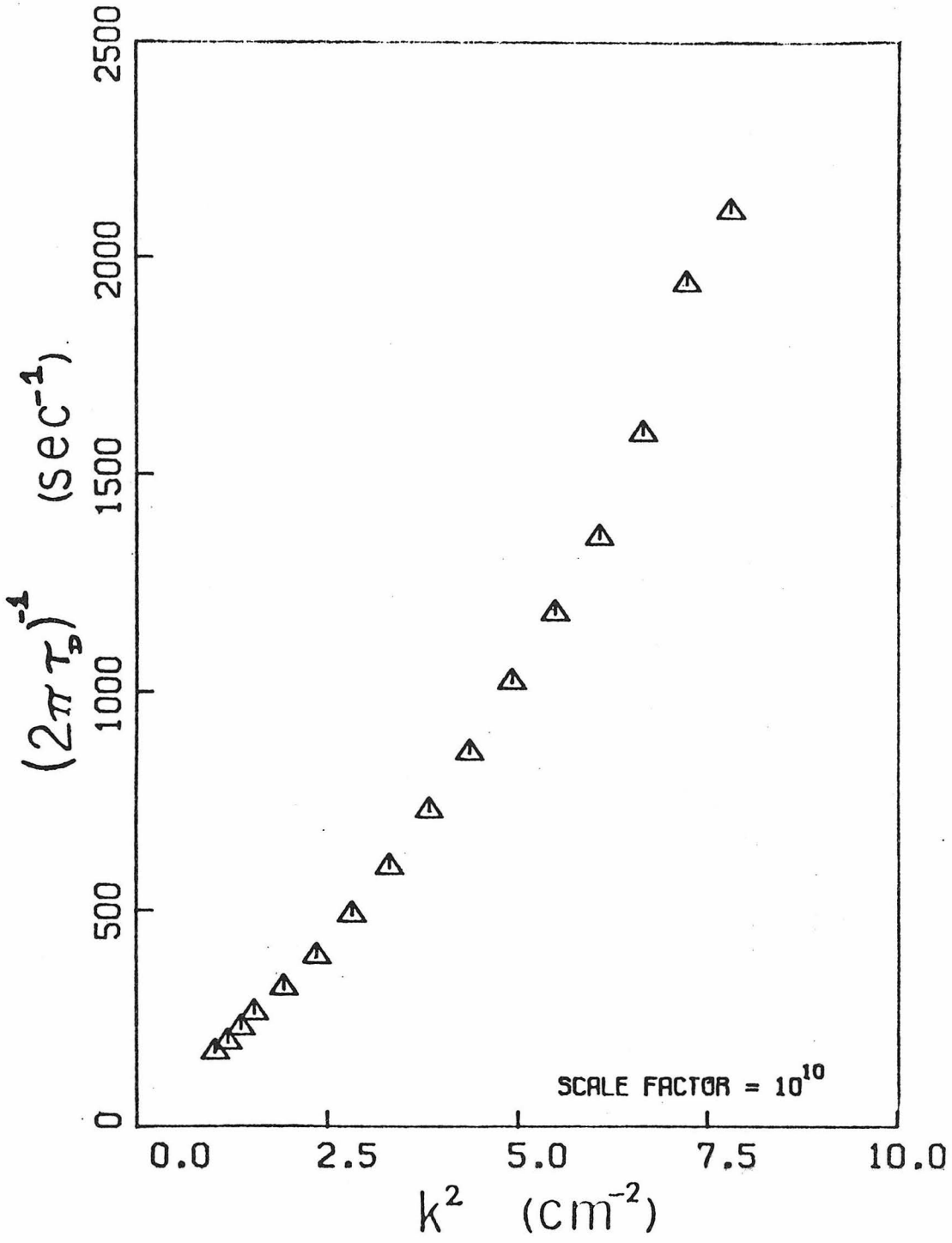

Fig. 21. The inverse decay time vs k^2 for seven million molecular weight polystyrene in cyclohexane (C = 115 μg/cc).

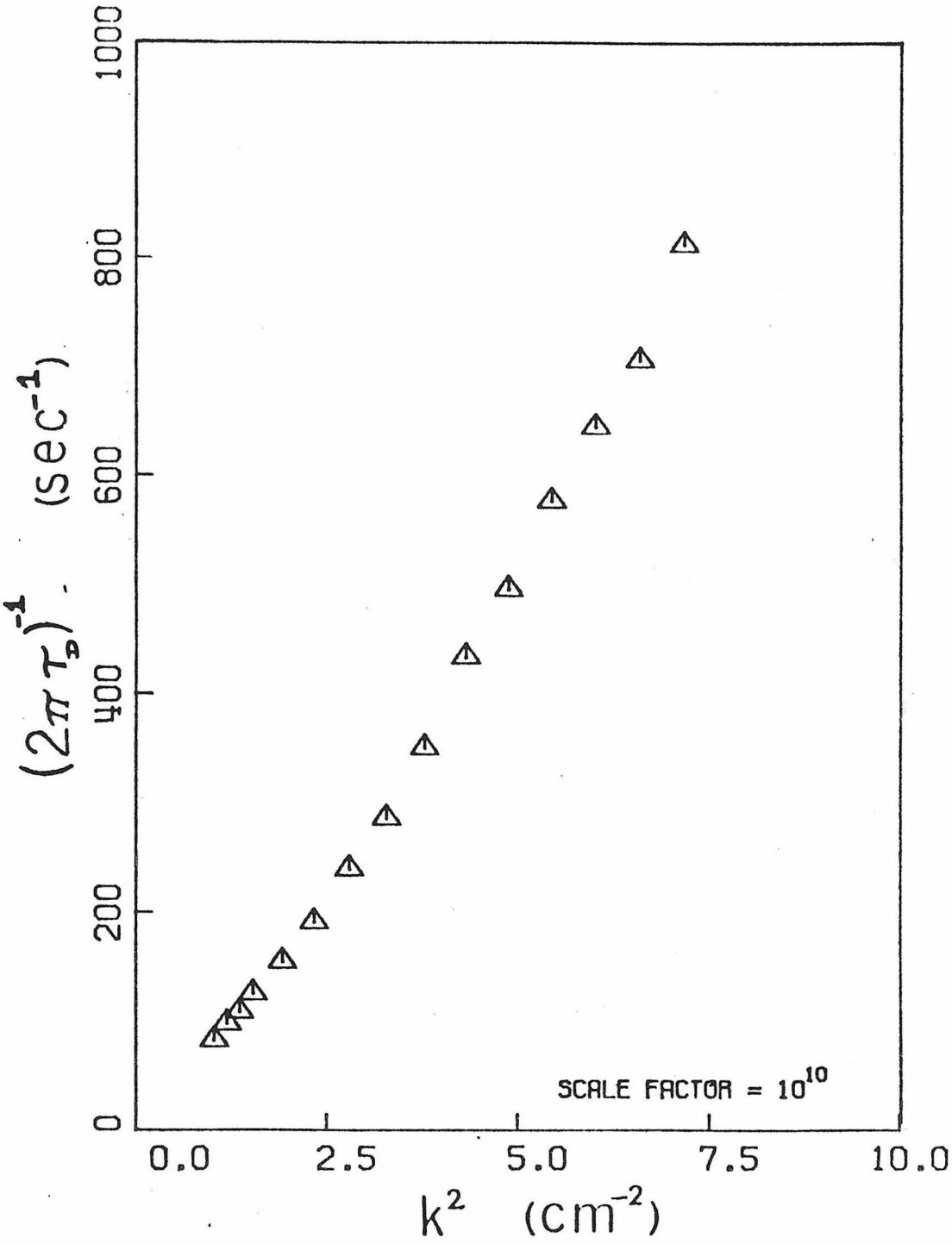

Fig. 22. The inverse decay time vs k^2 for seven million molecular weight polystyrene in diethylmalonate (C = 301 μg/cc).

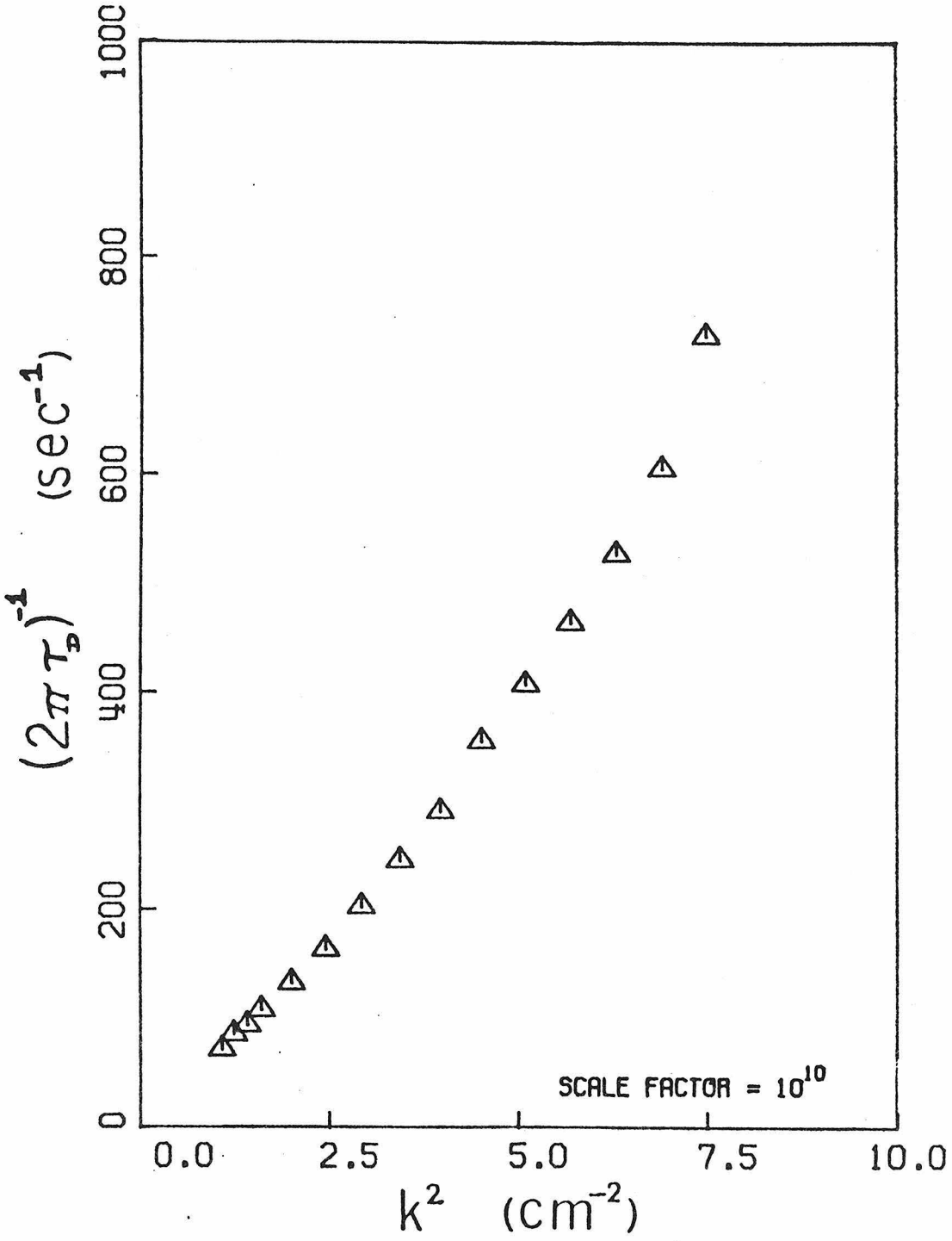

Fig. 23. The inverse decay time vs k^2 for seven million molecular weight polystyrene in 1-chloroundecane (C = 344 μg/cc).

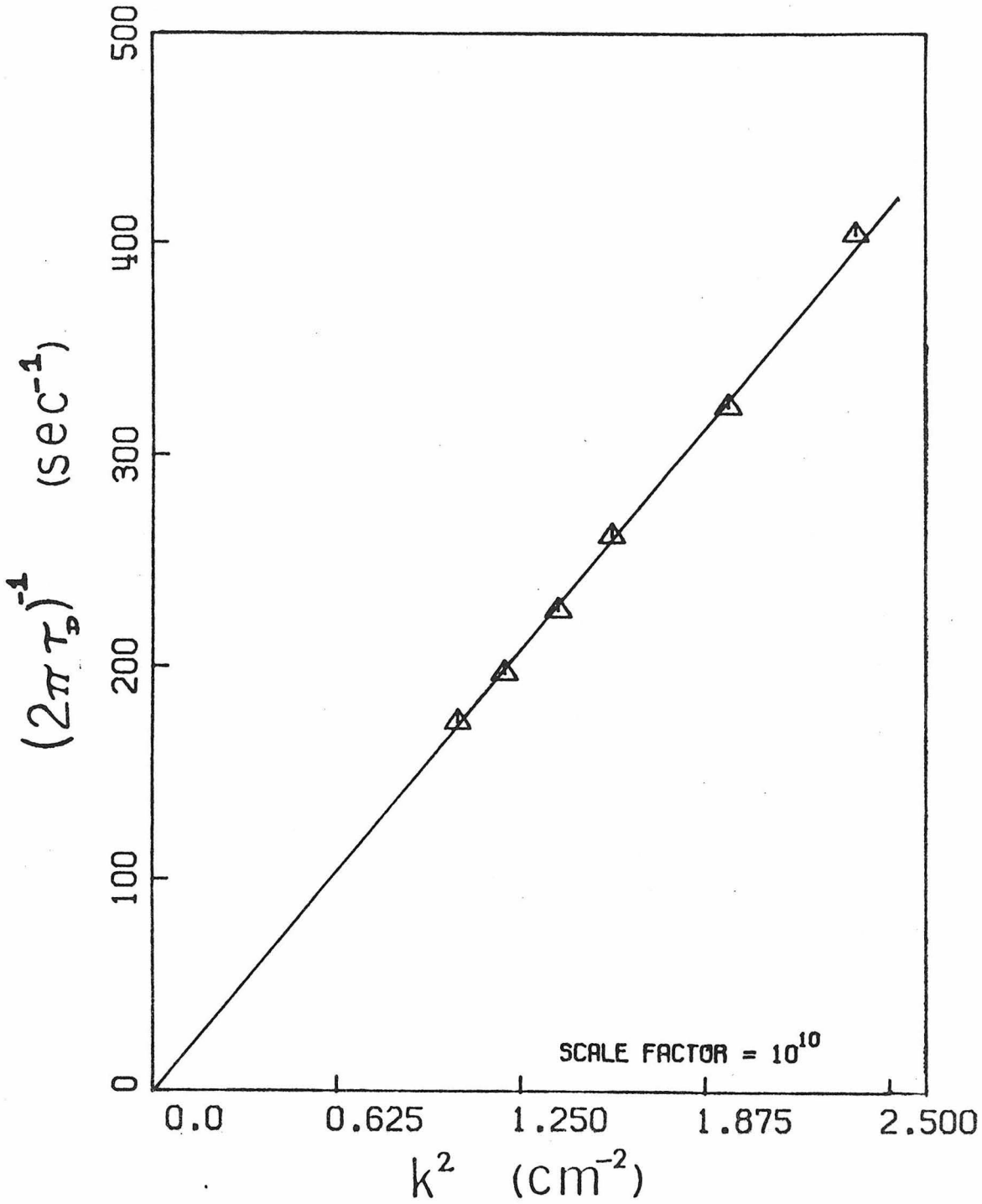

Fig. 24. The linear part of the inverse decay time vs k^2 plot for the seven million molecular weight polystyrene in cyclohexane (C = 322 μg/cc).

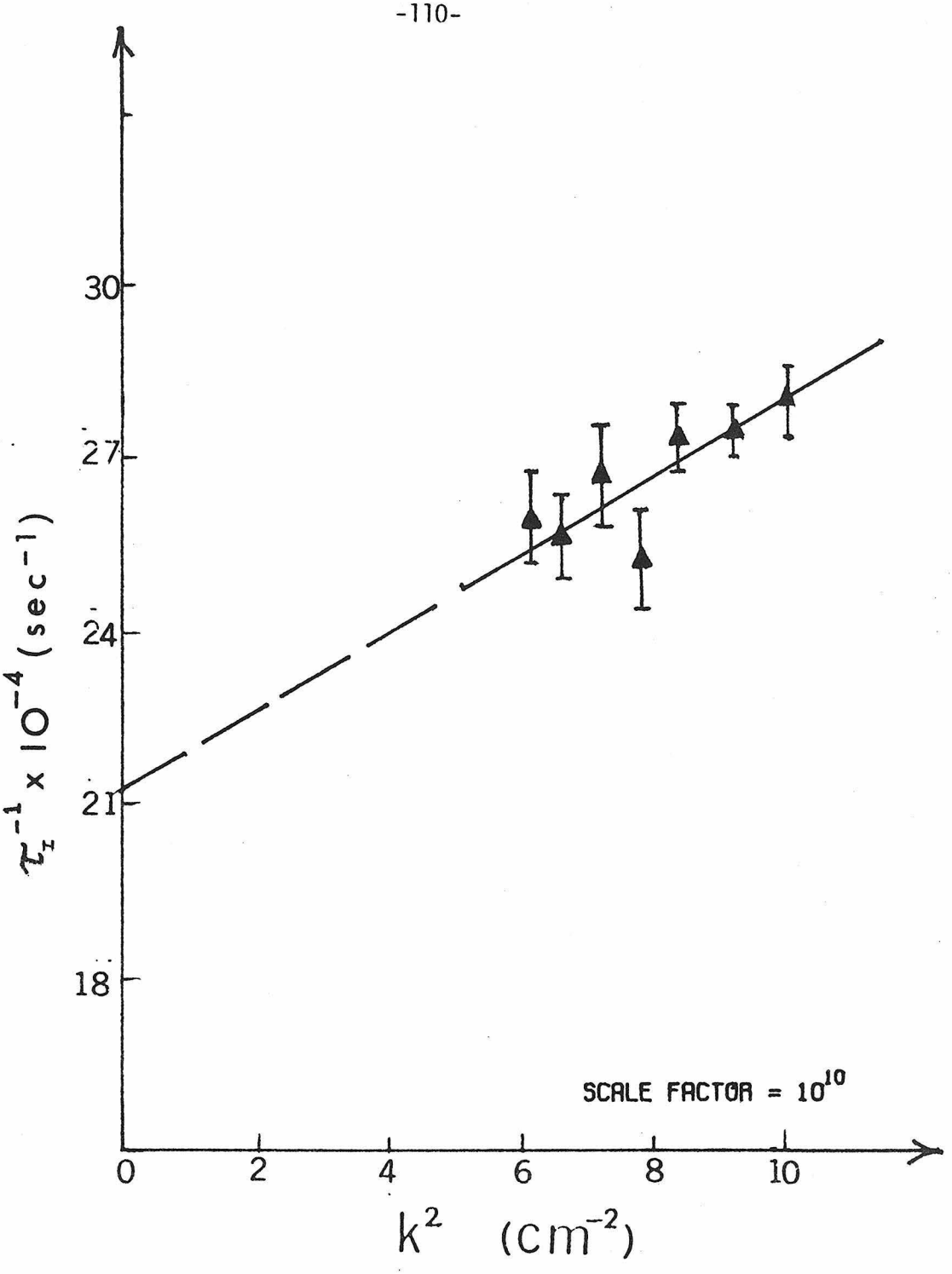

Fig. 25. τ_I^{-1} vs k^2 for the four million molecular weight polystyrene in cyclohexane. (C = 570 μg/cc).

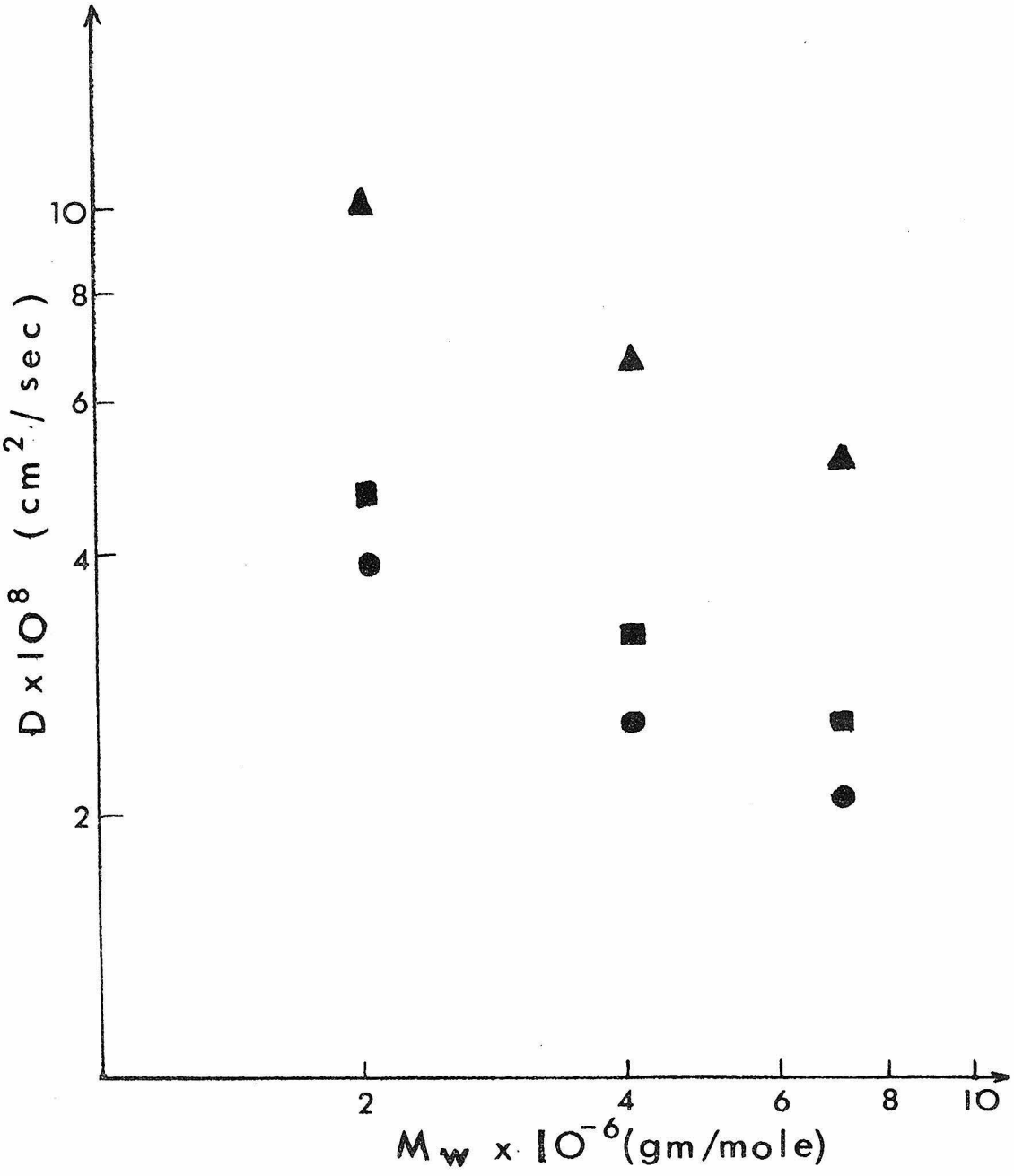

Fig. 26. The diffusion coefficients vs the molecular weight M_w. (▲) solutions in cyclohexane, (■) solutions in diethylmalonate, (●) solutions in 1-chloroundecane.

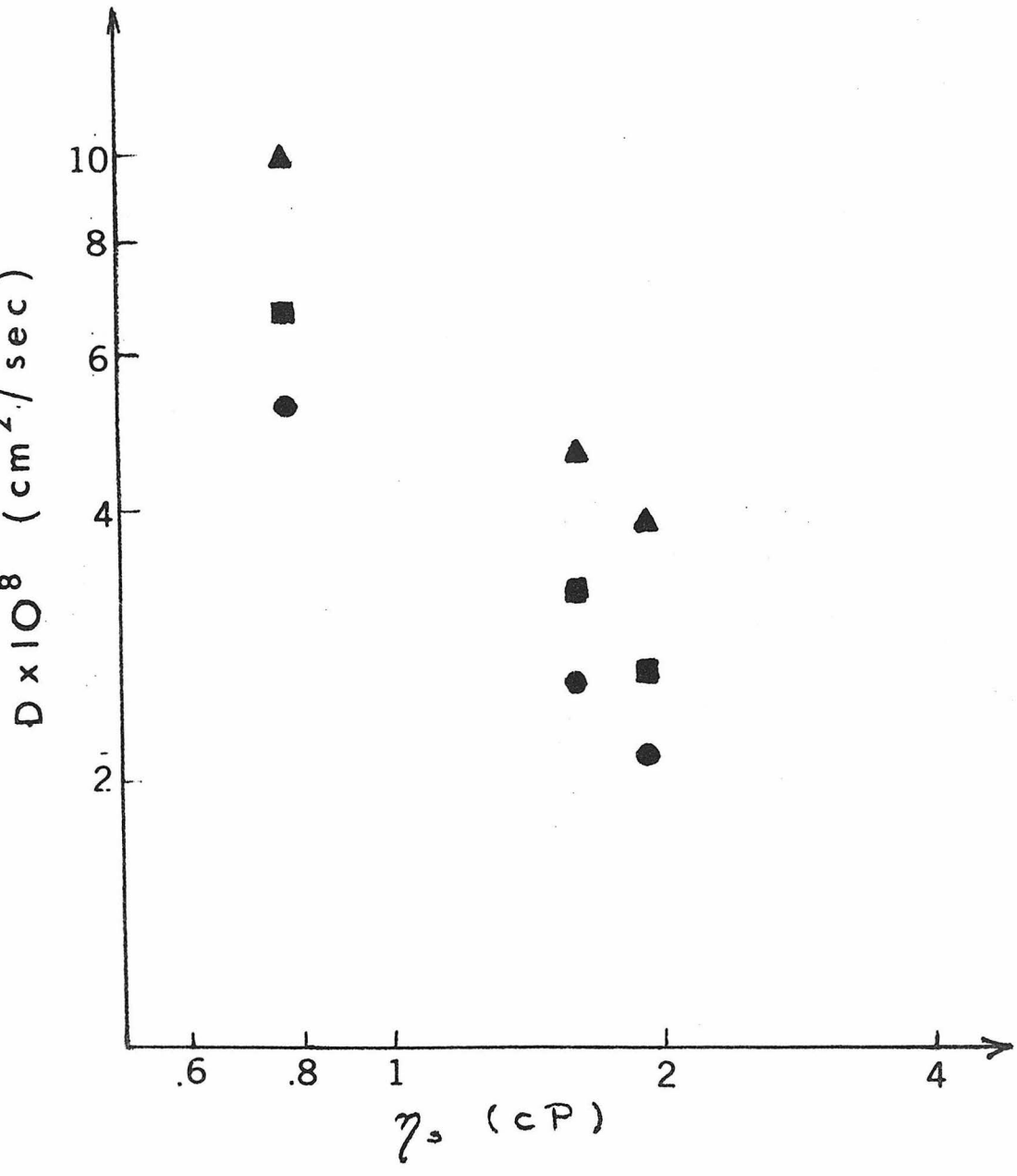

Fig. 27. The diffusion coefficients vs the solvent viscosity η_s. (△) MW = 2×10^6, (□) MW = 4.1×10^6, (o) MW = 7.1×10^6.

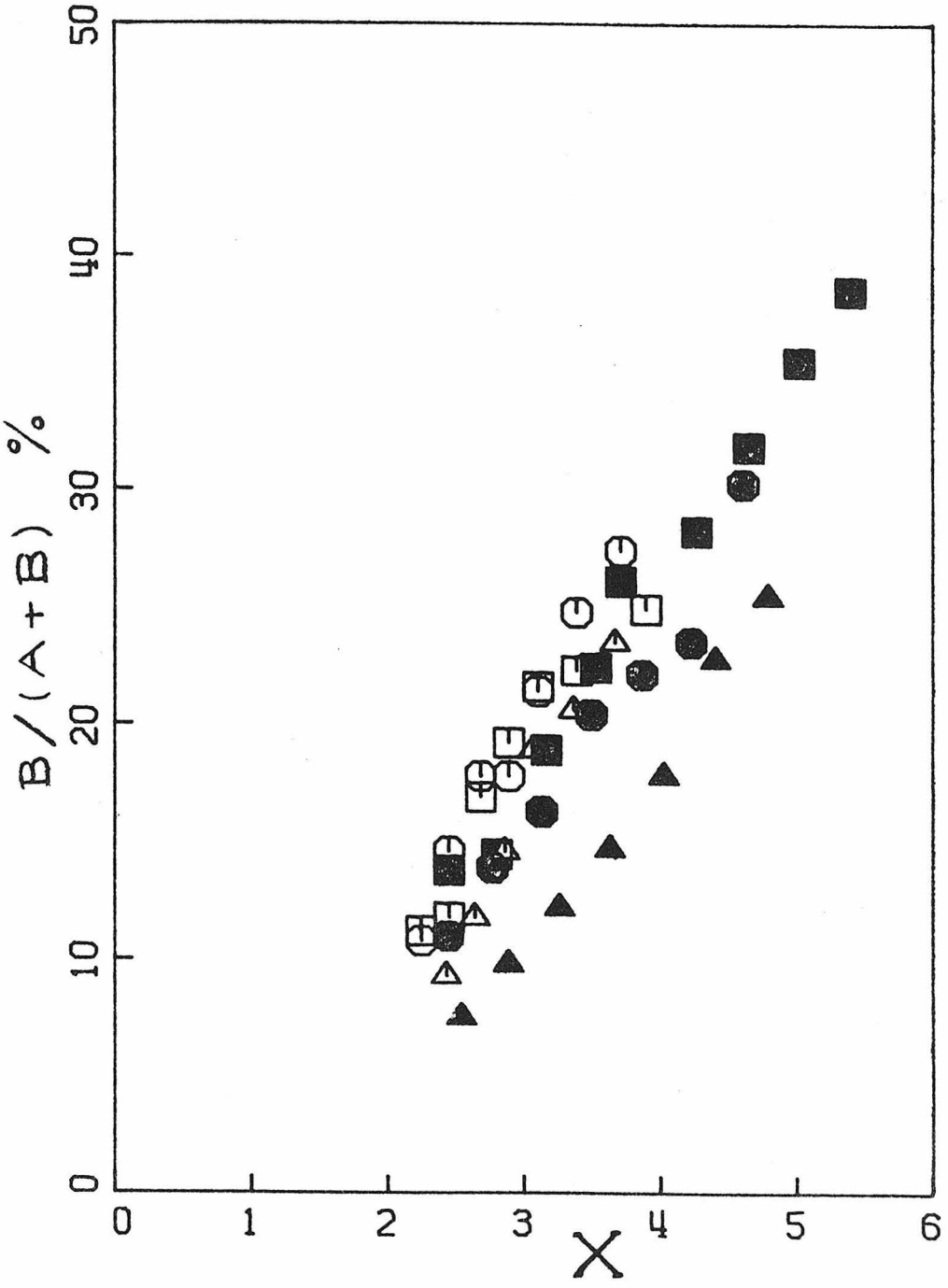

Fig. 28. The ratio A/(A+B) vs x: (□) in cyclohexane, (○) in diethylmalonate, (△) in 1-chloroundecane. The open symbols are for $M_w = 4.1 \times 10^2$, the filled ones are for $M_w = 7.1 \times 10^6$.

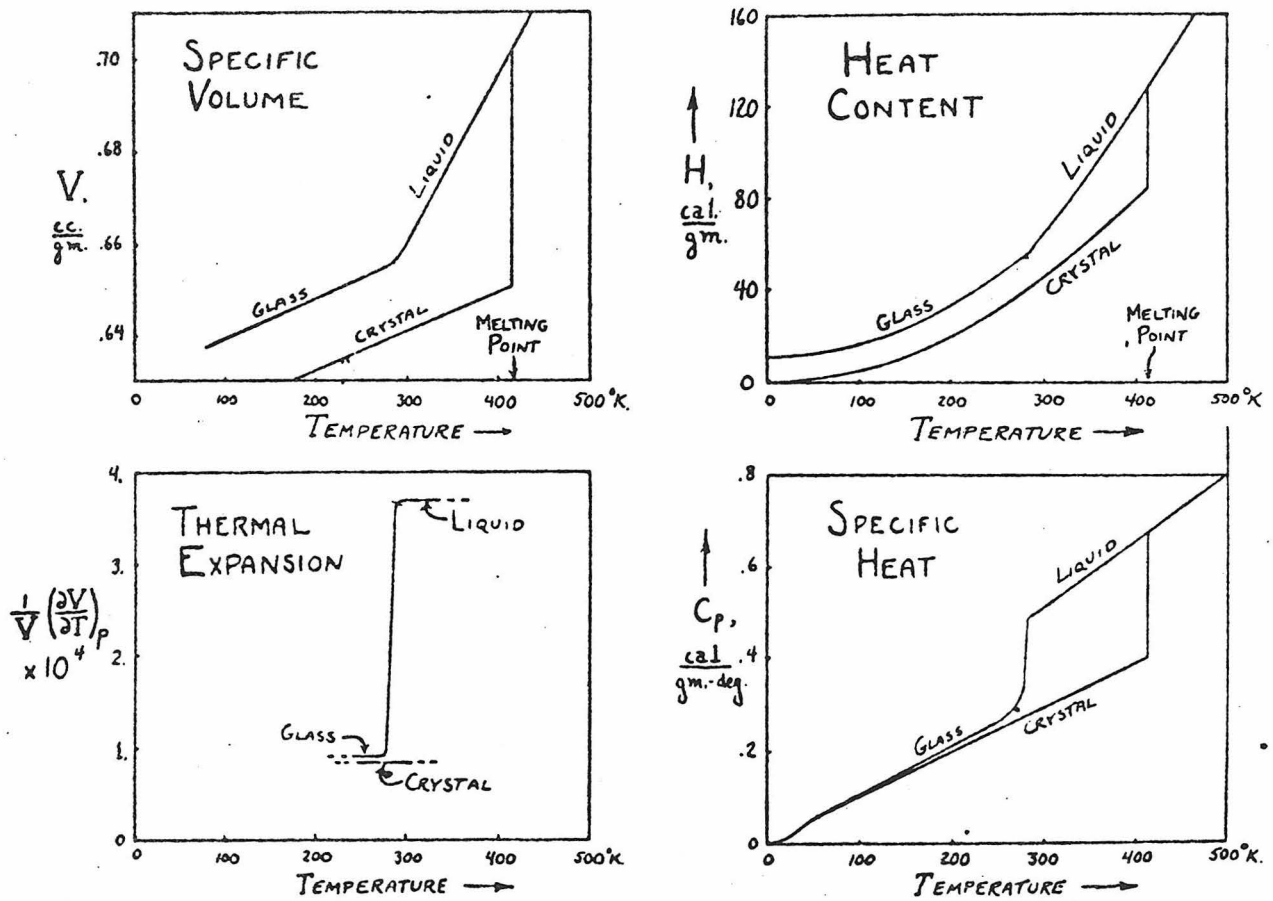

Fig. 29 Thermodynamic properties of glucose around glass transition temperature (from Kauzmann, 1948)

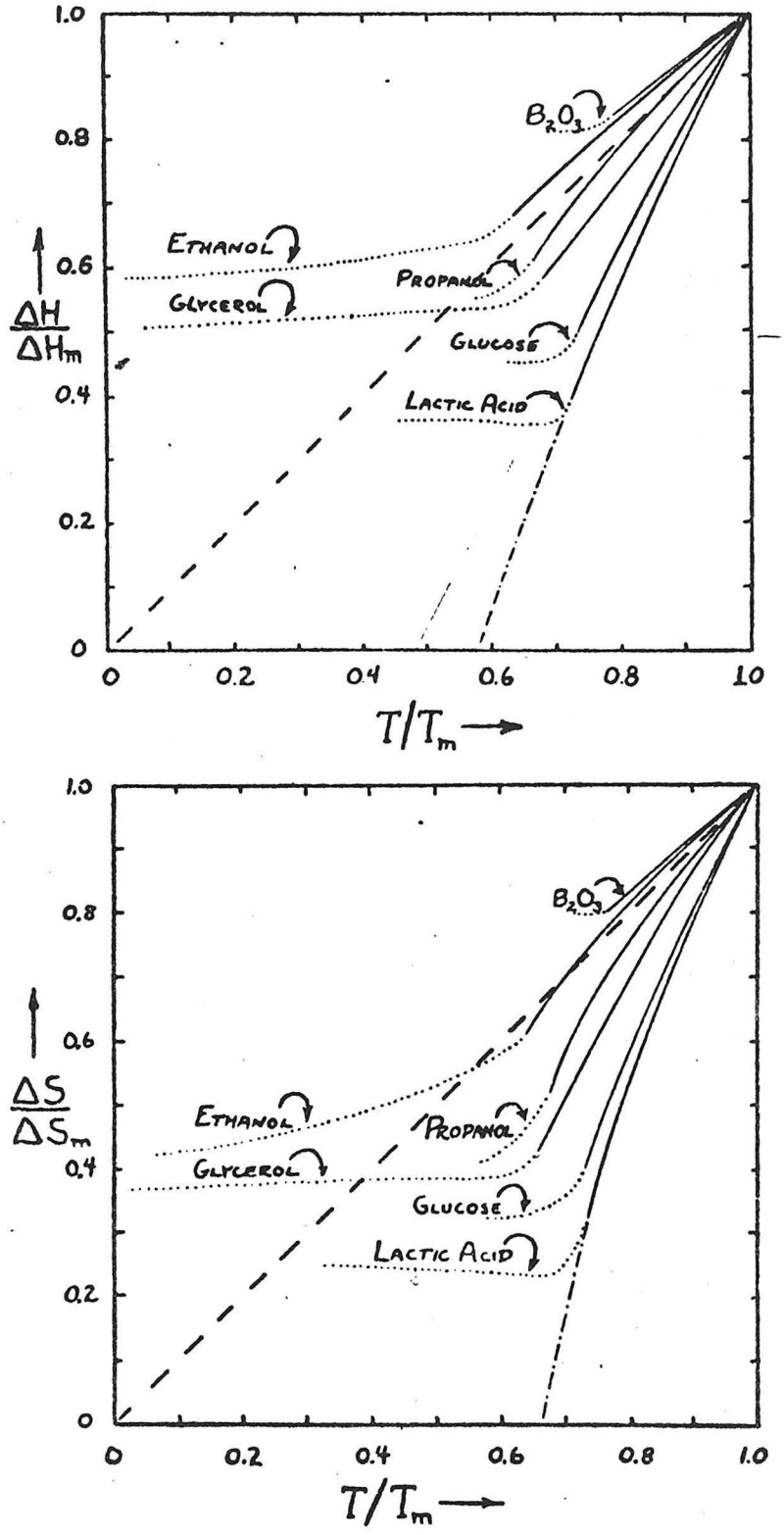

Fig. 30 Excess (that over the crystalline solid) heat content and entropy. —— normal supercooled liquid, ---- glassy state.

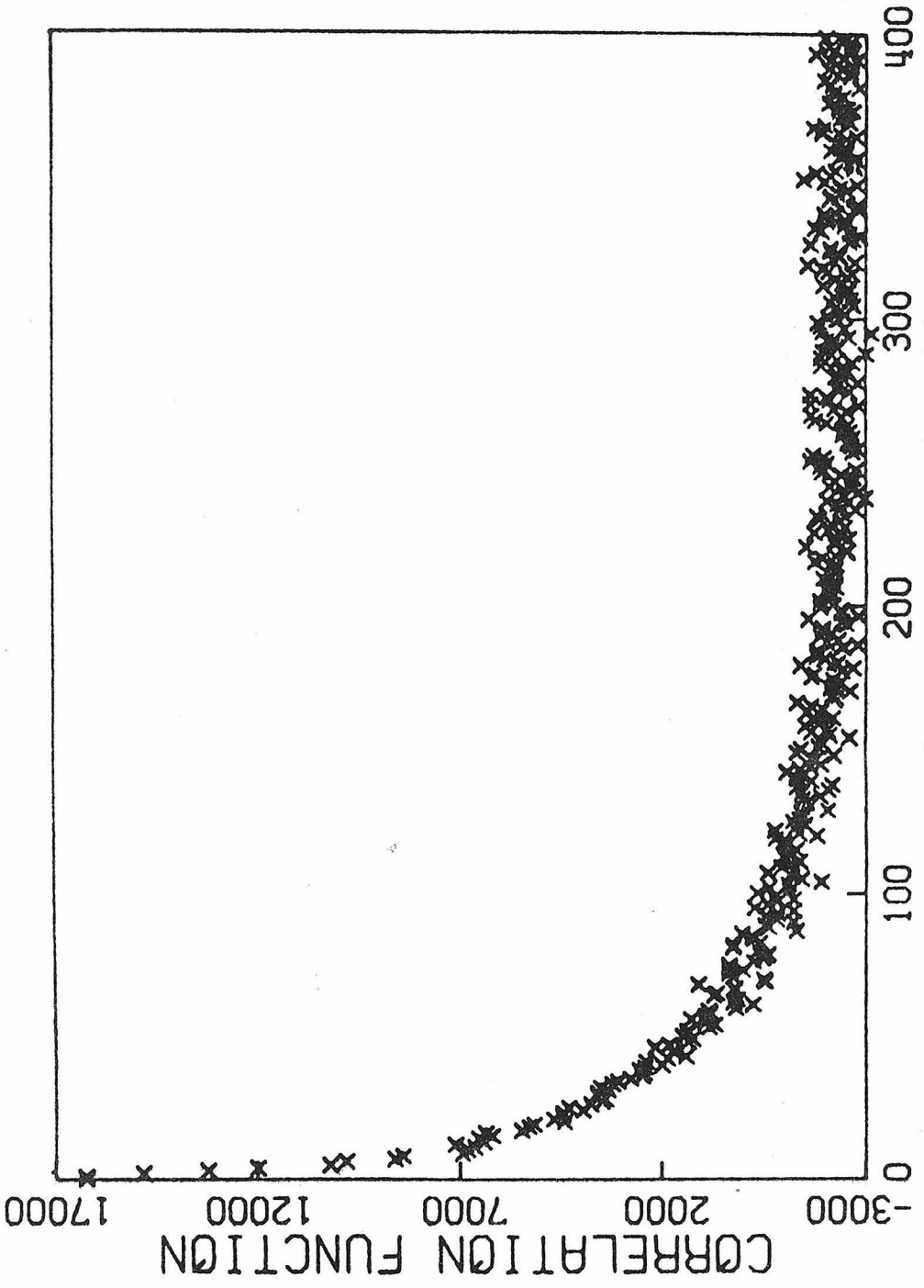

Fig. 31a Correlation function at 20°C, θ = 130° with the correlator increment time t= 1 msec

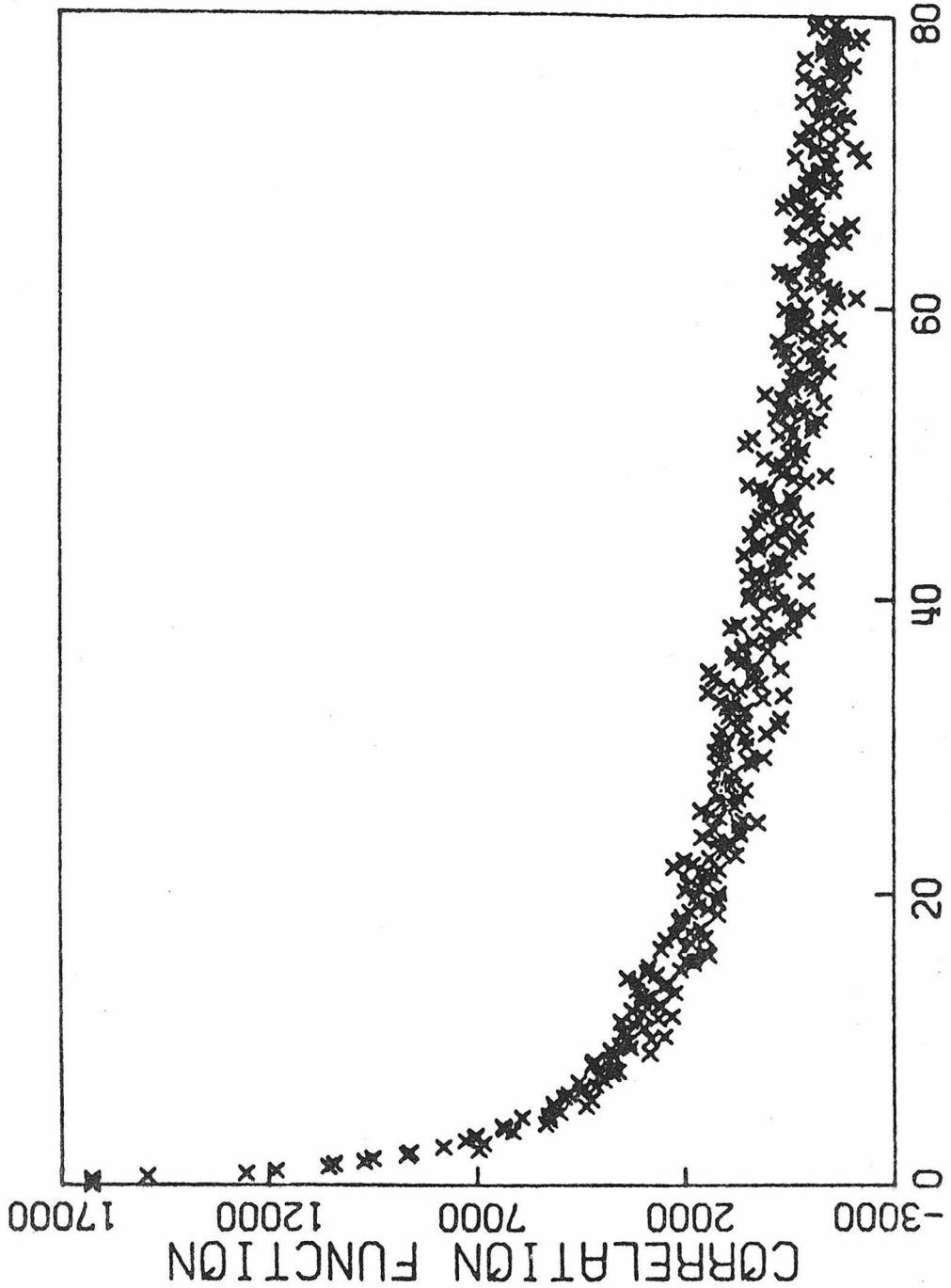

Fig. 31b Correlation function of Fig. 31a repeated with the correlator increment time t = 200 μsec

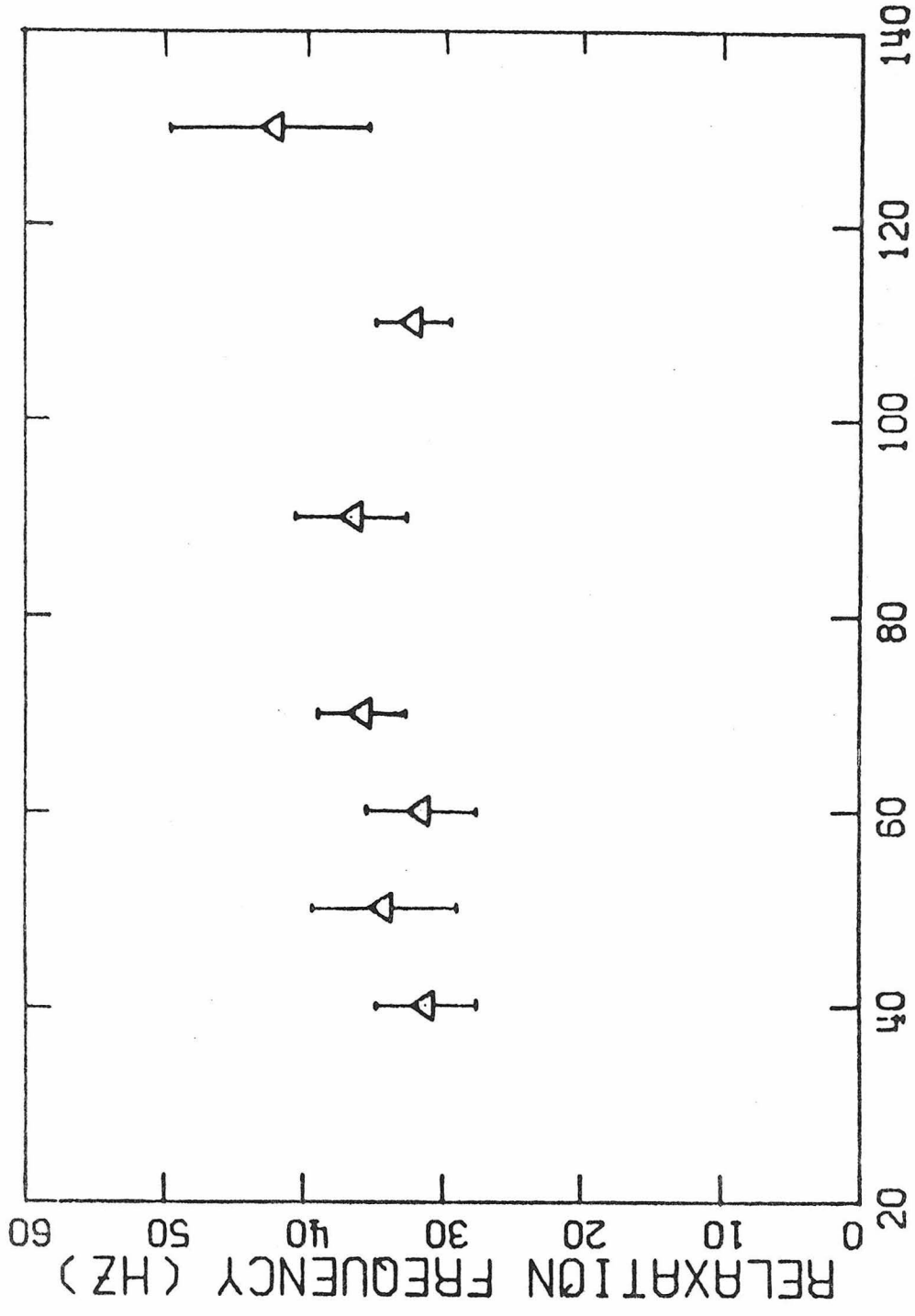

Fig. 32a Angular dependence of the high frequency relaxation performed on the same position of a sample at 20°C

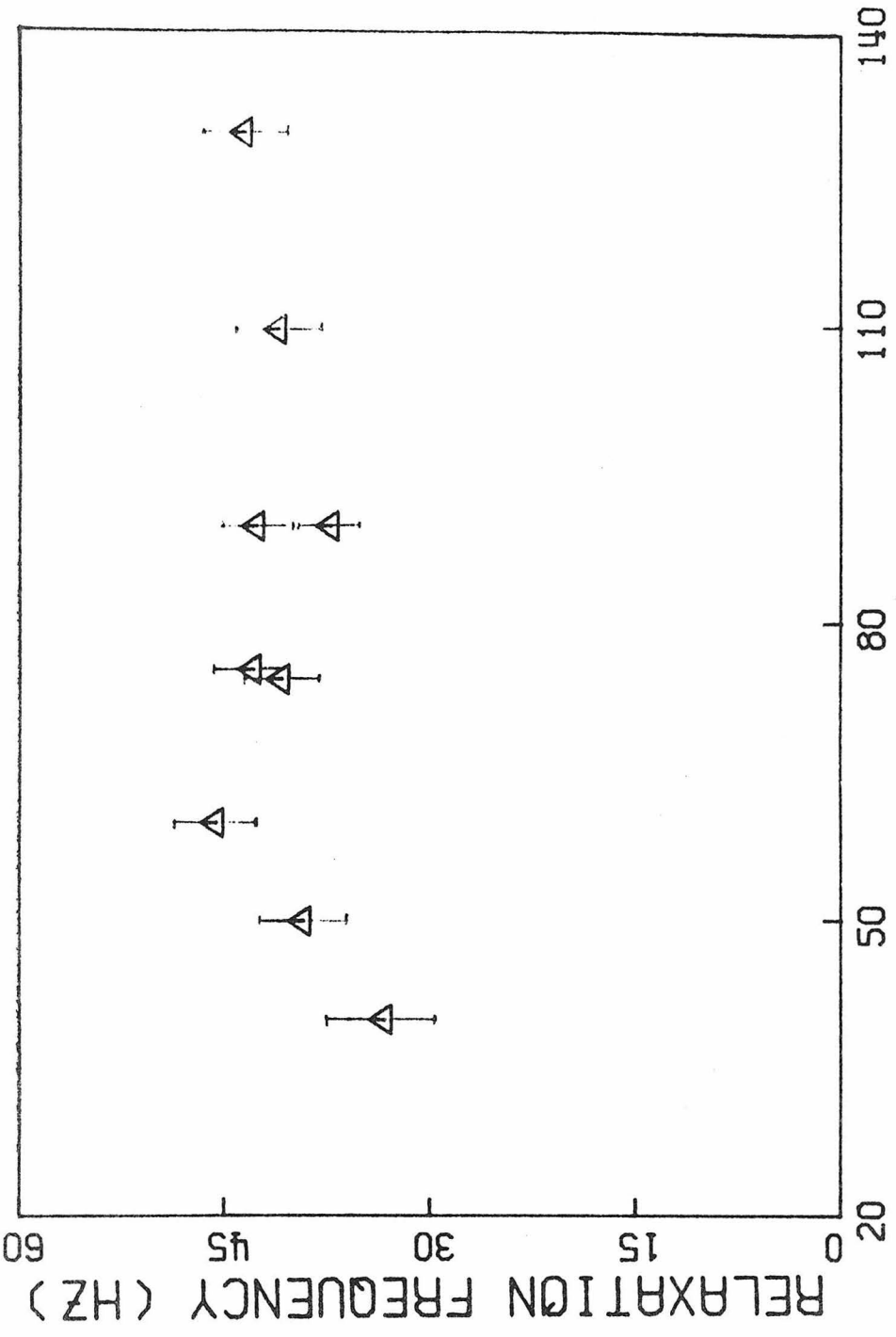

Fig. 32b Angular dependence of the high frequency relaxation performed on various positions of a sample at 20°C

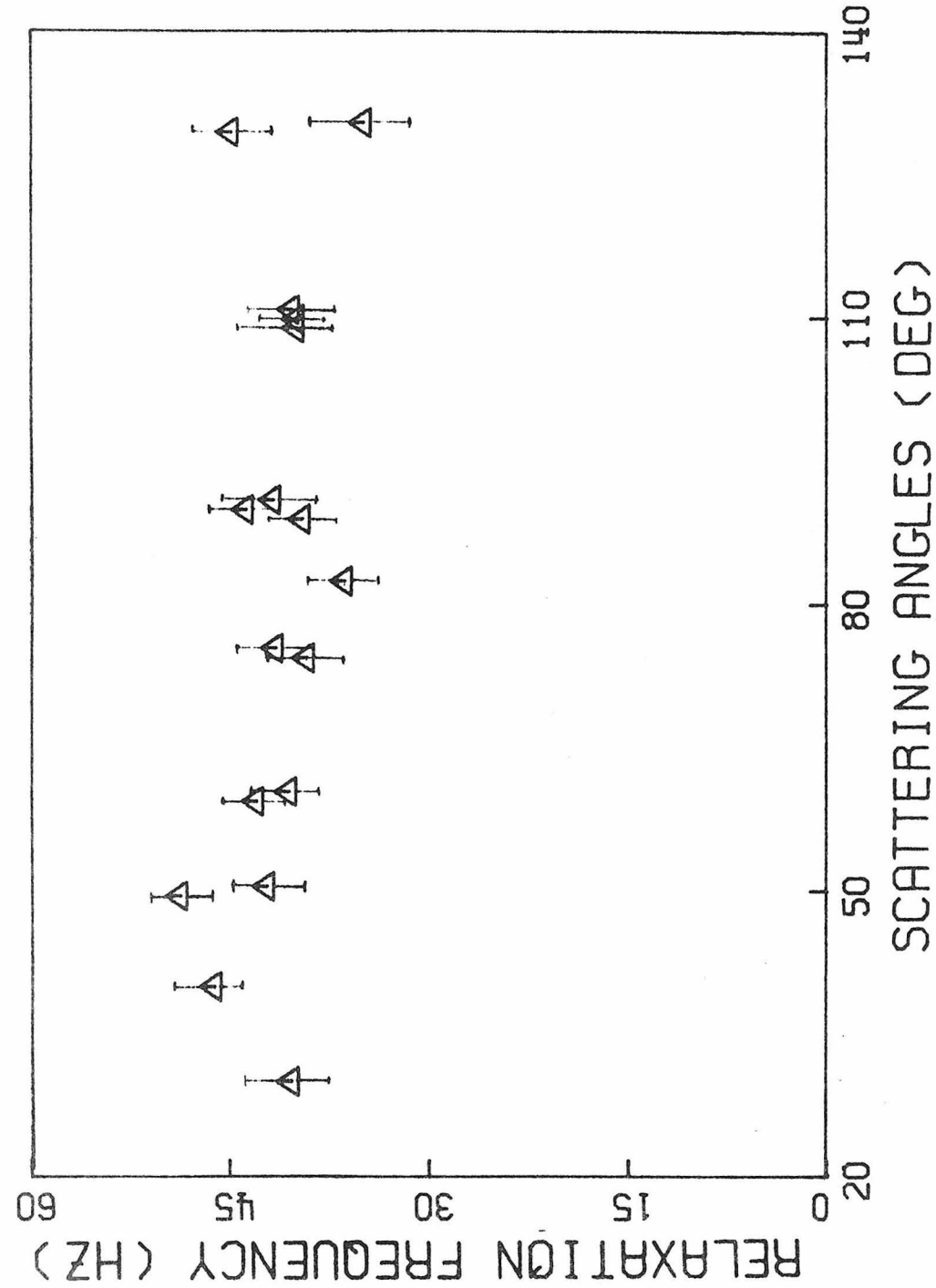

Fig. 33 Angular dependence of the high frequency relaxation performed on various positions of a sample at 40°C

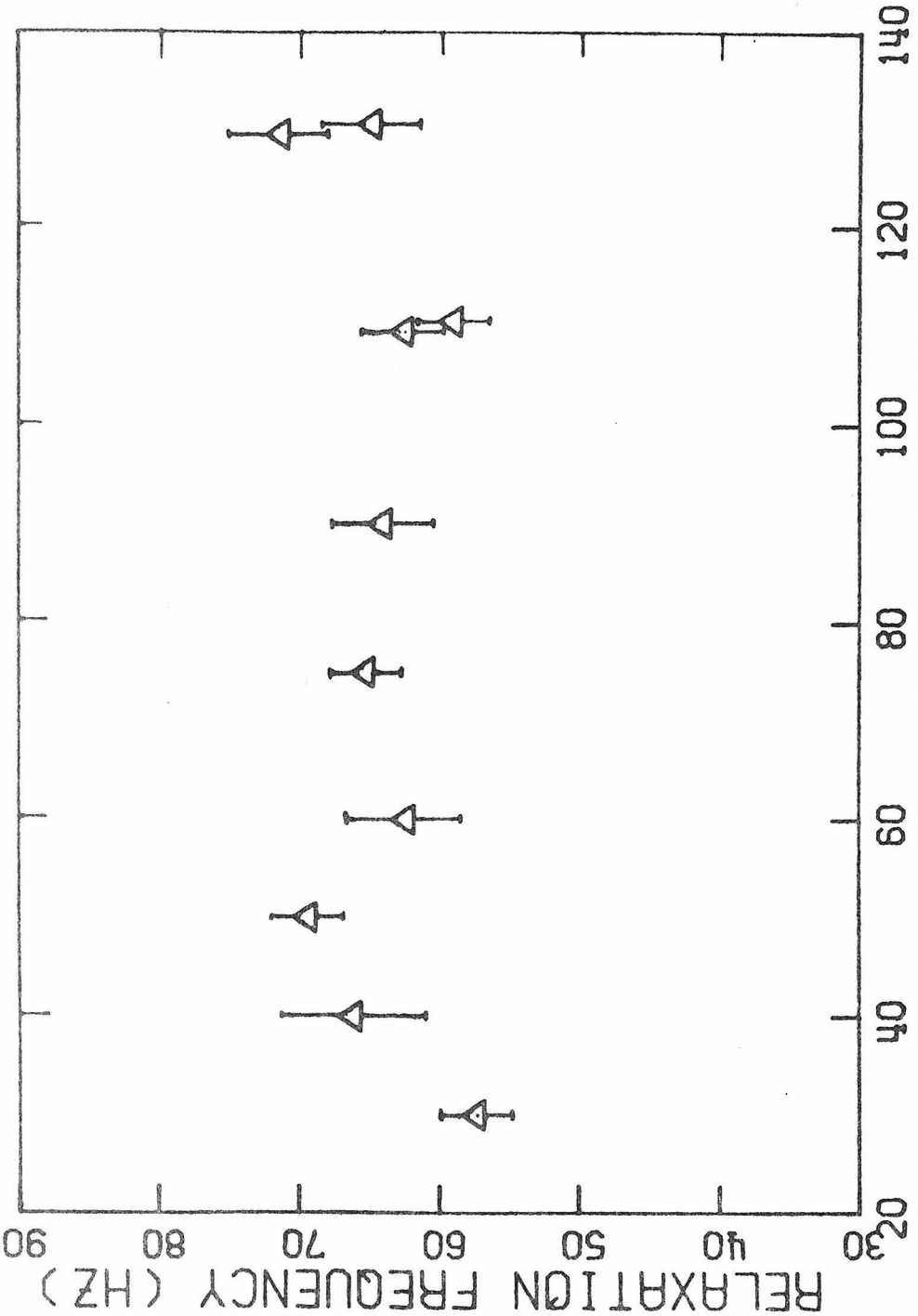

Fig. 34 Angular dependence of the high frequency relaxation performed on various positions of a sample at 55°C

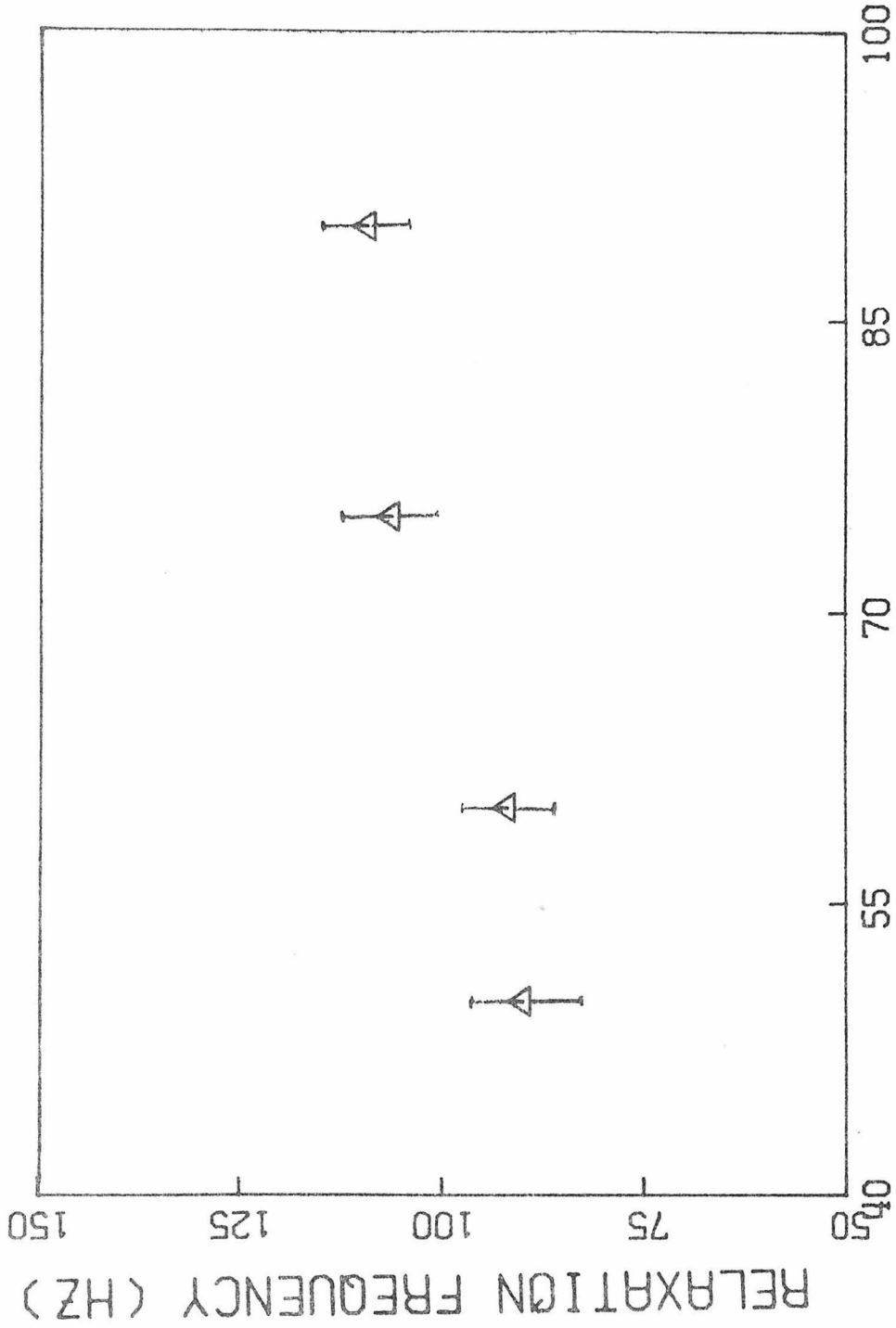

Fig. 35 Angular dependence of the high frequency relaxation performed on various positions of a sample at 81°C

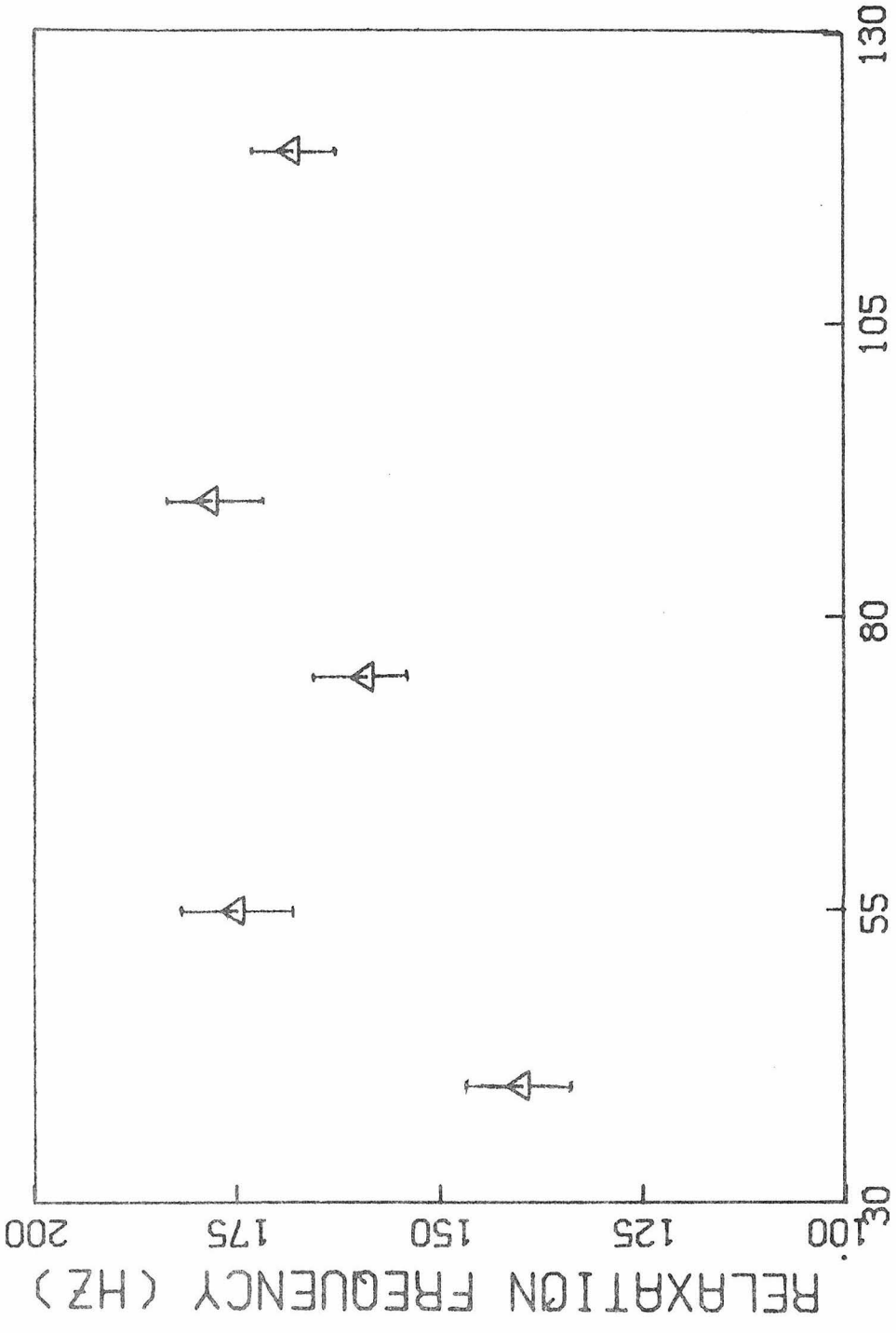

Fig. 36 Angular dependence of the high frequency relaxation performed on various positions of a sample at 100°C

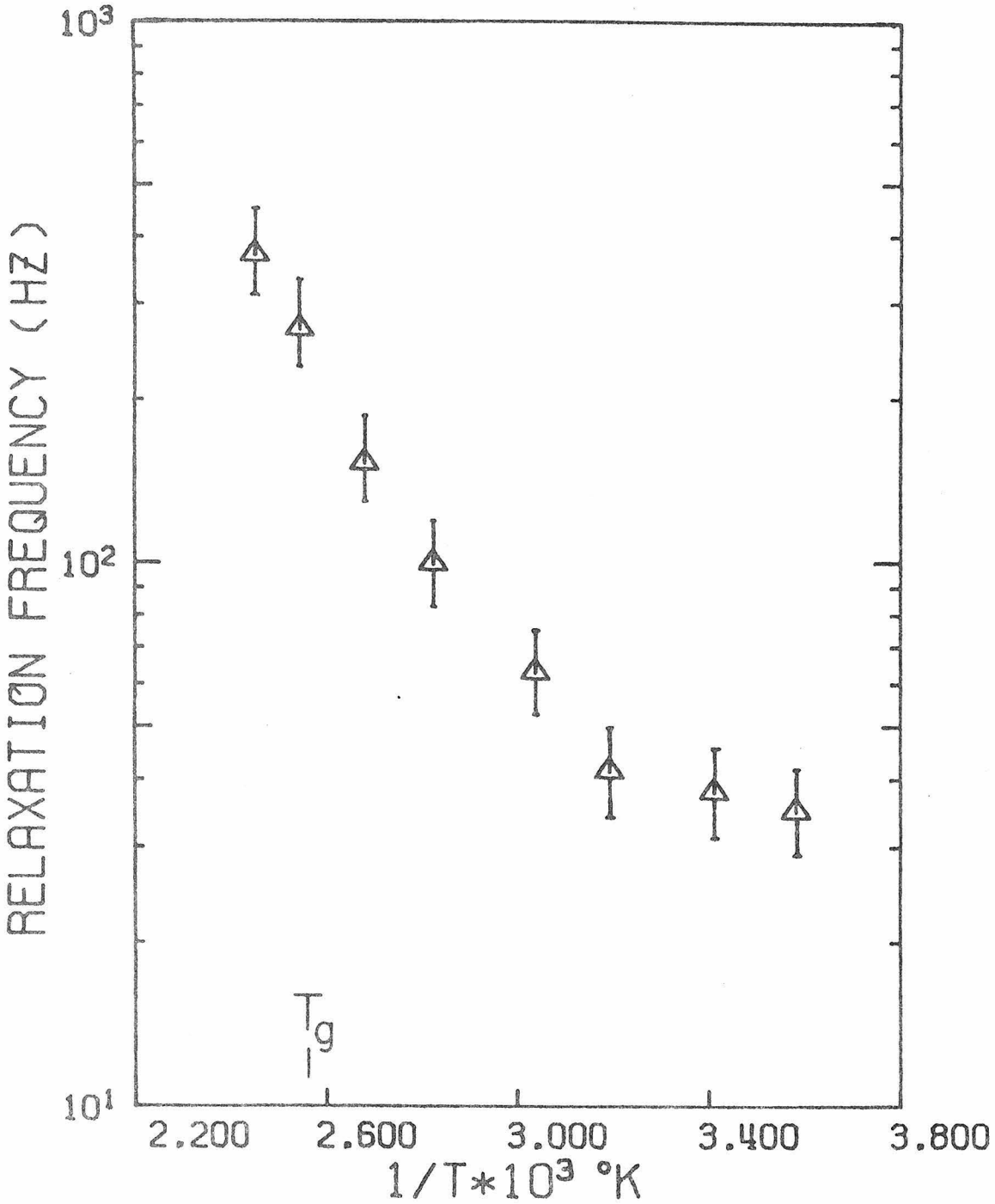

Fig. 37 Temperature dependence of the high frequency relaxation

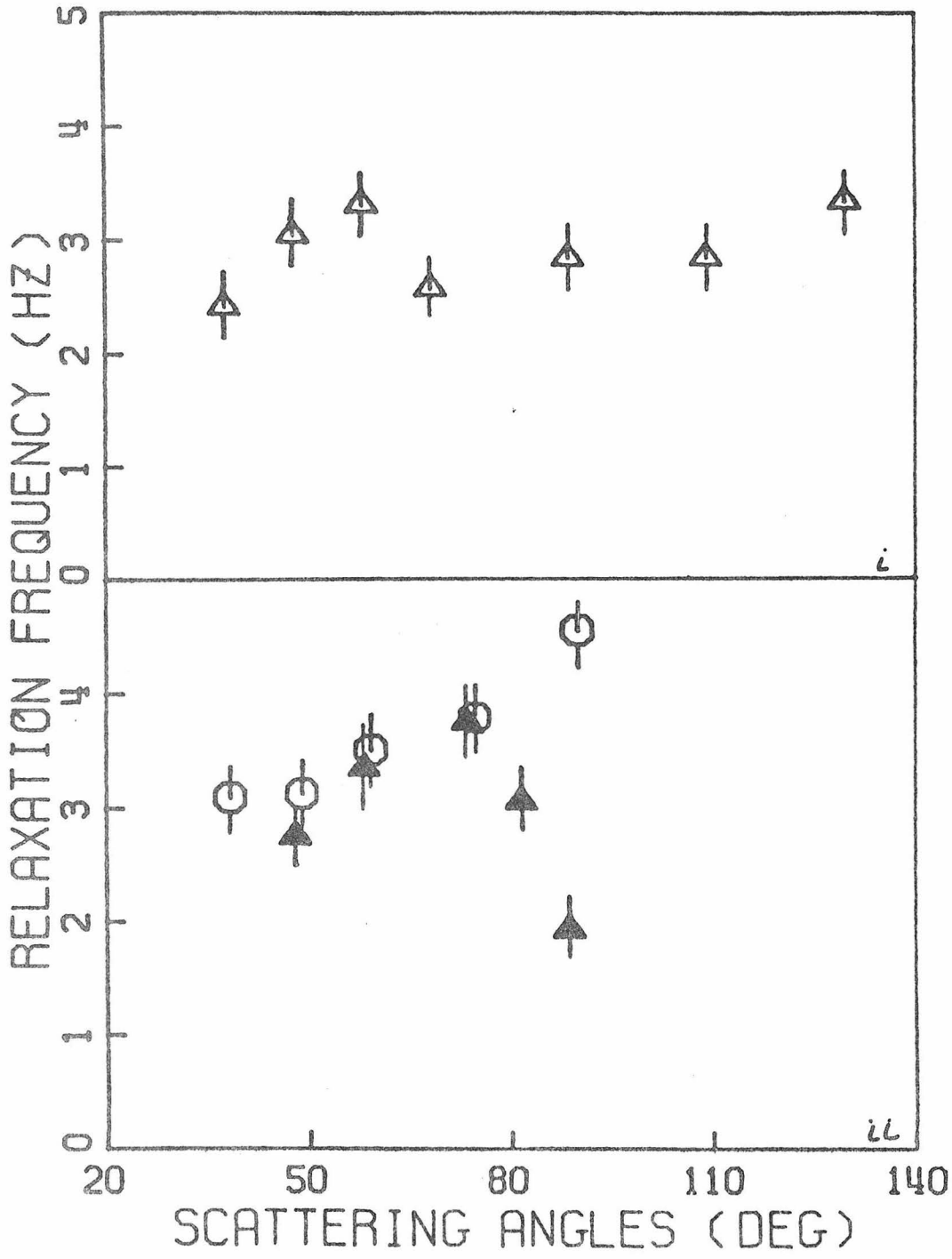

Fig. 38a Angular dependence of the low frequency relaxation performed on the same position of unannealed sample: i) at 20°C; ii) at 40°C for one position ( ) and at 40°C for another position ( ).

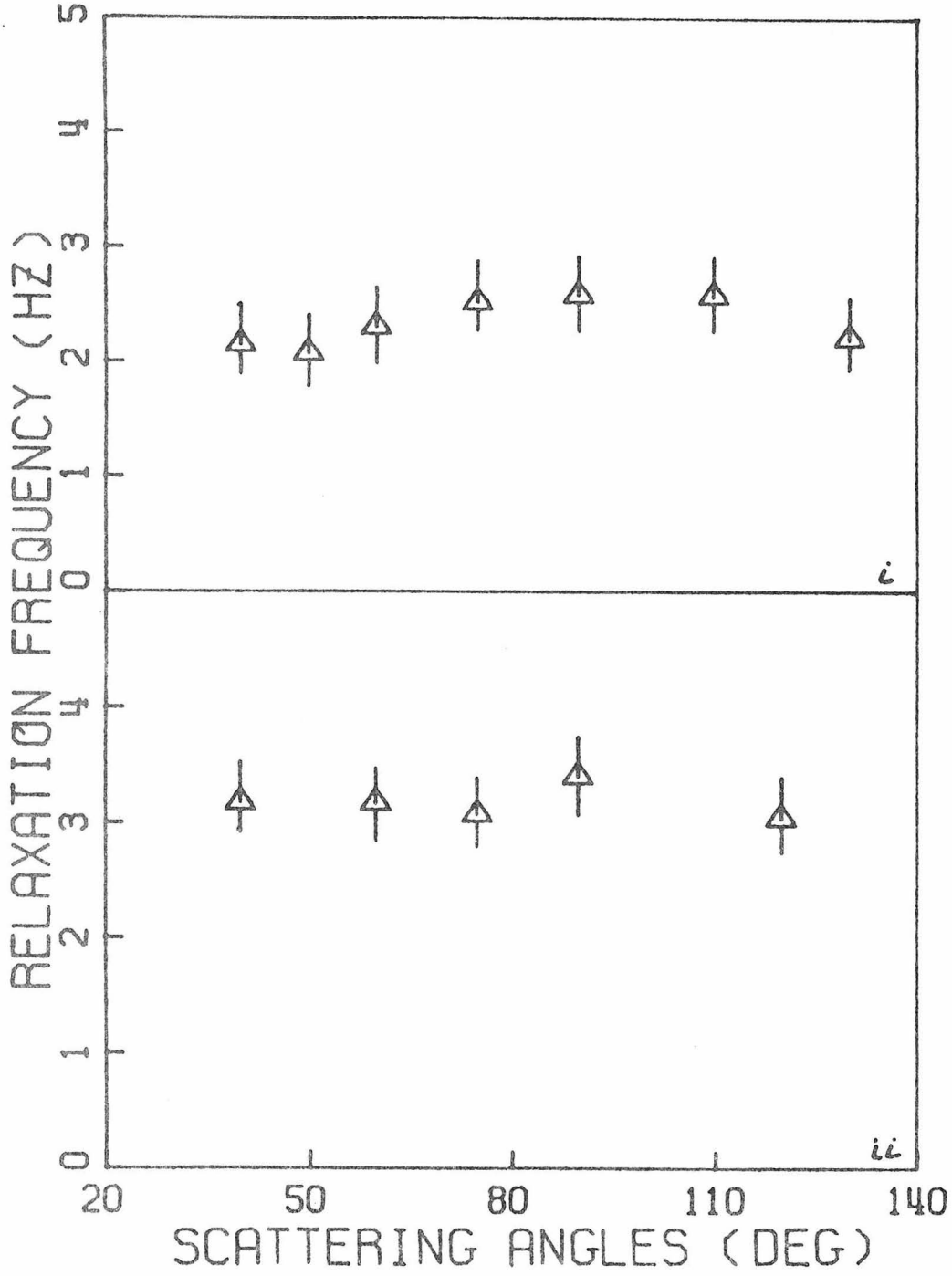

Fig. 38b Angular dependence of the low frequency relaxation performed on the same position of an unannealed sample: i) at 81°C; and ii) at 100°C

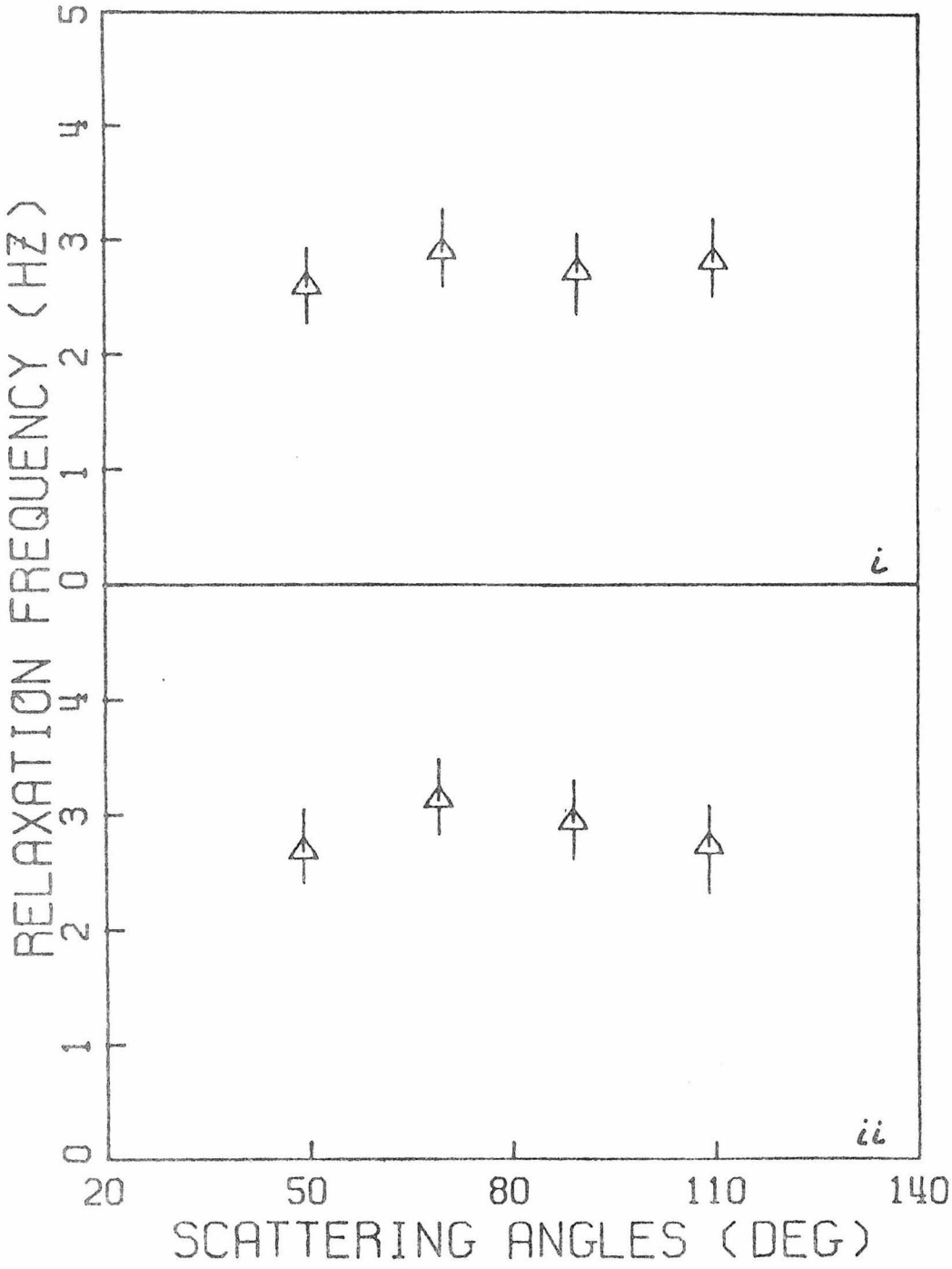

Fig. 38c Angular dependence of the low frequency relaxation performed on one position of an annealed sample at i) 6°C; and ii) 20°C

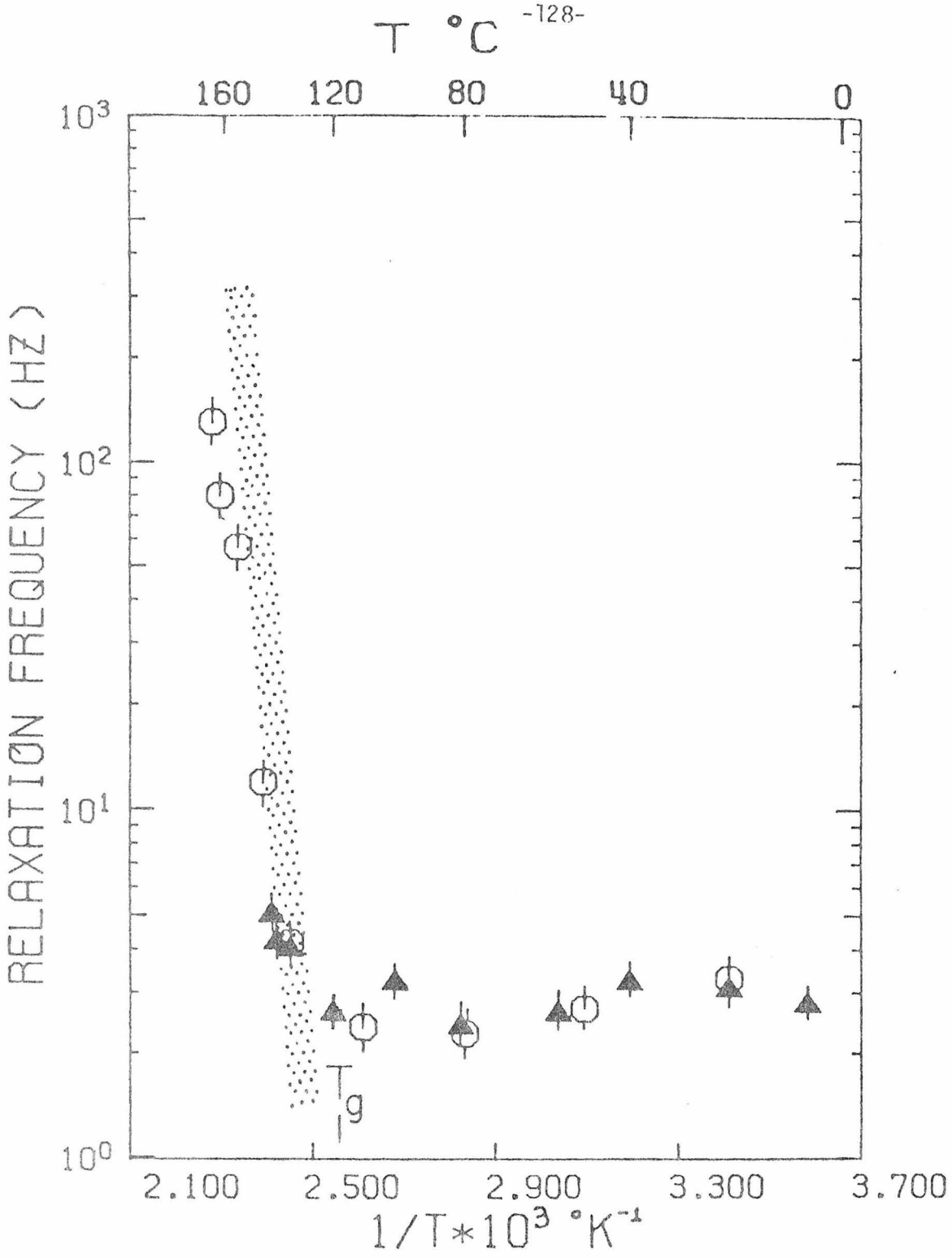

Fig. 39 Temperature dependence of the low frequency relaxation. Data from the commercial PMMA are denotet by ( ) and those from the Polysciences samples by ( ). The dotted area represents data and the attendant uncertainties from reference (10) obtained by other techniques